DESIGN AND EFFORTS TOWARDS SYNTHESES OF NIR-RESPONSIVE PHOTOSENSITIZERS BEYOND 700 nm VIA ENHANCED CONJUGATION

A THESIS SUBMITTED TO
THE GRADUATE SCHOOL OF NATURAL AND APPLIED SCIENCES
OF
MIDDLE EAST TECHNICAL UNIVERSITY

BY

GÖRKEM NAİL AYDIN

IN PARTIAL FULFILLMENT OF THE REQUIREMENTS
FOR
THE DEGREE OF MASTER OF SCIENCE
IN
CHEMISTRY

JANUARY 2024

Approval of the thesis:

THESIS TITLE

submitted by **GÖRKEM NAİL AYDIN** in partial fulfillment of the requirements for the degree of **Master of Science** i**n Chemistry, Middle East Technical University** by,

Prof. Dr. Halil Kalıpçılar
Dean, **Graduate School of Natural and Applied Sciences** _____

Prof. Dr. Özdemir Doğan
Head of the Department, **Chemistry** _____

Assoc. Prof. Dr. E. Görkem Günbaş
Supervisor, **Chemistry, METU** _____

Examining Committee Members:

Prof. Dr. Cihangir Tanyeli
Chemistry, METU _____

Assoc. Prof. Görkem Günbaş
Chemistry, METU _____

Prof. Dr. Ali Çırpan
Chemistry, METU _____

Assoc. Prof. Salih Özçubukçu
Chemistry, METU _____

Assoc. Prof. Safacan Köleman
Chemistry, Koc University _____

Date: 26.01.2024

I hereby declare that all information in this document has been obtained and presented in accordance with academic rules and ethical conduct. I also declare that, as required by these rules and conduct, I have fully cited and referenced all material and results that are not original to this work.

Name Last name : Görkem Nail Aydın

Signature :

ABSTRACT

DESIGN AND EFFORTS TOWARDS SYNTHESES OF NIR-RESPONSIVE PHOTOSENSITIZERS BEYOND 700 nm VIA ENHANCED CONJUGATION

Aydın, Görkem Nail
Master of Science, Chemistry
Supervisor: Assoc. Prof. Dr. Emrullah Görkem Günbaş

January 2024, 97 pages

Cancer, being a disease as ancient as the history of humanity, stands as one of the most challenging ailments faced by mankind today. Photodynamic therapy (PDT) is an effective, clinically proven treatment against various types of cancer. Compared to conventional treatment methods, PDT is minimally invasive and exhibits fewer side effects. However, despite these advantages, the usually visible light activation of photosensitizers used in PDT limits its effectiveness in deeper tissues due to the absorption of light by surrounding tissues. These agents often exhibit high phototoxicity and encounter solubility issues in aqueous environments. Consequently, researchers have been driven to design and synthesize next-generation photosensitizers to overcome such challenges.

Hybrid xanthene cores have gained considerable interest among the new generation of photosensitizers due to their impeccable photochemical properties, high fluorescence quantum yields, and remarkable photostability. Despite all these advantages, xanthene-based photosensitizers generally have limited use in deeper tissues due to their activation by visible light. In this study, four different selenium containing hybrid xanthene molecules were designed with enhanced conjugation through donor groups attached to the core structure to shift the absorbed light to the NIR region. The donor and Se-based hybrid xanthene core were successfully

synthesized and effectively brought together through Heck and Sonogashira type coupling reactions. Efforts towards realizing final oxidation reactions to reach the target photosensitizers, however, have not been fruitful yet. Several other oxidants are actively being pursued. Upon finalizing the synthesis of the target photosensitizers, their photophysical properties and potential as PDT agents will be investigated in detail.

Keywords: NIR-Photosensitizers, Photodynamic Therapy

ÖZ

ARTIRILMIŞ KONJUGASYON YOLUYLA 700 nm ÖTESİNDE NIR IŞIĞA DUYARLI FOTODUYARLAŞTIRICILARIN SENTEZİNE YÖNELİK TASARIM VE ÇALIŞMALAR

Aydın, Görkem Nail
Yüksek Lisans, Kimya
Tez Yöneticisi: Doç. Dr. Emrullah Görkem Günbaş

Ocak 2024, 97 sayfa

Kanser, varlığı canlılık tarihi kadar eski olan bir hastalık olmakla beraber insalığın günümüzdeki karşılaştığı en zorlu hastalıklarından biridir. Fotodinamik terapi efektif ve klinik olarak kanıtlanmış birçok kanser türüne karşı kullanılan bir tedavi metodudur ve günümüzde kullanılan klasik tedavi yöntemlerine kıyaslandığında minimally invasive ve daha az yan etkiye sahiptir bu avantajlarına rağmen kullanılmakta olan fotodinamik terapi ajanları görünür bölge ışıkla aktifleşmelerinden dolayı kullanılan ışık dokular tarafından absorblanmakta ve tedavinin daha derin dokularda efektif olarak kullanılamamasına sebebiyet vermektedir. Ek olarak kullanılan bu ajanların yüksek fototoksisiteye sahip olması ve suda çözünürlük problemleri yaşaması bilim insanlarını bu problemlerin üstesinden gelecek yeni nesil fotoduyarlaştırıcıların dizayn edilmesi ve sentezlenmesine itmiştir.

Hibrit ksanten çekirdekleri, kusursuz fotokimyasal özellikleri, yüksek floresans kuantum verimleri ve dikkate değer fotostabiliteleri nedeniyle yeni nesil ışığa duyarlılaştırıcılar arasında büyük ilgi görmüştür. Tüm bu avantajlara rağmen, ksanten bazlı ışığa duyarlılaştırıcıların görünür ışıkla aktivasyonları nedeniyle daha

derin dokularda kullanımı genellikle sınırlıdır. Bu çalışmada, soğurulan ışığı NIR bölgesine kaydırmak için çekirdek yapıya bağlanan donör grupları aracılığıyla gelişmiş konjugasyonla selenyum içeren dört farklı hibrit ksanten molekülü tasarlandı. Donör ve Se bazlı hibrit ksanten çekirdeği, Heck ve Sonogashira tipi birleştirme reaksiyonları yoluyla başarılı bir şekilde sentezlendi ve etkili bir şekilde bir araya getirildi. Ancak hedef ışığa duyarlılaştırıcılara ulaşmak için son oksidasyon reaksiyonlarını gerçekleştirmeye yönelik çabalar henüz sonuç vermedi. Diğer bazı oksidanlar aktif olarak araştırılmaktadır. Hedef ışığa duyarlılaştırıcıların sentezi tamamlandıktan sonra bunların fotofiziksel özellikleri ve PDT ajanları olarak potansiyelleri ayrıntılı olarak araştırılacaktır.

Anahtar Kelimeler: Fotodinamik Terapi, NIR-Fotoduyarlaştırıcı

To Serap and Gürsoy Aydın

ACKNOWLEDGMENTS

Firstly, I would like to express my heartfelt gratitude to my advisor and one of the best teachers I have ever known, Assoc. Prof. Dr. E. Görkem Günbaş, for providing us with these opportunities and for never allowing the flame of scientific curiosity within us to extinguish. Additionally, I am deeply thankful for his boundless support and extensive knowledge, and working together with him during this process was an invaluable experience.

A heartfelt thanks extends to the members of Flair Lab, particularly my friends Emre Özgan, Çağlayan Kızıleniş, and Doğuşcan Dönmez. Their collaborative spirit, constructive feedback, and shared enthusiasm have fostered a positive and motivating research environment. Furthermore, I would like to express my gratitude to Osman Karaman, who assisted in the process of joining the Flair lab and always shared his knowledge and guidance.

I would like to thank Assoc. Prof. Dr. Salih Özçubukçu, one of the best teachers I have ever known, for patiently welcoming me throughout all the courses I took from him.

Special thanks are reserved for my supportive girlfriend Dilan Batur, her belief in my capabilities has been a motivating force, and I am grateful for her unwavering support.

I would also thank to my examining committee members, Prof. Dr. Cihangir Tanyeli, Prof. Dr. Ali Çırpan, Assist Prof. Dr. Salih Özçubukçu and Assist Prof. Dr. Safacan Kölemen for accepting to evaluate my thesis and their valuable suggestions.

Lastly, I extend my deepest gratitude to my beloved family for their unconditional love, encouragement, and sacrifices. Their steadfast support has been the cornerstone of my academic achievements and the driving force behind my perseverance.

TABLE OF CONTENTS

LIST OF TABLES

TABLES

LIST OF FIGURES

FIGURES

LIST OF SCHEMES

LIST OF ABBREVIATIONS

ALA	5-aminolevulinic acid
DDQ	2,3-dichloro-5,6-dicyano-1,4-benzoquinone
FDA	Food and Drug Administration
Hp	hematoporphyrin
HpD	hematoporphyrin derivative
ISC	intersystem crossing
PDT	photodynamic therapy
PMB	para-methoxybenzyl
PS	photosensitizer
ROS	reactive oxygen species
DCM	Dichloromethane
DMF	Dimethylformamide
EtOAc	Ethyl Acetate
THF	Tetrahydrofuran
n-BuLi	n-Butyl Lithium
DIPA	Di-isopropylamine
DMEDA	N, N-Dimethylethylenediamine
TEOA	Triethanolamine

LIST OF SYMBOLS

SYMBOLS

λ_{abs}	Maximum Absorption Wavelength
λ_{fl}	Maximum Fluorescence Wavelength
ϕ_{fl}	Fluorescence Quantum Yield

CHAPTER 1

INTRODUCTION

Photodynamic therapy (PDT) is a fascinating medical treatment that harnesses the power of light to fight cancer. Imagine a light-activated agent, like a nano assassin, selectively targeting and eliminating malignant cells while leaving healthy ones unharmed. That's the essence of PDT. PDT relies on three key ingredients: a photosensitizer, light, and molecular oxygen. The photosensitizer, injected or applied topically, accumulates in target cells like cancerous or diseased tissues. When exposed to specific wavelengths of light, the photosensitizer gets energized and reacts with molecular oxygen to generate reactive oxygen species (ROS) or singlet oxygen, which will be the assassin of the diseased tissues. *(1)*

1.1 1.1 The History of Photodynamic Therapy

Light therapy has been used for medical purposes since ancient times. Sunlight was a widely used agent in ancient Egypt to treat skin diseases, particularly infections and lesions. The Egyptians used treatments for various skin conditions, including sunbaths and ointments containing naturally occurring compounds found in plants called psoralens, which are photosensitizing substances.*(2)* The much later development of photodynamic therapy (PDT) was made possible by the early use of light therapy despite the lack of scientific knowledge. Likewise, “heliotherapy” was another medical treatment employed by ancient Greeks effectively for various ailments. This practice involves prolonged exposure to the sun to treat conditions such as skin diseases, muscle pain, and even neurological disorders.*(3)* Although its

exact mode of action is still unknown, heliotherapy is an early example of light therapy experiments in humans.

With the groundbreaking work of German medical student Oscar Raab. PDT entered its modern era. In 1900, when Raab was researching the behavior of single-celled organisms called Paramecia, he made an astonishing discovery. He found that Paramecia died rapidly when exposed to light in the presence of an acridine (Figure 1) dye.*(4)* This phenomenon later became known as the “photodynamic effect” and represented a turning point in the history of PDT. Raab's discovery sparked interest in science and opened new avenues for studying biological interactions mediated by light.

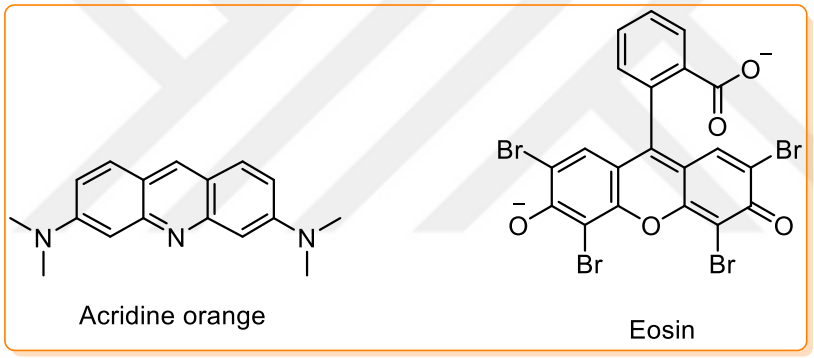

Figure 1.

Shortly after Oscar Raab's groundbreaking discovery, Danish scientist Niels Finsen discovered that some diseases could be treated with light. He found that exposing people with smallpox to red light for specific periods of time prevented the formation of smallpox pustules and could be used to treat the disease. Finsen's work would later earn him the Nobel Prize in medicine and be recognized as a cornerstone of modern photodynamic therapy.*(5)*

In 1903, the same year Neil Finsen won the Nobel Prize, Herman von Tappeiner and A. Jesionek used topically applied eosin (Figure 1) and white light to treat skin cancer.*(6)* Herman von Tappeiner, in his studies, realized that molecular oxygen plays a direct role in the functionality of the treatment. He coined the term "photodynamic action" in the literature for the interaction of oxygen with the photosensitizer used.*(7,8)* In later years, W. Hausmann, who worked in Vienna, reported that the haematoporphyrin (Figure 2) could kill the paramecium bacterium by interacting with light and the skin reactions of mice exposed to light after haematoporphyrin administration.*(9)*

The structure of porphyrin (Figure 2) was first obtained in 1841 by boiling blood with sulfuric acid and then washing it with ethanol. The discovery of its fluorescent properties and the naming of it took place in later years.*(10,11)*

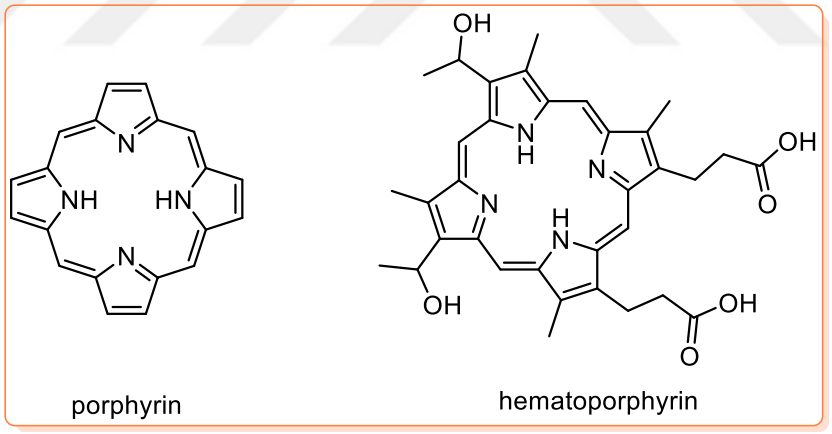

Figure 2

In 1913, German chemist Friedrich Meyer-Betz showed that similar effects could be observed in humans by injecting 200 mg of hematoporphyrin into his skin. He observed swelling and pain after hematoporphyrin injection, particularly in areas exposed to light. *(12)* In 1955, Samuel Schwartz synthesized the hematoporphyrin derivative (HPD) by subjecting hematoporphyrin to a series of chemical processes.*(13)* Then, in 1960, Richard Lipson and his colleagues at the Mayo Clinic showed that HPD accumulated in cancer cells, allowing cancer to be imaged. With this study, they started the golden era of photodynamic therapy.*(14)* 12 years after this study, I. Diamond and his colleagues suggested that porphyrins could accumulate in cancer cells and kill cancer cells by exploiting their cytotoxic properties. Animal studies showed that the growth of gliomas implanted in mice could be suppressed for 10 to 20 days, but after some time, the tumor began to grow again in deeper tissues.*(15)* In 1975, Thomas Dougherty and his colleagues reported that breast cancer tumors in mice could be wholly stopped using red light and HPD.*(16)* A year after this study, J.F. Kelly and colleagues conducted the first human experiments with bladder cancer using HPD.*(17)* Shortly after these successes, Y. Hayata used PDT to treat lung tumors and gastric carcinoma.*(16,17)* Photofrin, the first photosensitizer approved by the FDA in 1995, was isolated from HPD by Dougherty and co-workers.*(14)*

The areas of application for photodynamic therapy have constantly been expanding since 1995. Over time, it has found its place not only in cancer treatment but also in numerous medical regions.

1.2 Work of Action

The concept of photodynamic therapy (PDT) is the targeted killing of specific cells or tissues using light, photosensitizer (PS), and molecular oxygen. Patients with malignant cells can accumulate (PS) topically or via circulation. The PS in the patient's tumor area is then activated by specific wavelengths of light. The PS is usually triggered by light with a wavelength greater than 600 nm, called a therapeutic window. ROS are formed when the PS interacts with molecular oxygen or cellular components after activation. Under normal conditions, the PS should not be cytotoxic to the cell; however, after harvesting energy of light, it causes the production of ROS that ultimately leads to cell death.*(18)*

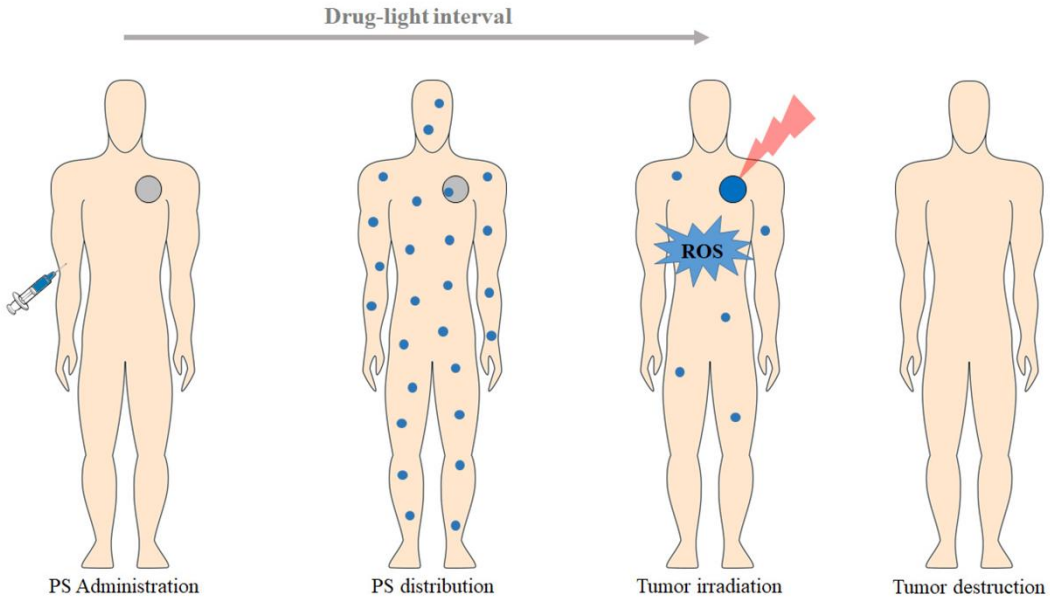

Figure 3. Therapeutic Application of PDT *(19)*

1.2.1 Harvesting Energy of Light

The use of photosensitizers to harvest light energy and transfer it to biological components is the core principle of photodynamic therapy. This section examines the interactions between PS and light to understand the energy transfer that occurs.

The Photodynamic action begins with light exposure of PS accumulated in cancerous cells or tumors. After light exposure, excited PS transitions from the singlet ground state (^1PS) to the singlet excited state ($^1PS^*$); the excited electrons are naturally more unstable than in the ground state and can exist only for nanoseconds. In a singlet excited state, PS can release energy in two different ways to return to the singlet ground state. One is radiative decay, also known as fluorescence, which can be used for imaging. Another way is to release heat through internal conversation.

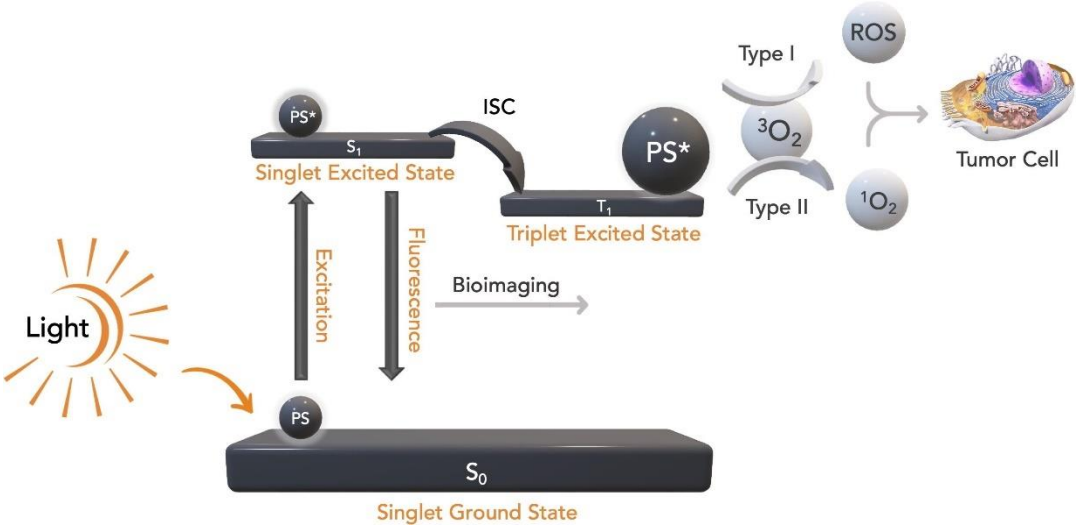

Figure 4. Schematic illustration of PDT and bioimaging & Jablonski Diagram *(1)*

However, the singlet state can also transition into an electronically excited, longer-lasting (triplet state, $^3PS^*$) by changing the electron's spin in the higher energy orbital through intersystem crossing. This extended excited state can undergo two different processes or return to the ground state by emitting light (phosphorescence). The triplet state has an extended lifetime (microseconds), which provides sufficient time

for direct energy transfers to molecular oxygen (O_2). The Type II reaction within the PS begins with the production of singlet oxygen ($^1O_2$), precipitated by this energy exchange, which also returns the PS to its original form. Singlet oxygen is highly reactive and interacts with various biological substrates, leading to oxidative stress and, ultimately, cell death. When the PS in the triplet excited state reacts with a substrate rather than molecular oxygen, the cell death mechanism progresses through Type I. In the Type I mechanism, the PS interacts with the cell membrane, leading to either electron transfer or hydrogen atom abstraction, generating free radicals. These produced free radicals that reacted with molecular oxygen, producing ROS such as oxygen radicals, hydroxyl radicals, and hydrogen peroxide.*(1,19)*

1.2.2 Cell Death

The leading cause of cell death in PDT is the reactive species that arise from Type I and Type II reactions.*(14,20)* Although Type II mechanisms generate singlet oxygen and dominate cell death, Type I and Type II mechanisms act simultaneously. The process is responsible for cell death is determined by several factors, including the concentration of molecular oxygen, the affinity of the substrate for binding to the cell, and the presence of photosensitizers (PS). These factors control the process that leads to cell death. The three pathways for cell death facilitated by the ROS produced by the PS are necrosis (unprogrammed), apoptosis (programmed), and indirect death (hypoxia), which results from the PS disrupting the surrounding tissues and cutting off the blood supply to the cancerous tissue, preventing the cancer cells from accessing oxygen and nutrients.*(21) (19)*

1.2.2.1 Apoptosis & Necrosis

In PDT, cell death can occur through apoptosis or necrosis.*(22)* High-intensity light generally leads to rapid (necrotic) cell death. Necrosis can be described as rapid cell

death and can be characterized by the breakdown of the cell membrane and the resulting inflammation.*(23)*

Apoptosis, called programmed cell death, can be triggered by low-intensity light. It is characterized by chromosomal DNA damage, cell and membrane shrinkage, and apoptotic bodies outside the cell membrane. Unlike necrosis, apoptosis does not elicit an immune response, and no toxic chemicals are released into the environment because the cell does not rupture.*(24)*

1.3 Key Components of Photodynamic Therapy

As mentioned earlier, photodynamic therapy (PDT) consists of three main components: photosensitizer, light, and molecular oxygen. We will examine each component in detail to gain a deeper understanding of PDT.

1.3.1 Photosensitizers

Photosensitizers are one of the three critical components of PDT. These are chemical compounds, dyes, or naturally occurring molecules that can be defined as chemicals that trigger photochemical reactions through the light they absorb of a specific wavelength.*(25)*

It is possible to identify several features and circumstances that characterize the perfect photosensitizer; stability at ambient temperature and a high degree of chemical purity are necessary. Only the presence of a specific wavelength of light should activate the PS. A strong photochemical reactivity is essential, with wavelengths between 600 and 800 nm absorbing light the most. There should be a minimum absorption in the 400–600 nm region to avoid extreme photosensitivity from sunshine. Furthermore, there should be no overlap between the absorption bands and any other material in the body, including melatonin, hemoglobin, or oxyhemoglobin. The photosensitizer must be readily soluble in bodily tissues and

exhibit negligible cytotoxicity in the dark. It should also have a high selectivity for neoplastic tissues to reduce phototoxic side effects, staying in afflicted areas for several hours while leaving healthy tissues swiftly. Finally, the synthesis must be affordable, uncomplicated, and readily available.*(26)*

1.3.1.1 First Generation Photosensitizers

In the 20th century, naturally occurring porphyrin derivatives produced the first generation of photosensitizers.*(14)* Initially, it was believed that they had excellent photodynamic action, but over time, it became clear that they had severe disadvantages.*(27)* Despite these drawbacks, the FDA-approved first-generation photosensitizer photofrin is the most used photosensitizer in cancer, including lung, esophageal, and cervical cancer. Dark cytotoxicity, poor absorption within the therapeutic window, and persistent skin hypersensitivity after treatment due to the long half-life of PS are the main problems with first-generation photosensitizers. The first generation of PS is limited to absorbing light between 625 and 635 nm in the near-infrared (NIR) spectrum.*(28)* The low absorption of near-infrared radiation results in low skin penetration and low chemical purity, paving the way for second-generation photosensitizers. *(27)*

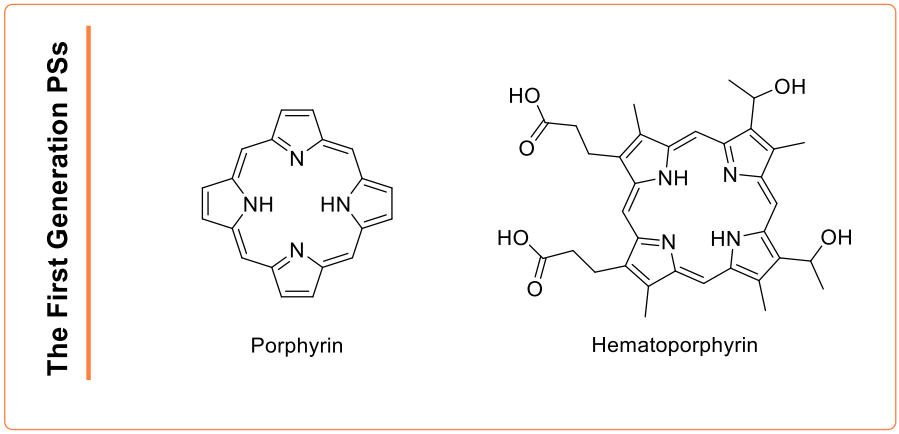

Figure 5. The first-generation photosensitizers

1.3.1.2 Second Generation Photosensitizers

Second-generation photosensitizers were developed to solve the problems encountered with first-generation PSs. Compared to the 1st generation, the 2nd generation PSs are activated by higher wavelength light (>650 nm), can be removed from cells more quickly than Photofrin, and show lower phototoxicity. They also have a higher singlet oxygen quantum yield and better aqueous solubility.*(27)*

1.3.1.2.1 Porphyrin Based

5- Aminolevulinic acid (ALA) is a prodrug. Upon application to the body, it undergoes enzymatic conversion into protoporphyrin, which exhibits a maximum absorption wavelength of 630 nm. The topical application of light does not cause photosensitivity except in the treated area. While a wavelength of 630 nm is effective for achieving deeper penetration, it is impossible to penetrate deep tissues by topical treatments. Due to its inherently low activity, the treatment process of ALA is either high light intensity or prolonged exposure.*(29)*

Chlorins are porphyrin-based second-generation PSs consisting of two saturated tetrapyrrole rings. The saturation of these double bonds has resulted in their absorption shifting to the NIR region, making them highly interesting due to their ability to provide the necessary penetration. HPPH, Foscan, and Temoporfin are used in the treatment of neck and prostate cancers, and their high fluorescence properties make them potential imaging agents. However, their low solubility in water limits their clinical applications.*(27)*

In clinical applications, the maximum absorption peak of bacteriachlorin, known as TOOKAD, is approximately 800nm. Due to its ability to absorb light with a long wavelength is used to treat deep cancer tissues. Unlike photofrin, it has a much shorter elimination time from the body, resulting in significantly lower photosensitivity. Moreover, it does not have any severe side effects.*(30,31)*

Phthalocyanines are derivatives of azoporphyrin, formed by the binding of four isoindolic rings through four nitrogen atoms and typically containing a coordinated metal. The increased conjugation with the nitrogen atoms involved in the porphyrin ring enables their activation with light in the NIR region.*(32)*

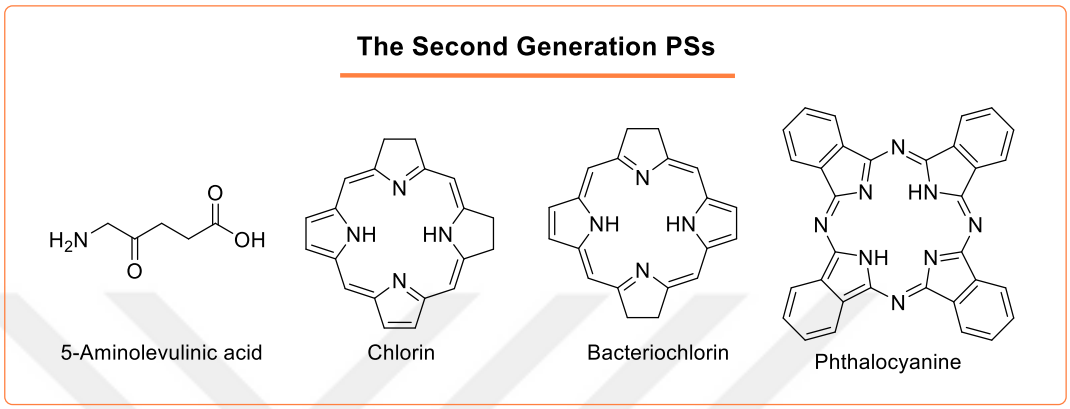

Figure 6. Second generation photosensitizers

1.3.1.2.2 Non-Porphyrin-Based Photosensitizers

Two different groups of example PSs, namely natural and synthetic, are provided in Figure 7. These PSs have provided some solutions to the water solubility and low absorption problems that porphyrin-based PSs cannot overcome.

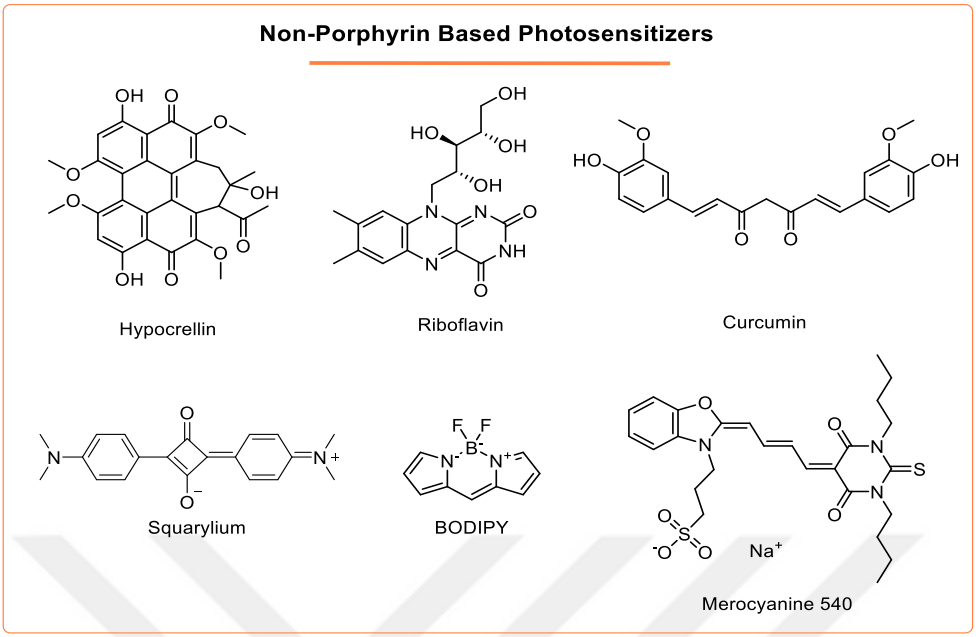

Figure 7. Non-porphyrin-based photosensitizers.

1.3.2 Xanthene Dyes

Xanthene dyes are a type of synthetic dyes consisting of many different members, including second and third generations. The general structure of xanthene dyes is to replace the benzene ring in the middle of the anthracene with a pyran ring. Second-generation dyes were developed to solve the problems of photosensitivity, slow excretion from the body, and poor water solubility that occurred with 1st generation dyes. Xanthene dyes are one of the best choices for overcoming these problems. The promising properties of xanthene dyes include water solubility, photostability, and ease of synthetic modification. Classical xanthene dyes such as fluoresceins, rhodoles and rhodamines (Figure 8) successfully utilized in cancer imaging*(33)* and modified with heavy atom for photodynamic action.*(34)* Even though classical xanthene dyes have these promising properties due to their large bandgap, they generally absorb the green region of the visible spectrum; therefore, this property limits in vivo studies. *(35)*

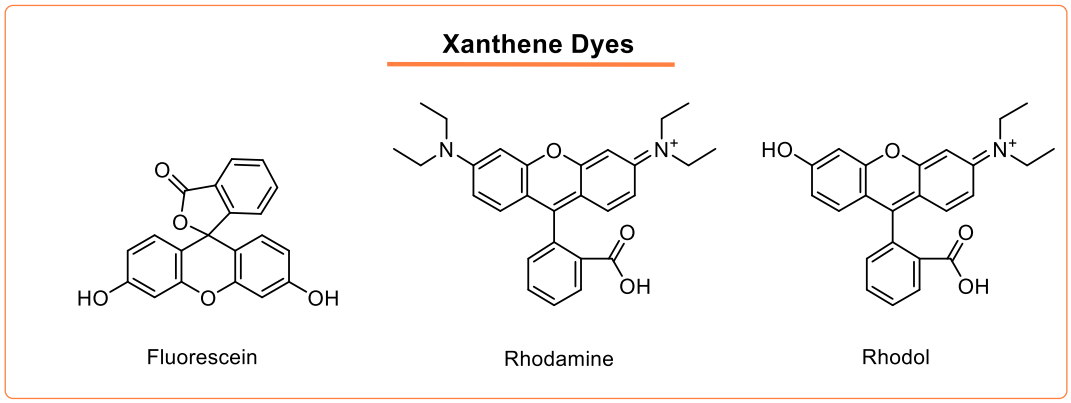

Figure 8. Examples of classical xanthene dyes

Hybrid xanthene cores were developed by replacing the oxygen atom at position 10 with heteroatoms such as silicon, phosphorus, selenium, and tellurium in xanthene dyes, which can be easily modified synthetically.*(1)* Xiao and Qian first proposed the idea of replacing the oxygen atom with silicon in 2008. Replacing oxygen with silicon at position 10 of the rhodamine core has resulted in a bathochromic shift of about 90 nm*(36)* It also has a high molar extinction coefficient compared to the rhodamine dye, and the promising results of this study paved the way for the synthesis of hybrid xanthene dyes with various heteroatoms (Si, P, Se, Te).*(1)* Some hybrid xanthene dyes are listed in figure 9.

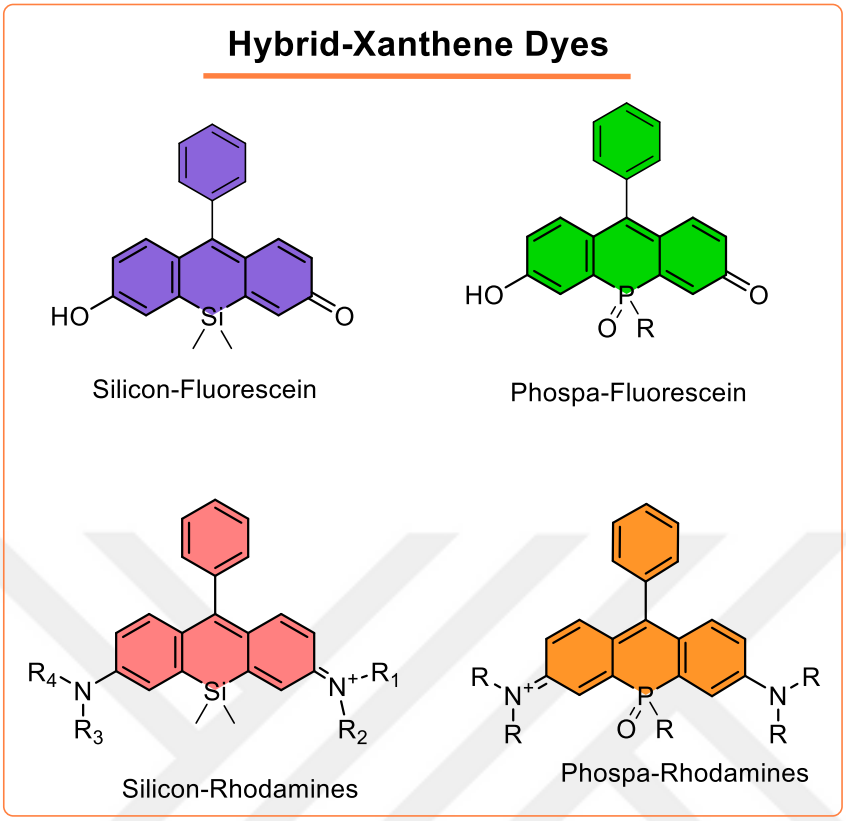

Figure 9. General structures of hybrid xanthene dyes

After the 90 nm bathochromic shift achieved by silicon modification by Xiao and Qian, the modification of different xanthene cores with heteroatoms (Figure 9) has become a burgeoning research area.*(36–40)* In 2018, Adam Choi and Stephen C. Miller made alterations to the oxygen atom within the oxazine dye by substituting it with a silicon atom (Figure 10). As a result of this modification, they achieved a significant bathochromic shift of approximately 80 nm in the oxazine dye.*(41)*

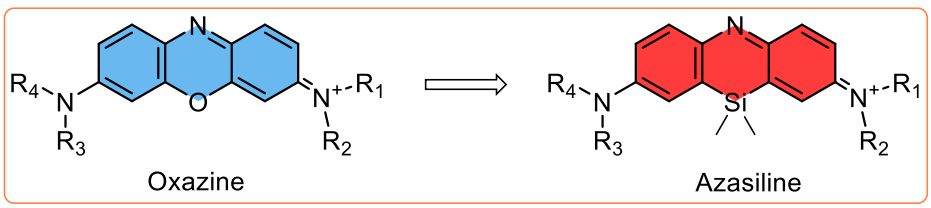

Figure 10. Structure of oxazine and azasiline dyes

1.3.3 Light

Light, one of the fundamental components of photodynamic therapy (PDT), can be divided into two main groups: laser and non-laser light sources. The light sources used in PDT are shown in Figure 11. Laser sources used in PDT include argon lasers, argon-pumped dye lasers, metal vapor-pumped dye lasers, solid-state lasers, optical parametric oscillators, and diode lasers. On the other hand, non-laser light sources include tungsten-quartz halogen lamps, xenon arc lamps, metal halide lamps, phosphor-coated sodium lamps, and fluorescent lamps. In addition, non-laser light sources also include light-emitting diodes (LEDs).*(42,43)*

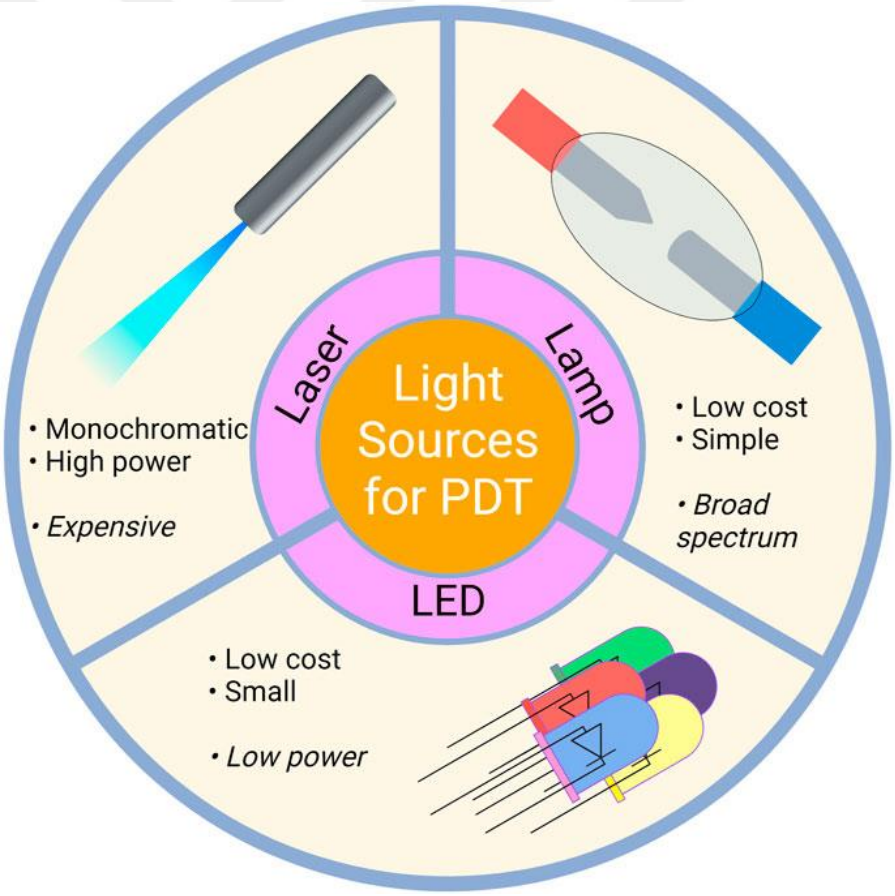

Figure 11. Light sources utilized in PDT.*(43)*

The wavelength of the light used is as important as the light source, and PSs are used to increase the effectiveness of PDT. As seen in Figure 12, the wavelengths that can penetrate deepest into the tissue are red and infrared. It is called the optical window for the tissue from 600 nm to 1200 nm, but it is not possible to produce singlet oxygen ($^1O_2$) above 800 nm because the transmitted light does not have enough energy to stimulate PS.*(44,45)*

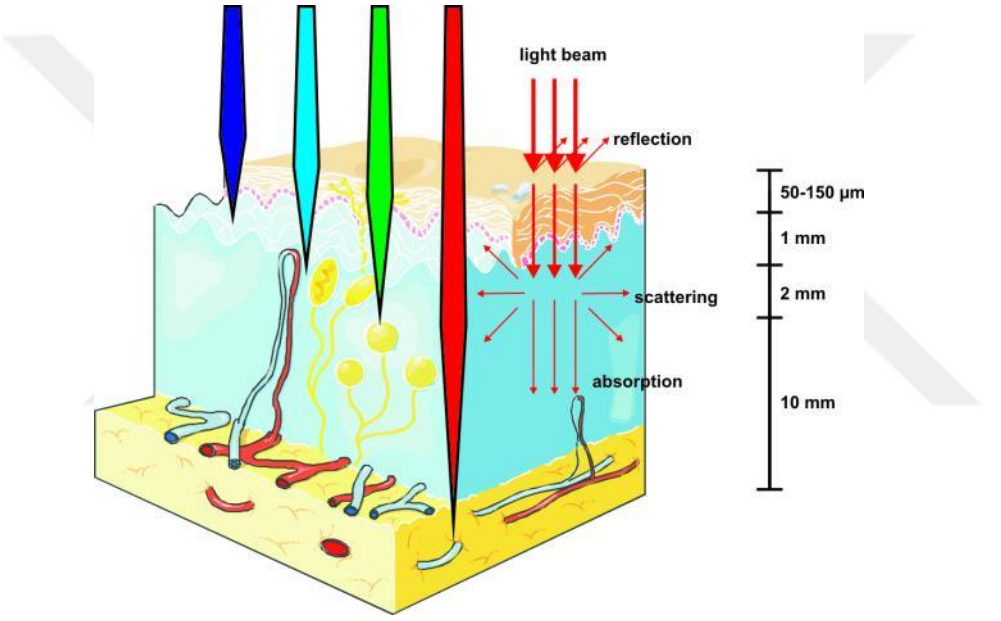

Figure 12. Light propagation through the tissues.*(44)*

1.3.4 Oxygen

Oxygen, one of the three main components of PDT, is another factor that directly affects the effectiveness of the treatment. The low oxygen concentration in cancer tissue reduces the efficacy of PDT.*(46)* Low oxygen conditions, known as hypoxia, are resistant to PDT in cells. It has been shown that the singlet oxygen ($^1O_2$) produced can only penetrate up to 0.05 µm without interacting with cell components or being quenched.*(47)* Therefore, singlet oxygen produced outside the cell does not cause

damage inside the cell. The subcellular localization of the photosensitizer influences the region where the damage occurs and the course of treatment.*(48)*

1.4 Synthetic Tools Used in the Synthesis of Xanthene Dyes

The Heck and Sonogashira coupling reactions have played a crucial role in the synthesis of the target molecules featuring N-Se-based enhanced conjugation, as illustrated in Figure 15. Achieving the synthesis of these target molecules without leveraging coupling reactions would be synthetically inefficient and considerably challenging. The utilization of coupling reactions is imperative for the efficient and favorable access to the desired compounds, underscoring their significance in the synthetic pathway.

1.4.1 Sonogashira Coupling

The Sonogashira reaction is a cross-coupling reaction widely employed in synthetic organic chemistry for the formation of carbon-carbon bonds. It involves the utilization of a palladium catalyst and a copper co-catalyst to facilitate the formation of a new carbon-carbon bond. In the presence of these catalysts, a carbon-carbon bond is established between a terminal alkyne and an aryl or vinyl halide. This reaction represents a pivotal method in the synthetic tool for the strategic creation of carbon-carbon linkages, contributing significantly to the synthesis of complex organic molecules.*(49)*

The Sonogashira reaction finds widespread utility in the synthesis of complex molecules, owing to its high efficiency under mild conditions. This versatile reaction has been successfully applied in various domains, including pharmaceuticals, natural products, organic materials, and nanomaterials. As an illustrative example, the synthesis of the tazorotene molecule, employed in the treatment of acne, involves the strategic application of the Sonogashira reaction.*(50)* The ability of this reaction to operate under mild conditions makes it particularly advantageous for the

construction of intricate molecular structures, highlighting its main role in contemporary synthetic methodologies.

The alkynylation reaction of aryl halides using aromatic acetylenes was initially reported by several research groups in 1975. Notably, the procedures outlined by Heck*(51)* and Cassar*(52)*, characterized by the solely use of a palladium catalyst, result in considerably harsher conditions compared to the Sonogashira reaction*(49)*, which incorporates a copper pre-catalyst. The catalytic cycle for the Sonogashira coupling reaction is depicted in figure 13.

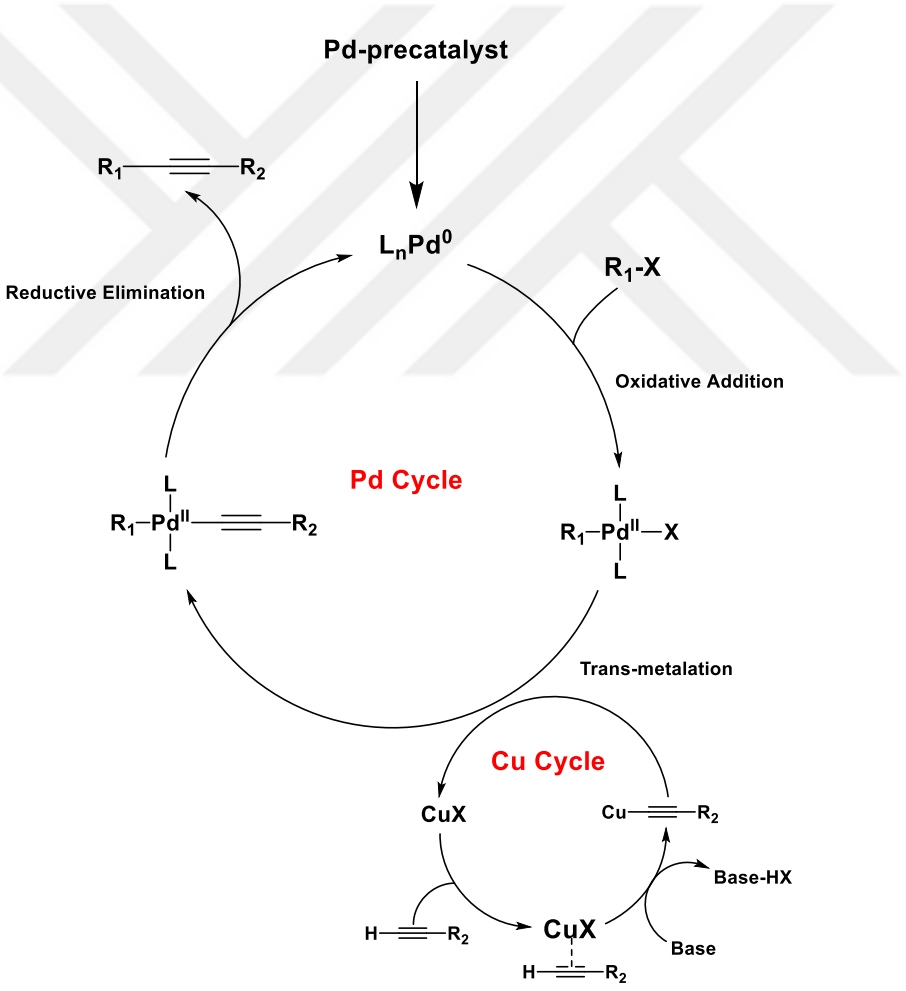

Figure 13. The catalytic cycle for Sonogashira reaction.*(49)*

1.4.2 Heck Coupling

The cornerstone of contemporary synthetic organic chemistry, the Heck coupling reaction transformed the area by creating carbon-carbon bonds unlike anything else. This palladium-catalyzed cross-coupling reaction was first described by Professor Richard F. Heck in 1969 and has since grown to be an essential tool for creating aryl-vinyl . A base and a palladium(0) or palladium(II) species usually form the catalytic system that facilitates the coupling of aryl halides with alkenes.*(53)* The Heck coupling reaction is an essential tool for the synthesis of complex molecules, such as medicines, agrochemicals, and materials with significant industrial value, due to its adaptability and efficiency. Its wide range of substrates includes a variety of functional groups, giving chemists access to a wide range of molecular structures. Heck coupling is also compatible with a variety of sensitive functional groups due to its mild reaction conditions, which increases its synthetic utility.The Heck reaction's catalytic cycle, which includes the steps of oxidative addition, syn addition, and beta-hydride elimination (Figure 14), sheds light on the complex mechanisms underlying this transformation process.

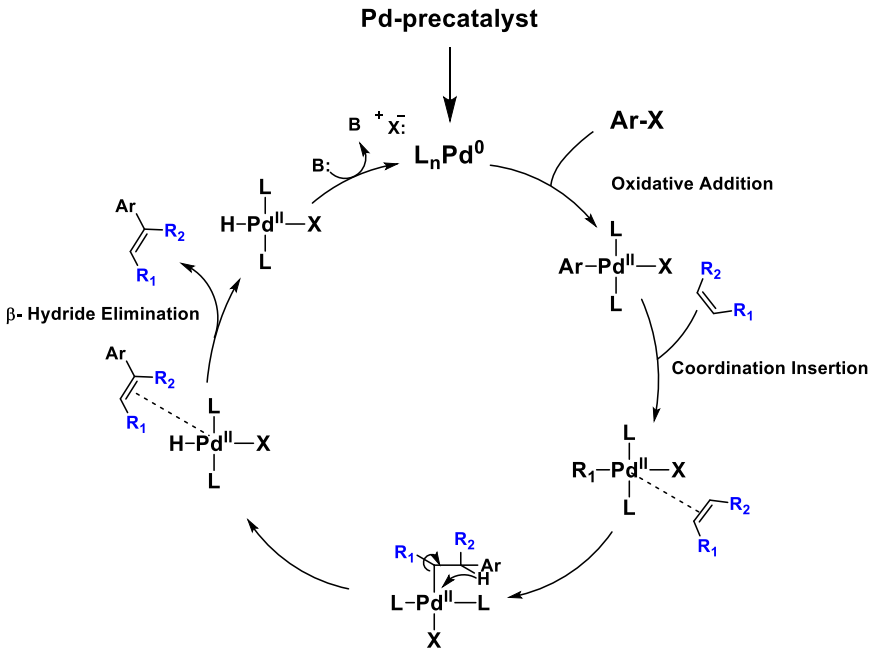

Figure 14. The catalytic cycle for Heck reaction.*(54)*

1.5 Aim of The Study

Hybrid xanthene cores have gained immense popularity as photosensitizers (PSs) in recent years due to their numerous advantages, including water solubility, photostability, and high quantum yield, as previously mentioned. However, a significant drawback of both classical and hybrid xanthene cores is the fact that most have their absorption maxima in the visible region, hence demonstrate limited utility for deep tumors.

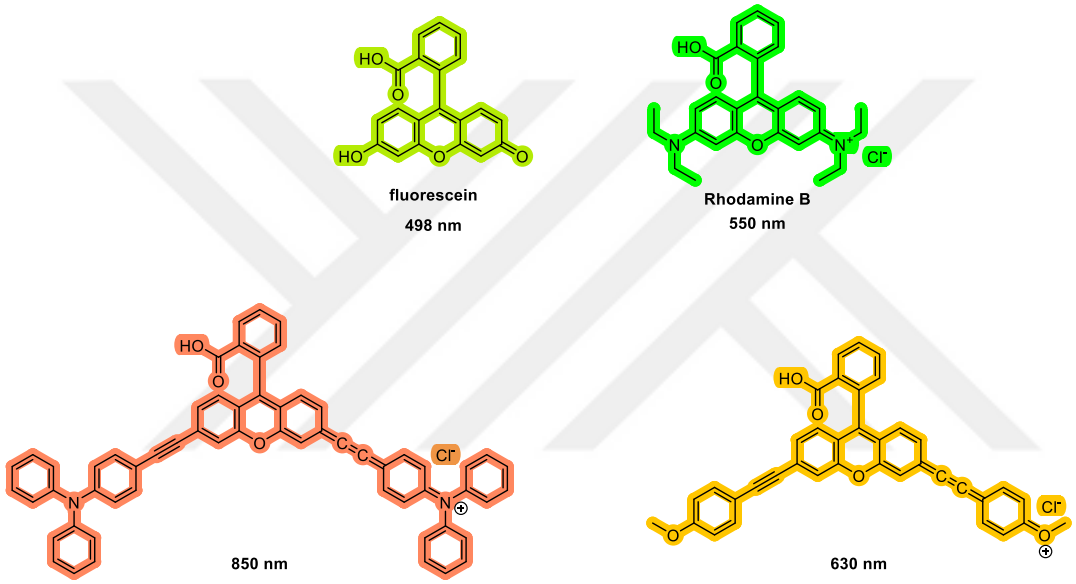

Figure 15. Examples of fluorophores with extended conjugation & absorption, based on classical Xanthene dyes.*(55,56)*

As demonstrated by Colleen N. Scott and colleagues (Figure 15), the enhancement of π-conjugation by extending the classical xanthene core has shown a significant increase in the absorption maximum of the resulting fluorophore, depending on the attached donor group. In 2021, xanthene-based fluorophores were reported to be activated by light in the NIR-I and NIR-II regions by expanding π-conjugation and enhancing the intramolecular charge transfer effect (Figure 16).

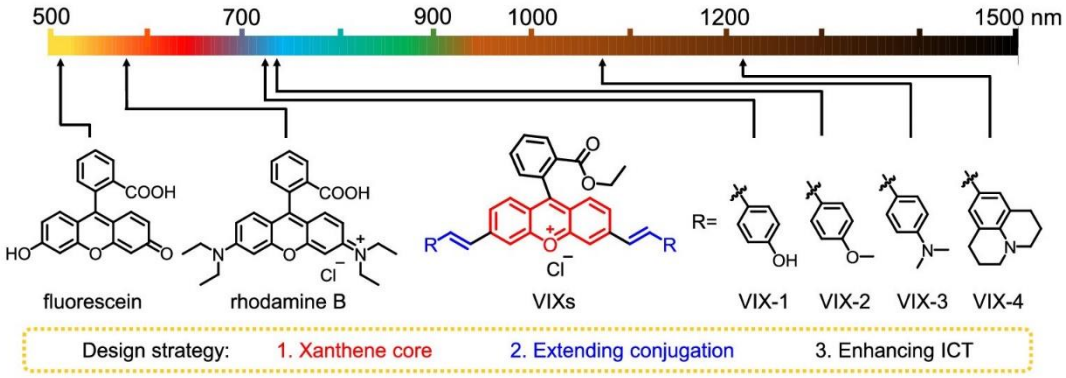

Figure 16. Structures of the fluorescent xanthene dyes with extended conjugation*(56)*

In literature, there are xanthene-based fluorophores that can be activated by light in the near-infrared (NIR) and NIR-II regions with extended conjugation.*(55,56)* However, it is important to note that these examples extend beyond the scope of PSs and primarily serve as imaging agents. Utilizing increased conjugation for the design of photosensitizers (PS) activated in the NIR region is a clear solution. The selection of Selenium as the heteroatom modification in the core structure enables PS function by enhancing intersystem crossing, and further modification with halogen-heavy atoms, which tends to render PSs with dark toxicity, is not required.

The pursuit of synthesizing photosensitizers that can be activated by near-infrared (NIR) light beyond 700 nm has been a fascinating and ambitious research endeavor. Though the synthesis of the intended molecules is still in progress, the methodology and initial stages of the synthesis have shown promising potential in the search for effective photosensitizers. The careful planning and theoretical framework used to design these molecules to use NIR light's more extended wavelength range provide a solid foundation for future work in this field. Incorporating extended conjugation into the molecular structure is expected to enhance the absorption properties and ultimately increase the photoactivation capabilities of the synthesized molecules in the desired near-infrared (NIR) spectrum.

With all these insights the following target PSs were designed, namely N-StyO, N-StyN, N-AcetO, and N-AcetN. (Figure 17)

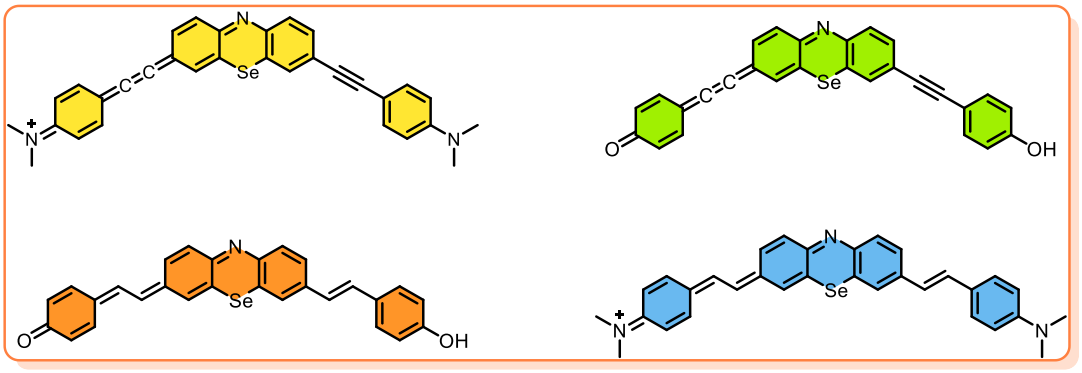

Figure 17. Schematic illustration of target NSe-based xanthene cores with enhanced conjugation

We envisioned that the incorporation of enhanced conjugation in N-Se-based hybrid xanthene photosensitizers can be achieved by assembling donor groups and core structures through straightforward Sonogashira and Heck coupling reactions. This approach holds the potential to yield photosensitizers activated by NIR light and could be synthesized with high efficiency and ease.

CHAPTER 2

RESULTS AND DISCUSSION

2.1 Synthetic Approach for Target Photosensitizers

This thesis uses a non-linear synthetic pathway for synthesizing novel N-Se-based hybrid xanthene cores, shown in Figure 18. Using a non-linear synthetic approach for the N-Se-based xanthene core with an extended conjugation is a fresh and inventive method in organic synthesis. Unlike the usual step-by-step procedures, this approach explores multiple synthetic paths simultaneously. Blending different reaction pathways aims to build the xanthene core efficiently while lengthening its conjugated structure. This elongation could enhance the xanthene's optical and electronic traits, possibly improving its ability to absorb or emit light. This non-linear method not only speeds up synthesis but also opens doors to new xanthene variations with longer conjugation.

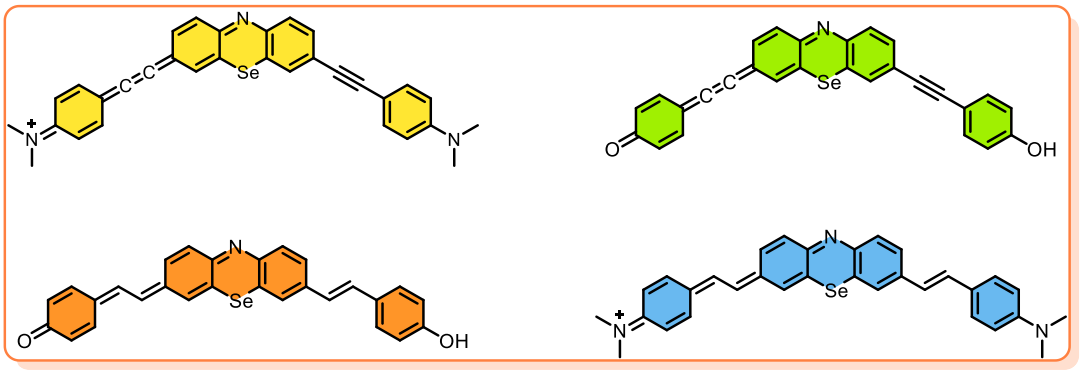

Figure 18. Schematic illustration of target NSe-based xanthene cores with enhanced conjugation

The synthesis plan involves dividing the molecular structure into two distinct segments, the xanthene core structure, and the donor part. A non-linear synthetic pathway is used to systematically assemble these segments, utilizing their unique

characteristics for efficient and tailored synthesis, resulting in a unique molecular design.

2.2 Synthesis of Donors

2.2.1 Synthesis of 4-Ethynylphenol

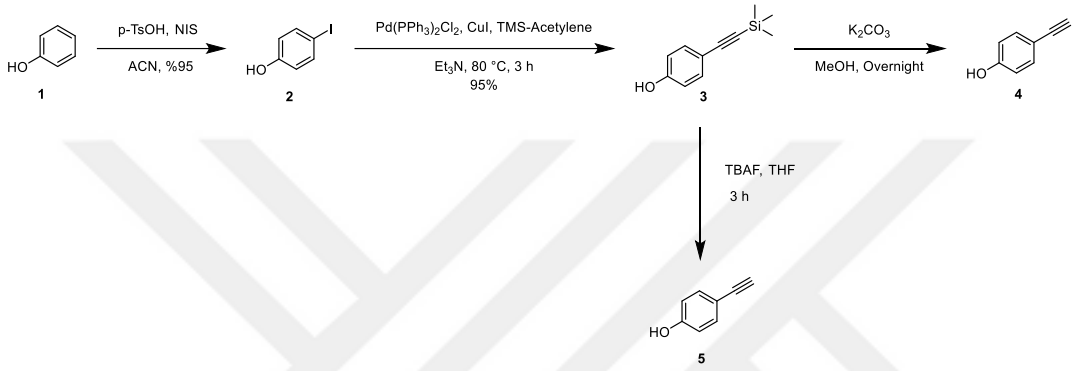

Scheme 1. Synthetic route of 4-Ethynylphenol

The synthesis of 4-ethynyl phenol is demonstrated in Scheme 1. Phenol was subjected to an iodination reaction with the presence of *p*-toluenesulfonic acid (*p*-TsOH) and *N*-iodosuccinimide (NIS) to yield compound **2** in high yield (95 %). In the second step, the Sonogashira coupling reaction was performed in the presence of $Pd(PPh_3)_2Cl_2$ and CuI catalysts in triethylamine. This step led to the successful formation of compound **3** with almost quantitative yield. Evalation of different solvents for the Sonogashira reaction and results are presented in Table 1.

Table 1. Solvent time screening for Sonogashira reaction

Entry	Solvent	Time	Yield
1	**DMF**	**12 h**	**98 %**
2	**Triethylamine**	**3 h**	**99 %**
3	**THF**	**4 d**	**96 %**
4	**Toluene**	**1-2 d**	**96 %**

Based on the data presented in Table 1, it can be inferred that there is no statistically significant variation in the yields of compound **3** when different solvents are employed. Nevertheless, it should be noted that the reaction time for the Sonogashira coupling reaction varies drastically depending on the solvent used.

Two distinct pathways were explored to deprotect the silyl protecting group. The outcomes of both pathways were satisfactory in crude NMR; however, it is important to note that the compound's inherent nature made it prone to decomposition when exposed to air, heat, or the purification procedures such as column chromatography.

Due to the rapid decomposition of compound **4**, we decided to protect the free hydroxyl in compound **2** by using a para-methoxybenzyl (PMB) as a protecting group.

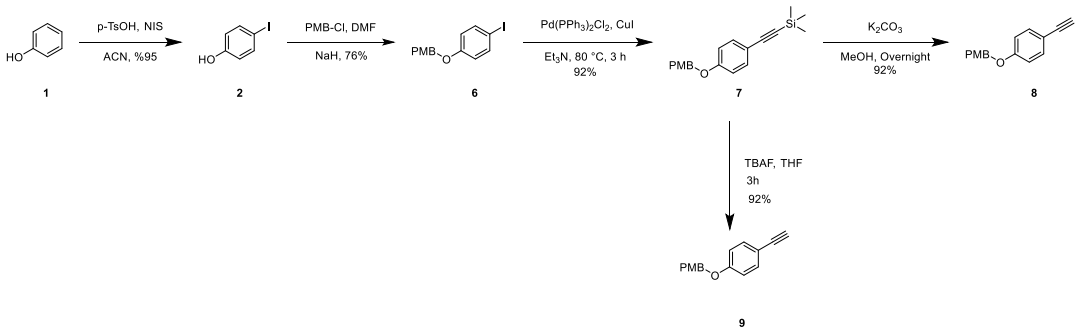

Scheme 2. Modified synthetic route for 4-ethynylphenol donor.

Following the iodination reaction of phenol, PMB protection was carried out in the presence of PMB-Cl and NaH in DMF, resulting in product **6** as a stable compound with 90% yield. The remaining reactions and conditions are identical to those in scheme 1.

2.2.2 Synthesis of 4-ethynylaniline

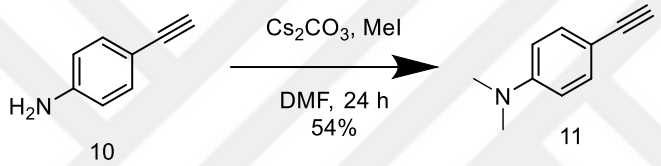

Scheme 3. Synthetic route for 4-ethynylaniline.

In order to obtain compound **11**, commercially available 4-ethynylaniline (**10**) was treated with cesium carbonate and methyl iodide in DMF for 24 hours. As a result of this reaction, 4-ethynyl-*N*, *N*-dimethylaniline (**11**) was obtained with a yield of 54%.

2.2.3 Synthesis of 4-vinyl phenol

The Wittig reaction has been widely recognized as one of the most effective methods for producing vinyl derivatives from aldehydes or ketones in the presence of phosphorus ylide. To synthesize 4-vinyl phenol, it was necessary first to synthesize the phosphorus ylide.

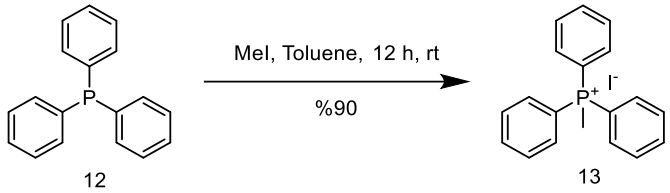

Scheme 4. Synthetic illustration of Wittig reagent.

The reaction between methyl iodide (MeI) and the commercially available triphenylphosphine (**12**) in toluene successfully yielded compound **13** (Scheme 4).

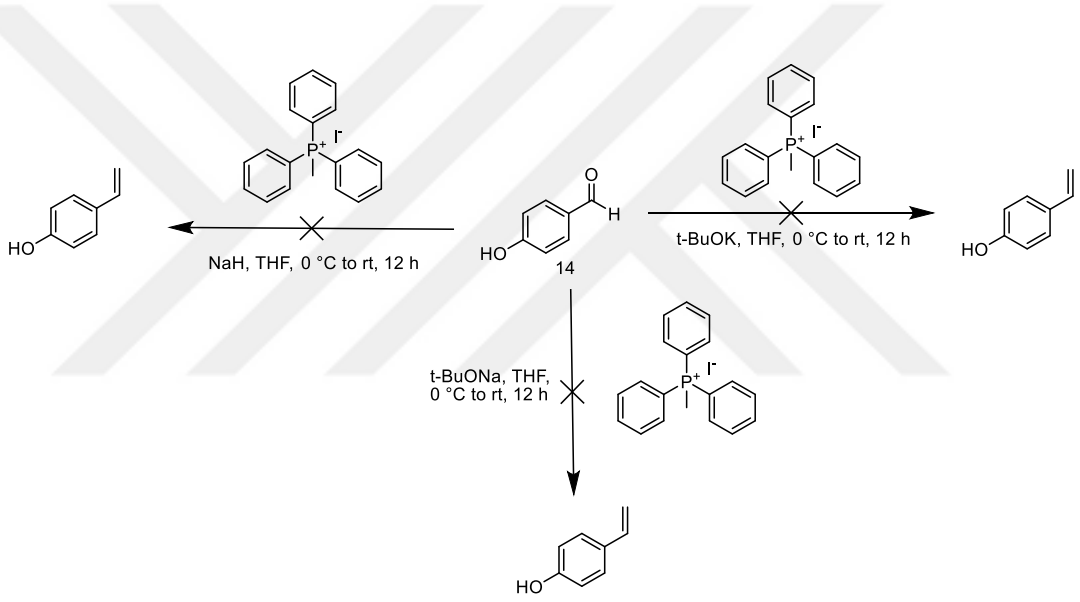

Scheme 5. Attempted Wittig reactions via different bases.

Several unsuccessful attempts to obtain 4-vinylphenol starting from compound **14** are shown in Scheme 5. The reaction of phosphorus reagents with some strong bases in scheme 5 typically leads to the formation of phosphorus ylides. However, when compound **13** was treated with sodium hydride (NaH), potassium *tert*-butoxide (*t*-BuOK), or sodium *tert*-butoxide (*t*-BuONa) in THF, the expected ylide formation reaction was not observed upon monitoring through thin-layer chromatography (TLC). It is important to note here that both the phosphonium salt and the base was used as 2 equivalents. After treating white compound **13** with the base, there was no

observable color change and changes in TLC proving no noticeable decomposition. Additionally, upon adding 4-hydroxybenzaldehyde (**14**) to the reaction mixture and allowing it to stir overnight, it was observed via TLC that compound **14** did not deplete, and as confirmed by nuclear magnetic resonance (NMR) reaction did not occur and starting material was recovered.

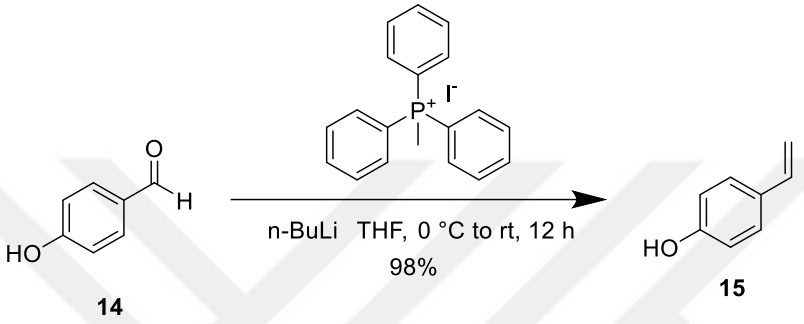

Scheme 6. Schematic illustration of successful attempt of Wittig reaction

A successful attempt has been made (Scheme 6) to synthesize 4-vinyl phenol (**15**) from compound **14** by changing the base to *n*-butyllithium (*n*-BuLi). The reason for the previous unsuccessful reactions was attributed to insufficient ylide formation.

2.2.4 Synthesis of N, N-dimethyl-4-vinylaniline

N, *N*-dimethyl-4-vinylaniline is analogous to compound **15**. This compound was synthesized following the same procedure as compound **15**. The starting material for the synthesis of *N*, *N*-dimethyl-4-vinylaniline was 4-(dimethylamino) benzaldehyde. (Scheme 7)

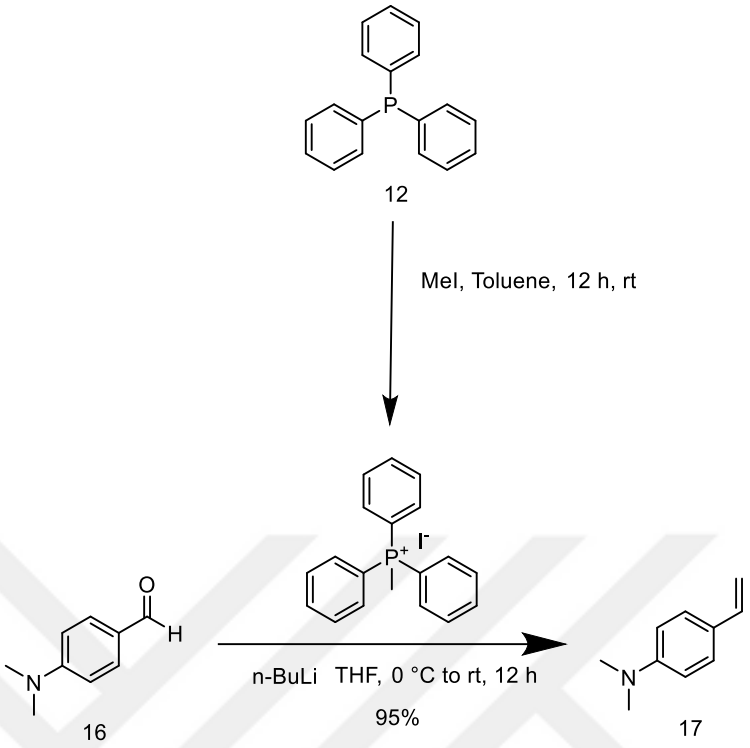

Scheme 7. Synthesis of Wittig reagent & Wittig reaction.

2.3 Synthesis of N-Se-Based Hybrid Xanthene Core

For the synthesis of the N-Se-based hybrid xanthene core (22), the initially intended synthetic pathway is shown in Scheme 8. Compound **18** is readily available and was used to introduce the selenium bridge to obtain compound **19**.

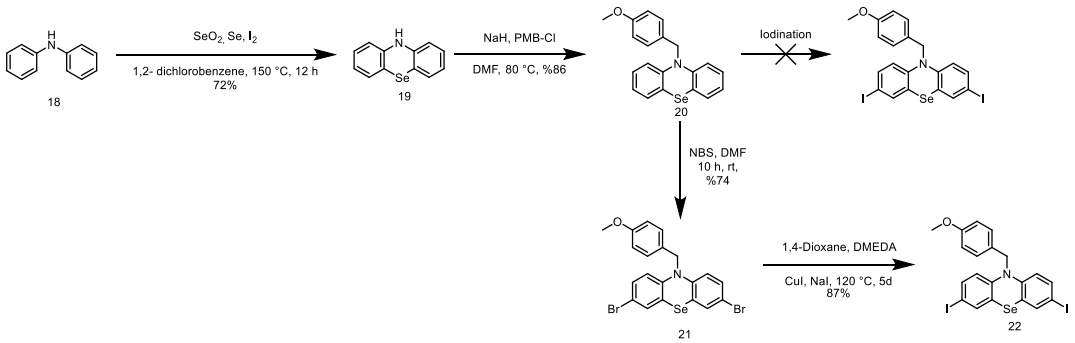

Scheme 8. Synthetic route for NSe-based xanthene core.

It is imperative to protect nitrogen to prevent potential interference from the free nitrogen present in compound **19** during subsequent coupling reactions aimed at combining the donor and core structures. PMB was chosen as the protective group due to its well-documented ease of removal for similar molecules in the literature. Additionally, PMB was selected to protect compound **2** to ensure global deprotection. Compound **20** was successfully attained using NaH and PMB-Cl in DMF starting from compound **19**.

It is important to note that the effectiness of the Sonogashira coupling reaction, which is used to combine donor molecules with the core structure, is influenced by the halogen atom attached to the aromatic ring. Specifically, the preference sequence is aryl iodide > aryl bromide >>> aryl chloride. Based on this, we preferred to incorporate iodine into our core structure. Unfortunately, as shown in Table 2, our attempts to use iodination methods to yield compound **20** have not produced conclusive results.

Table 2. Iodination attempts of xanthene core.

Entry	Source	Solvent	Additive
1	NIS	DMF (dry)	-
2	NIS	DCM	$AuCl_3$
3	NIS	MeOH	$AgSO_4$
4	I_2	EtOH	HIO_3

Following the unsuccessful attempts at iodination, a bromination reaction was achieved using NBS to yield compound **21**. The aromatic Finkelstein reaction was attempted next to get target product containing iodine atoms within the core structure (**22**). After several experiments, it was shown that the reaction did not occur in the Schlenk system. The synthesis of compound **22** could only be achieved under the conditions outlined in Scheme 8 with utilizing a sealed tube system.

2.4 Synthesis of NSe-AcetOH

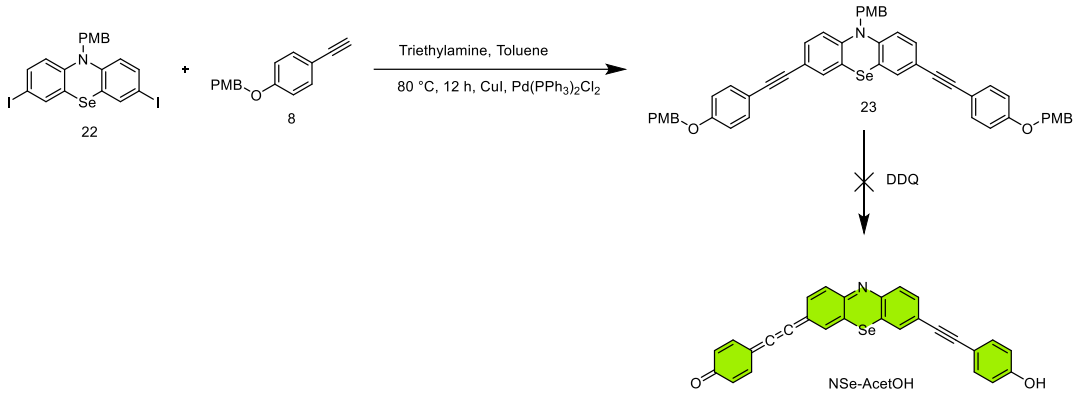

Scheme 9. Synthetic route for NSe-AcetO

As depicted in Scheme 9, a Sonogashira-type reaction was employed to obtain compound **23**. Monitoring the reaction via TLC was considerably challenging due to the proximity of spots, making it difficult to discern. Despite these challenges, after 12 hours, it was observed that nearly all of compound **22** had been consumed. However, employing column chromatography with various solvent systems did not yield compound **23**, resulting in isolation of mixtures. Attempts to reduce polarity led to solubility issues, preventing the isolation of compound **23** in its pure form. After numerous attempts, a decision was made to proceed to the oxidation step without employing any further purification method for compound **23**.

The partially purified compound **23** was treated with DDQ break the PMB groups and oxidize the molecule. Despite heating from room temperature to 80 ºC over 12 hours, the desired NSe-AcetO was not obtained. After considering the information, the protective group of Compound **8** was replaced with TBDMS (tert-butyldimethylsilane). This substitution was made because silyl ethers are easier to cleave than methoxybenzyl ethers. The purpose of this alteration was to address the isolation challenges experienced with compound **23**. By doing so, it's expected that the isolation of the final product (**28**) would be smoother.

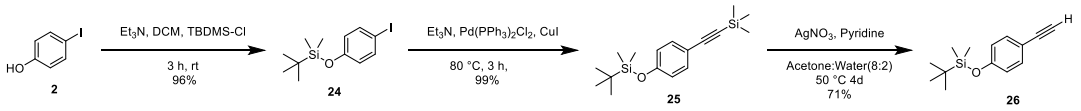

Scheme 10. Modified synthetic route for the donor.

Scheme 10 illustrates the modified synthesis pathway for our donor molecule. Compound **24** was obtained in notably high yield through the reaction of 4-iodophenol with Et_3N and TBDMS-Cl. The subsequent Sonogashira coupling reaction is similar to the one depicted in Scheme 2.

Ultimately, the selective removal of the TMS protecting group was carried out in the presence of the TBDMS protecting group to obtain compound **26**. During the deprotection reaction, reagents other than silver nitrate have proven ineffective. Despite its relatively high efficiency and robust performance, the reaction required approximately five days to complete, and no optimization attempts were fruitful for shorting the reaction time.

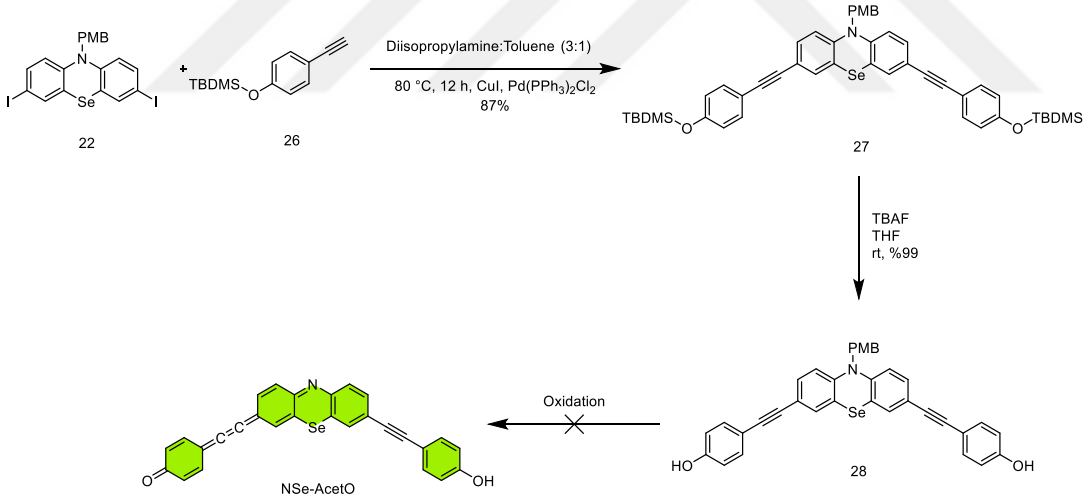

Scheme 11. Modified synthetic route for NSe-AcetO

Compound **27** was obtained by reacting TBDMS-protected donor molecule (**26**) with compound **22** via Sonogashira reaction. This synthesis avoided the solubility issues and isolation challenges encountered during the synthesis of compound **23**.

Simultaneously, optimization was achieved by substituting our base, initially triethylamine, with di-isopropylamine (DIPA), resulting in a cleaner reaction profile.

Subsequently, the TBDMS deprotection reaction was conducted within tetra-*n*-butylammonium fluoride (TBAF), demonstrating a notably high yield. The oxidation reactions performed to obtain our final product NSeAcetO (Scheme 12) have been illustrated in Table 3. The reason for attempting oxidation reactions without conducting PMB deprotection was due to the potential of PMB cleavage through an oxidative mechanism.

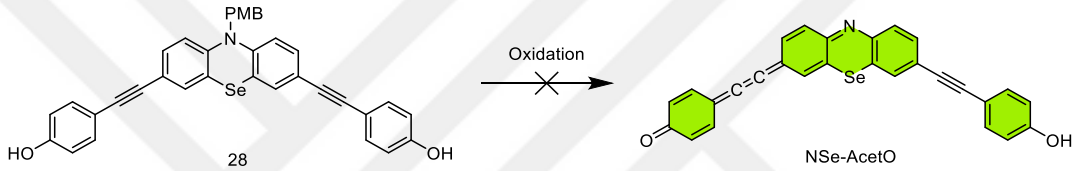

Scheme 12. Oxidation attempt of compound 28.

Table 3. Oxidation reagents and solvents

Entry	Source	Solvent
1	DDQ	Toluene
2	I_2	MeOH
3	DDQ	DCM
4	p-chloranil	DCM
5	Ag_2O	Acetone
6	Ag_2O	DMSO

All attempts to oxidize compound **28**, shown in Table 3, has failed. Numerous trials monitored by TLC have shown that the starting material is not consumed, and no

noticeable spot formed that would indicate the product. While changing the reaction time did not result in any changes in the course, temperature differences led to the degradation of compound **28**. During the oxidation experiment with DDQ in DCM, it was observed that compound **28** rapidly reacted and was consumed. However, the resulting product did not correspond to the desired NSe-AcetO.

The rapid progression of the reaction, despite attempts to slow it down by lowering the reaction temperature to 0 °C, did not result in NSe-AcetO. The presence of the PMB protecting group on nitrogen, complicating the oxidation, prompted trials involving PMB cleavage reactions. Nevertheless, these attempts did not yield satisfactory results. Consequently, to overcome these challenges, a decision was made to alter the synthesis route by replacing the PMB protecting group, essential to the core structure, with the *tert*-butyloxycarbonyl (Boc) protecting group. The new synthetic pathway of the core structure protected with Boc is illustrated in Scheme 14.

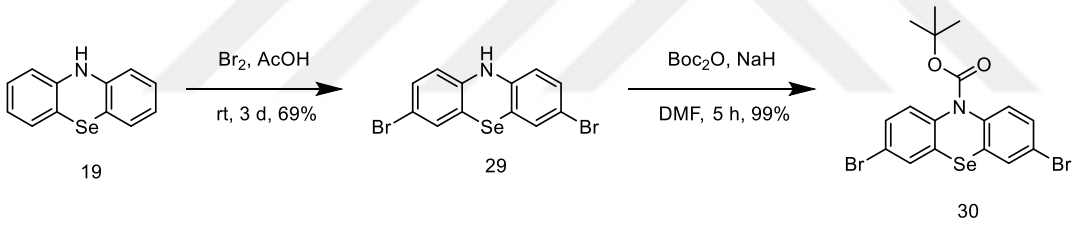

Scheme 13. Modified synthetic route for NSe-based core structure.

In contrast to the previous PMB protection reaction (see Scheme 8), compound 30 was obtained by first brominating compound **19** and then performing the protection reaction. The reason for swapping the positions of the protection and bromination reactions lies in the behavior observed after protecting compound **19** with Boc. The Boc group withdraw electron density through resonance from the nitrogen atom thus reducing its donating ability and hinders electrophilic aromatic substitution.

Contrary to what is stated in the literature, the bromination reaction does not take 8 hours but three days (Scheme 14). The starting material **19** and its mono-brominated

derivative are expected to be fully converted into compound **29**, which requires the continuous addition of bromine. Without the continuous addition of bromine, purification by chromatographic methods is impossible due to the very similar polarities of the mono-brominated, di-brominated species and the starting material.

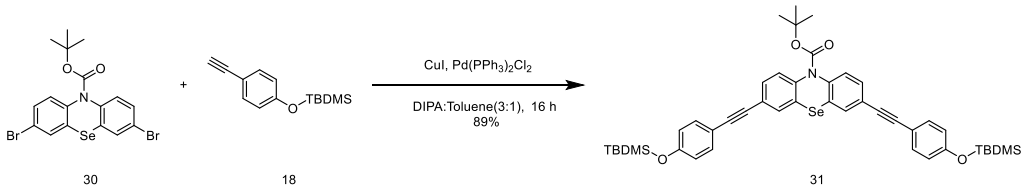

Scheme 14. Sonogashira coupling reaction

Compound **31** was obtained via the Sonogashira coupling reaction, with a high yield. Despite employing identical conditions as the Sonogashira reaction depicted in Scheme 11, the yield of the Sonogashira reaction of compound **31** (Scheme 15) exhibited a slightly reduced yield. This decline in yield was attributed to the fact that compound **30** containing bromine as a halogen substituent. The synthetic pathway, successfully achieving the cleavage of Boc and TBDMS protecting groups, is illustrated in Scheme 16.

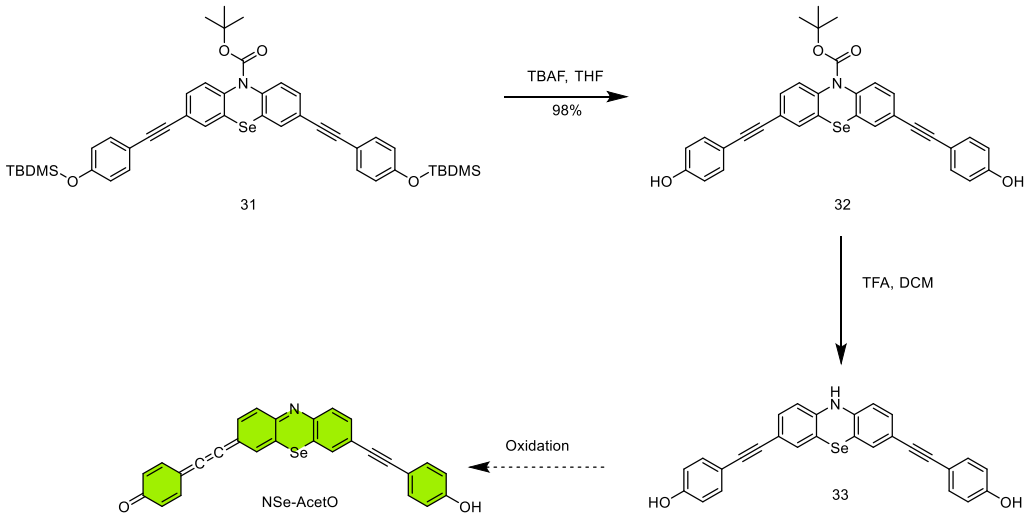

Scheme 15. Modified synthetic route for NSe-AcetO

To obtain Compound **33**, a sequential process involving TBDMS deprotection using TBAF followed by Boc group cleavage using TFA was conducted (Scheme 16). The reason for this specific sequence was that performing Boc deprotection initially resulted in the rapid degradation of the product when exposed to air.

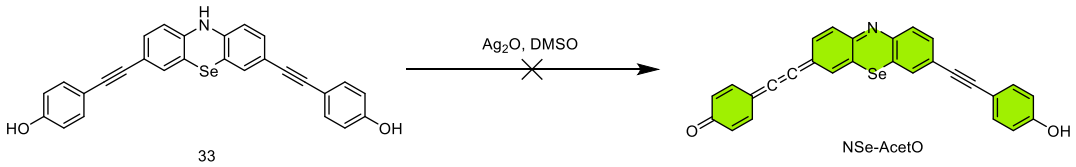

Scheme 16. Oxidation attempt of compound 33.

The oxidation experiment (Scheme 17) was monitored by NMR in DMSO-d6 and unfortunately proved unsuccessful. Despite the gradual increase in temperature, the addition of reagents and extended duration did not yield NSe-AcetO.

2.5 Synthesis of NSe-AcetN

The syntheses of NSe-AcetN and NSe-AcetO, which are analogs of each other, were carried out simultaneously due to their similar reaction pathways.

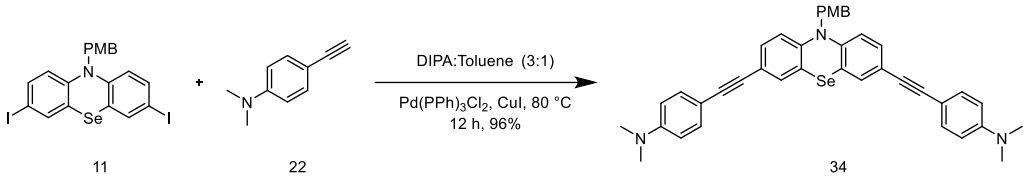

Scheme 17. Synthesis of Compound 34 via Sonogashira reaction

The synthesis of Compound **34** involved utilizing the Sonogashira coupling reaction (Scheme 18). Subsequently, compound **34** was utilized in similar oxidation reactions as compound **28** (refer to Table 3).

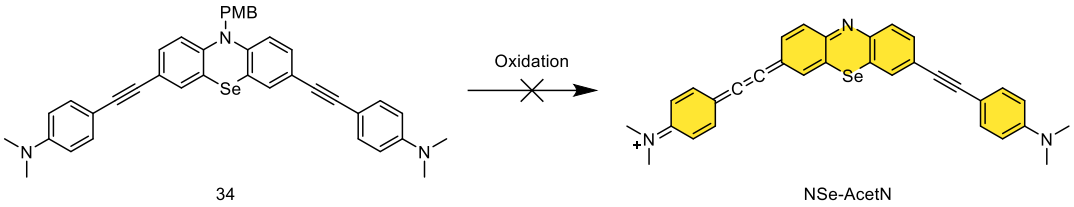

Scheme 18. Schematic illustration of oxidation reaction

Table 4. Oxidation reagents and solvents

Entry	Reagent	Solvent
1	I_2	MeOH
2	DDQ	DCM
3	p-chloranil	DCM
4	Ag_2O	Acetone
5	Ag_2O	DMSO

Despite attempt with different reagents, reactions times and temperatures during the oxidation attempts detailed in Table 4, the NSe-AcetN synthesis was unsuccessful. In each oxidation reaction, either the starting material recovered or its degradation resulted in the formation of complex mixtures.

As illustrated in Scheme 14, a Boc modification was applied to our core structure, compound **30**, and the coupling reaction was performed, yielding compound 35 with high efficiency (Scheme 20). Subsequently, Boc deprotection was carried out using TFA, successfully acquiring compound **36** (Scheme 20).

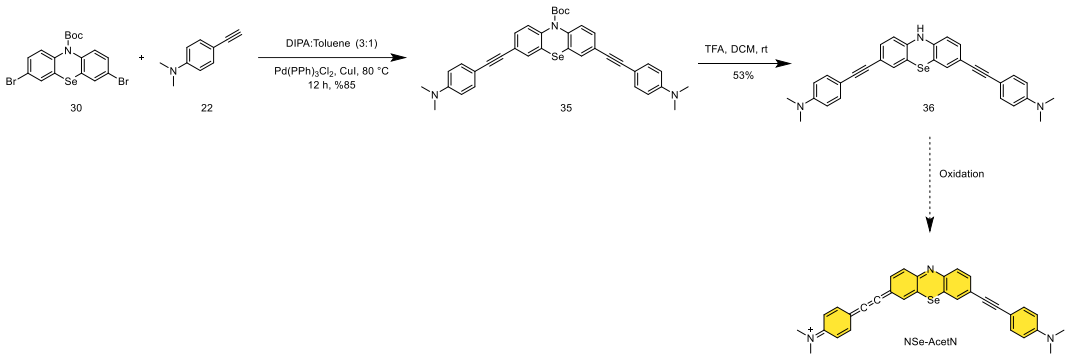

Scheme 19. Modified synthetic pathway for NSe-AcetN

The main problem is that compound **36**, obtained after extraction and column chromatography, lacks a protecting group for its bridging nitrogen, leading to rapid degradation in the presence of moisture/air. We attempted to oxidize compound **36** in DMSO to obtain our final product, the NSe-AcetN molecule (as illustrated in Scheme 21).

Unfortunately, this attempt proved unsuccessful. Despite alterations in the quantities of reagents and temperature adjustments during the reaction, the outcome consistently resulted in the retrieval of the starting material, compound **36**, as confirmed by TLC and NMR analyses.

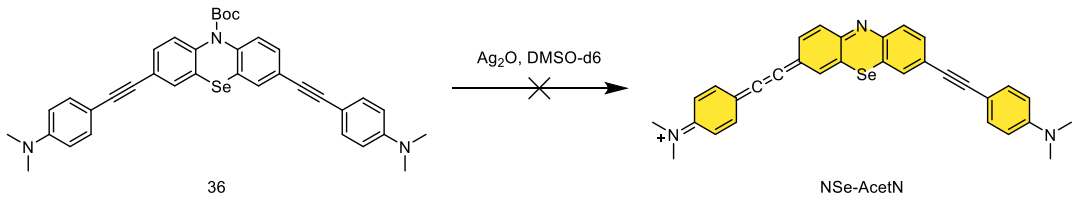

Scheme 20. Oxidation attempt by silver (I) oxide

As a future work several other oxidation methodologies with be implemented towards the synthesis of NSe-AcetN. Upon successful synthesis its photophysical properties and potential as a PDT agent will be evaluated.

2.6 Synthesis of NSe-StyN

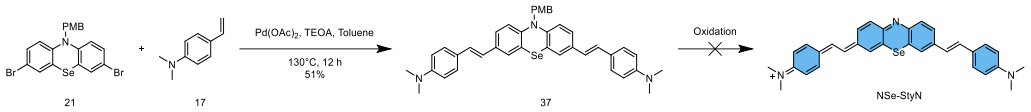

Scheme 21. Synthetic route for NSe-StyN

The attempted adaptation of Heck coupling reactions for similar transformations from the literature (Scheme 23) did not yield the target compound **37**. Complex reaction mixtures formed in all four different procedures, and compound **37** could not be obtained.

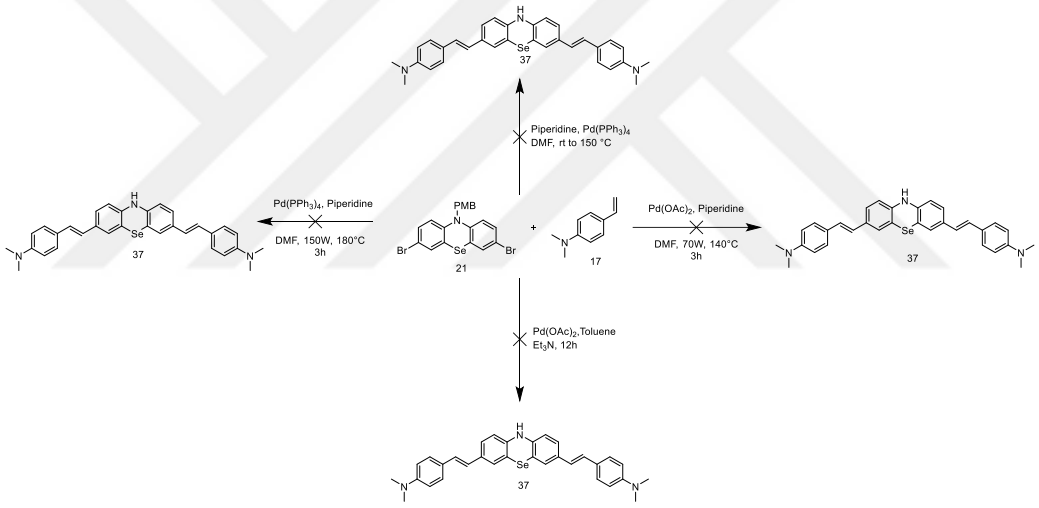

Scheme 22. Attempted Heck coupling reactions

As a result of replacing the base with triethanolamine (TEOA), compound **37** was obtained with a yield of 51% (Scheme 23). The reagents and conditions utilized for the oxidation of compound **37** were similar as those used in the oxidation of compound **34** (see Table 4).

Attempts to obtain the NSe-StyN molecule via oxidation were unsuccessful, resulting in the degradation of the starting material and the formation of complex reaction mixtures. Consequently, an alternative reaction pathway involving the

substitution of the protecting group with Boc is illustrated in Scheme 24.

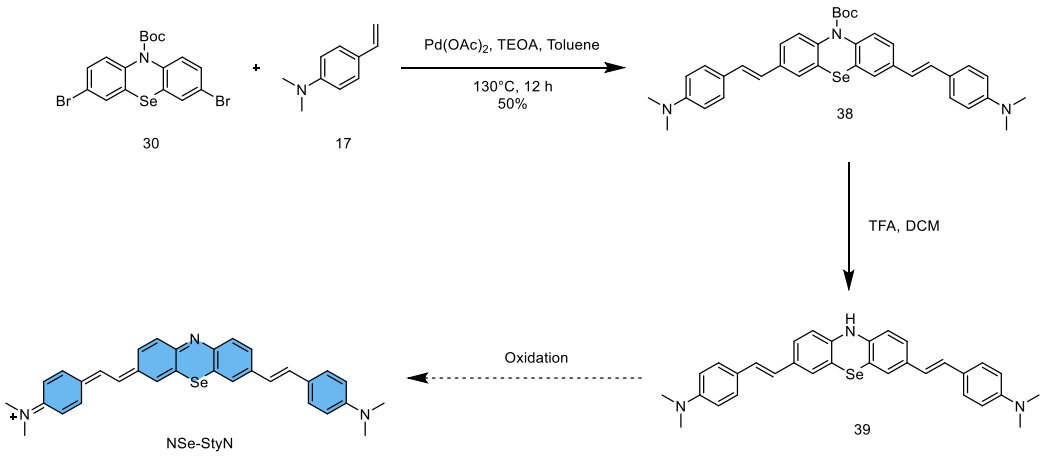

Scheme 23. Modified synthetic route of NSe-StyN

Compound 38 was obtained through Heck coupling, followed by a Boc deprotection reaction using TFA (Scheme 24), forming a blue-colored product. We presume that this product, rather than compound **39**, is a more stable form, the oxidized version of NSe-StyN. Although confirmation studies using NMR did not yield conclusive results, promising outcomes were observed through analyses conducted via HPLC.

Subsequent investigations will involve the isolation of the NSe-StyN molecule, which will be pursued, and its photophysical properties will be examined. Additionally, it will be tested as a potential photodynamic therapy (PDT) agent in various cancer cell lines.

2.7 Synthesis of NSe-StyO

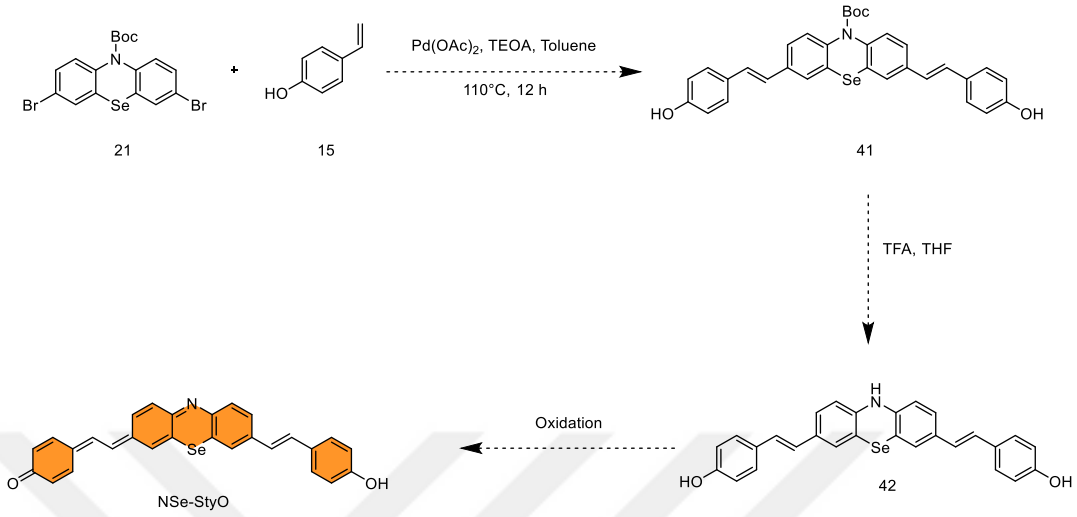

Scheme 24. Synthetic route of NSe-StyO

The molecule NSe-StyO is an analog of the molecule NSe-StyN; hence, the synthesis scheme for the molecule NSe-StyN is identical. However, the compound **41** obtained after the Heck reaction could not be completely isolated due to its possession of two hydroxyl groups, making the isolation process challenging.

As a future work, to isolate compound **41**, a Biotage Isolera flash column will be employed. In the event of incomplete isolation of the product, the reaction will proceed to the next step of cleaving the Boc protecting group with TFA from the crude material to obtain compound **42**. An attempt will be made to isolate compound **42** by taking advantage of its high polarity. Subsequently, utilizing the oxidation agents previously employed, as seen in Table (4), compound **42** will undergo oxidation to yield N-StyO. Furthermore, cell culture trials will be conducted to evaluate its potential as a photosensitizer (PS).

CHAPTER 3

CONCLUSIONS

The pursuit of synthesizing photosensitizers that can be activated by near-infrared (NIR) light beyond 700 nm has been a fascinating and ambitious research endeavor. Though the synthesis of the intended molecules is still in progress, the methodology and initial stages of the synthesis have shown promising potential in the search for effective photosensitizers. The careful planning and theoretical framework used to design these molecules to use NIR light's more extended wavelength range provide a solid foundation for future work in this field. Incorporating extended conjugation into the molecular structure is expected to enhance the absorption properties and ultimately increase the photoactivation capabilities of the synthesized molecules in the desired near-infrared (NIR) spectrum.

In this study four different target molecules with enhenced conjugation, have been identified. The donor and core segments of the targeted molecules were successfully synthesized, and Sonogashira and Heck coupling technologies were employed to bring these two segments together. The challenges encountered during the synthesis stages have provided valuable learning opportunities for incorporating extended conjugation into molecular structures. These challenges have led to refining synthetic methodologies and optimizing synthetic routes.

Despite significant progress in the synthesis of these four different N-Se-based hybrid xanthene cores, our main challenge has arisen during the oxidation step, where achieving conjugation across the entire molecule. The difficulty in the oxidation of molecules containing a triple bond, such as N-AcetO and N-AcetN, is believed to be attributed to the high energy demand associated with the rotation barrier during allene/cumulene formation. In the case of containing a double bond, the N-StyN molecule, the primary issue encountered is chemical oxidation, and it is

hypothesized that employing different oxidation agents could lead to the successful synthesis of the target molecule. For the N-StyO derivative, a more thorough assessment can be conducted after the necessary purification processes are completed. In conclusion, the incorporation of extended conjugation into the molecular design of the targeted photosensitizers responsive to NIR light beyond 700 nm is a promising and novel strategy, even if the synthesis process is yet to be completed. It is anticipated that ongoing synthesis efforts will clarify the full potential and implications of extended conjugation in enhancing the effectiveness and applications of these photosensitizer molecules in photodynamic therapy and related fields.

CHAPTER 4

EXPERIMENTAL

4.1 General Information

The ^{1}H and ^{13}C-NMR spectra were meticulously recorded in the spectroscopic analysis using a Bruker Avance III Ultrashield spectrometer operating at 400 MHz. The chemical shifts, referenced against TMS (tetramethylsilane), were noted in parts per million (ppm). J-coupling constants were detailed in hertz (Hz), and the signal multiplicities were indicated by standard symbols: s (singlet), d (doublet), t (triplet), and m (multiplet). MestReNova software facilitated the processing of NMR spectra for precise interpretation. Column chromatography procedures were conducted using robust glass columns packed with silica Gel 60 (Merck 230-400 mesh). Thin-layer chromatography (TLC) involved utilizing 0.25 mm silica gel plates (Merck Silica Gel 60 F254), and visualization was accomplished using a UV lamp for accurate compound detection. All chemicals and reagents were procured commercially and used without additional purification unless specified. Dry solvents utilized in reactions were acquired directly from the Mbraun MBSPS5 solvent drying system to ensure high purity. Argon gas was employed to maintain an inert atmosphere during experiments.

4.2 Synthesis of Donors

4.2.1 Synthesis of 4-iodophenol

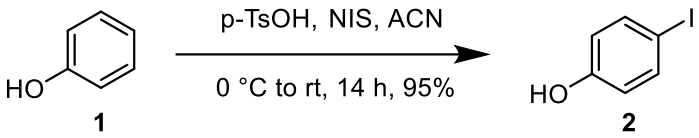

Scheme 25. Synthesis of Compound 2

Phenol (500 mg, 5.31 mmol) was dissolved in 50 mL dry acetonitrile in a 100 mL Schlenk tube under an argon atmosphere and cooled to 0 °C. *p*-TsOH (914.85 mg, 5.31 mmol) was added to the solution and stirred for 30 minutes. NIS (1.20 g, 5.31 mmol) added solution in one portion and the resulting mixture was warmed to room temperature and stirred for 14 hours. The reaction was monitored by GC-MS, and product composition was determined by GC/MS. After completion of the reaction, the resulting mixture was extracted with 3x50 mL ethyl acetate. The organic layer was dried over anhydrous Na_2SO_4 and the solvent was evaporated under reduced pressure. The crude product was purified by column chromatography on silica gel with Hexane: DCM (2:0.2) system yielding the product reddish white powder (95%): ^{1}H NMR (400 MHz, Chloroform-d) δ 7.44 (d, *J* = 8.8 Hz, 2H), 6.55 (d, *J* = 8.9 Hz, 2H), 4.95 (s, 1H). ^{13}C NMR (100 MHz, MeOD) δ 158.6, 139.3, 118.8, 81.3.

4.2.2 Synthesis of 4-((trimethylsilyl)ethynyl)phenol

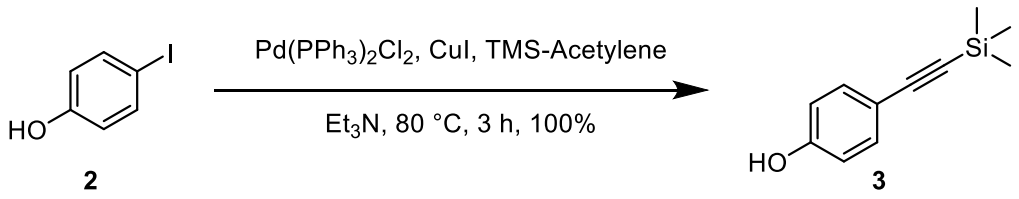

Scheme 26. Synthesis of Compound 3

A solution of 4-iodophenol (102 mg, 0.46 mmol), $Pd(PPh_3)_2Cl_2$, (9.7 mg, 0.014 mmol) and CuI (3 mg, 0.01 mmol) in Et_3N (3mL) was degassed for 30 minutes. Ethynyltrimethylsilane (0.0950 mL, 0.67 mmol) was added, and the reaction mixture was refluxed at 80 °C for three hours under an argon atmosphere. Reaction monitored with GC/MS. Upon completion, the mixtures was filtered through a pad of celite and the solvent was removed under reduced pressure. The residue was purified by column chromatography on silica gel with Hexane: EtOAc (2:0.1) yielding the product as yellow viscous oil (99%): ^{1}H NMR (400 MHz, $CDCl_3$): δ 7.36 (d, *J* = 8.8 Hz, 2H), 6.75 (d, *J* = 8.8 Hz, 2H), 5.02 (brs, 1H), 0.23 (s, 9H); MS (m/z): [M - H]- 189.2 (100%).

4.2.3 Synthesis of 1-iodo-4-((4-methoxybenzyl)oxy)benzene

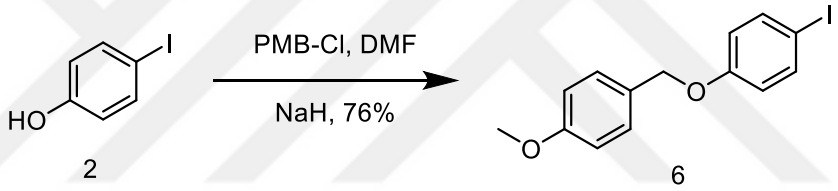

Scheme 27. Synthesis of Compound 6

To a solution of 4-iodophenol (600 mg 2.73 mmol) in 10 mL DMF, NaH (218 mg, 5.45 mmol) was added under an argon atmosphere and the mixture was stirred for one hour at rt. PMB-Cl (0.736 mL, 5.45 mmol) was added dropwise, and the reaction mixture was heated to 80 °C and stirred overnight. The resulting mixture was poured into cold water, extracted with 3x30 mL Et_2O, dried over $MgSO_4$, and concentrated in vacuo. The crude product was purified by column chromatography on silica gel using Hexane: DCM (20:5) to yield the target product as a white solid (76%): ^{1}H NMR (400 MHz, $CDCl_3$) δ 7.46 (d, *J* = 9.0 Hz, 2H), 7.25 (d, *J* = 8.6 Hz, 2H), 6.83 (d, *J* = 8.7 Hz, 2H), 6.66 (d, *J* = 8.9 Hz, 2H), 4.86 (s, 2H), 3.73 (s, 3H). ^{13}C NMR (100 MHz, $CDCl_3$) δ154.2, 152.7, 137.6, 137.1, 129.2, 115.9, 114.7, 93.3, 70.1, 55.7.

4.2.4 Synthesis of((4-((4-ethoxybenzyl)oxy)phenyl)ethynyl)trimethylsilane

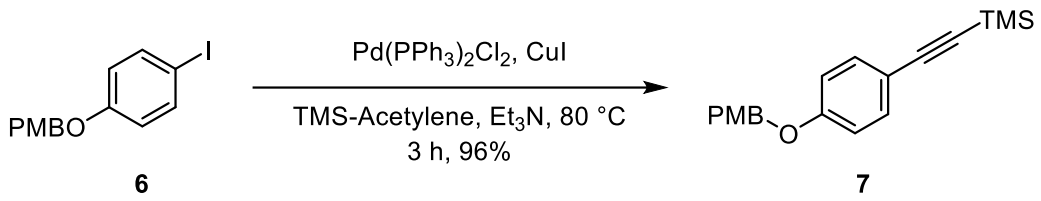

Scheme 28. Synthesis of Compound 7

Compound 6 (280 mg, 823 µmole) dissolved in Et_3N (5 mL), and toluene (2 mL) was added to the solution to increase the solubility of compound 6. To a solution of compound 6, $Pd(PPh_3)_2Cl_2$ (32 mg, 65.85 µmol) and CuI (9.41 mg, 49 µmol) were added and degassed for 30 min. TMS-acetylene (128 µL, 905µmol) was added to the reaction mixture and refluxed for three hours. The mixture was filtered through a thin celite pad, and the solvent evaporated under reduced pressure. Crude product was purified by column chromatography on silica gel Hexane: EtOAc (10:1) yielding the product as yellow solid (92%): ^{1}H NMR (400 MHz,) δ 7.44 (d, *J* = 8.7 Hz, 2H), 7.38 (d, *J* = 8.5 Hz, 2H), δ 7.00 – 6.89 (m, 4H), 5.00 (s, 2H), 3.85 (s, 3H), 0.28 (s, 9H). ^{13}C NMR (100 MHz, $CDCl_3$) δ 159.5, 158.8, 133.4, 129.3, 128.4, 115.3, 114.6, 113.9, 105.1, 92.5, 69.6, 55.2, 0.06.

4.2.5 Synthesis of 1-ethynyl-4-((4-methoxybenzyl)oxy)benzene

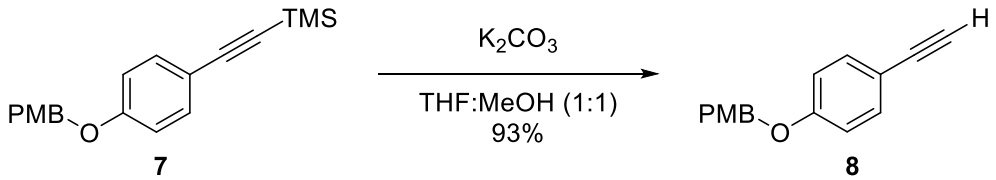

Scheme 29. Synthesis of Compound 8

To solution of compound 7 (323 mg, 1.02 mmol) in THF: MeOH (5:5 mL) K_2CO_3 (575 mg, 4.16 mmol) was added in one portion. The reaction was stirred for 3 hours,

the crude product was filtered and extracted with DCM 3x30 mL. Organic layers were combined and dried over Na_2SO_4 afterwards concentrated in vacuo. The residue was purified by column chromatography on neutral alumina Hexane: DCM (10:1) yielding the compound **8** as white solid (93%): ^{1}H NMR (400 MHz,) δ 7.47 (d, *J* = 8.3 Hz, 2H), 7.38 (d, *J* = 8.4 Hz, 2H), 6.98 – 6.92 (m, 4H), 5.02 (s, 2H), 3.85 (s, 3H), 3.05 (s, 1H). ^{13}C NMR (100 MHz, $CDCl_3$) δ 159.4, 159.1, 138.1, 133.5, 129.2, 128.3, 114.7, 113.9, 83.6, 75.8, 69.7, 55.2.

4.2.6 Synthesis of tert-butyl(4-iodophenoxy)dimethylsilane

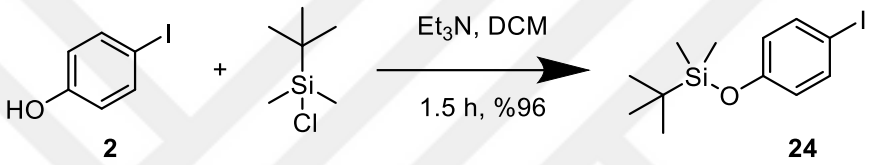

Scheme 30. Synthesis of Compound 24

A mixture of 4-iodophenol (3 g, 13.64 mmol), TBS-Cl (2.47 g, 16.36 mmol), and Et_3N (2.85 mL, 20.45 mmol) in 5 mL DCM was stirred for 1.5 h at room temperature. The reaction mixture was extracted 3x50 mL EtOAc, and the organic layer was dried over Na_2SO_4 and concentrated in vacuo. Crude product purified by column chromatography on silica gel with n-hexane yielding compound **24** as yellow oil (96%): ^{1}H NMR (400 MHz,) δ 7.32 (d, *J* = 8.8 Hz, 2H), 6.43 (d, *J* = 8.8 Hz, 2H), 0.79 (s, 9H), 0.00 (s, 6H). ^{13}C NMR (100 MHz, Chloroform-d) δ 155.0, 138.8, 122.5, 85.1, 25.6, 18.10, -4.5.

4.2.7 Synthesis of tert-butyldimethyl(4-((trimethylsilyl)ethynyl)phenoxy)silane

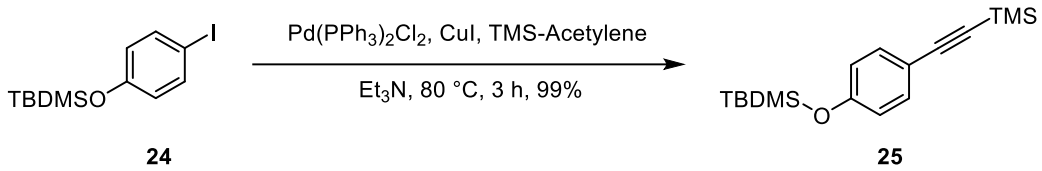

Scheme 31. Synthesis of Compound 25

The solution of compound **24** (320 mg, 957 µmole), $Pd(PPh_3)_2Cl_2$ (27 mg, 37 µmol) and CuI (15 mg, 76 µmol) in Et_3N was degassed by 30 min. After the addition of TMS-Acetylene (190 µL, 1.34 mmol), the reaction mixture was refluxed at 80 °C for three hours and monitored with GC/MS. The crude product was cooled to room temperature, filtered through a thin pad of celite, and concentrated under reduced pressure. The reaction mixture was purified by column chromatography on silica gel Hexane: EtOAc (10:1) yielding the product **25** as a yellowish oil (99%): ^{1}H NMR (400 MHz, Chloroform-d) δ 7.17 (d, *J* = 8.5 Hz, 2H), 6.57 (d, *J* = 8.5 Hz, 2H), 0.78 (s, 9H), 0.05 (s, 9H), 0.00 (s, 6H). ^{13}C NMR (100 MHz, $CDCl_3$) δ 155.9, 133.3, 119.9, 115.8, 105.1, 92.4, 25.5, 18.1, -0.0, -0.6.

4.2.8 Synthesis of tert-butyl(4-ethynylphenoxy)dimethylsilane

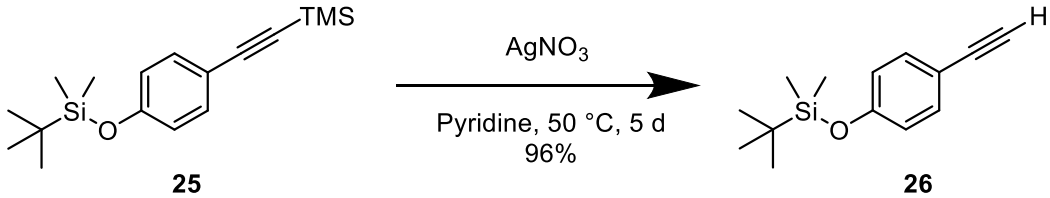

Scheme 32. Synthesis of Compound 26

Compound **25** (465 mg, 1.50 mmol) was dissolved in 2 mL acetone under Argon atmosphere, pyridine (37 µL 450 µmol), and solution of $AgNO_3$ (25 mg, 149.0 µmol) in 8 mL water was added and reaction mixture was heated up to 50 °C and stirred 12 h. After 48 hours, $AgNO_3$ (25 mg) was added and stirred 40 hours more. On the 4th

day TLC indicated that compound **25** was consumed, and the reaction mixture was cooled down to room temperature, filtered through a thin pad of celite, and concentrated in vacuo. The crude product purified by column chromatography on silica gel with Hexane: EtOAc (10:1) yielding the **26** as colorless oil (96%): ^{1}H NMR ($CDCl_3$, 400 MHz): δ = 7.4 (d, *J* = 8.6 Hz, 2 H), 6.8 (d, *J* = 8.7 Hz, 2 H), 3.0 (s, 1 H), 1.0 (s, 9 H), 0.2 (s, 6 H). ^{13}C NMR ($CDCl_3$, 100 MHz): δ = 156.3, 133.6, 127.1, 120.2, 114.8, 83.7, 75.9, 25.6, 18.2, –4.4.

4.2.9 Synthesis of 4-ethynyl-N,N-dimethylaniline

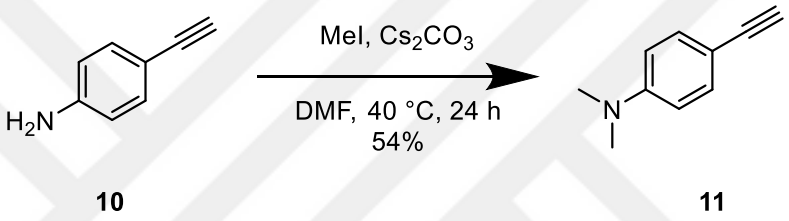

Scheme 33. Synthesis of Compound 11

To a 20 mL Schlenk tube, compound **10** (500 mg, 4.27 mmol) was added and dissolved in 5 mL DMF. Cs_2CO_3 (4.17 g, 12.80 mmol) and MeI (797 µL, 12.80 mmol) were added, and the reaction mixture was heated to 40 °C and stirred 24 h under argon atmosphere. Upon completion, the mixture was cooled down to room temperature and diluted with EtOAc. The organic layer was washed with water 3x50 mL and brine 3x50 mL and dried over anhydrous Na_2SO_4. The organic layer concentrated under reduced pressure and crude product was purified by column chromatography on silica gel hexane: EtOAc (98:2) solvent system yielding the **11** as yellow solid (54%): ^{1}H NMR (400 MHz, Chloroform-d) *δ* 7.37 (d, *J* = 8.9 Hz, 2H), 6.62 (d, *J* = 8.9 Hz, 2H), 2.98 (s, 7H). ^{13}C NMR (100 MHz, $CDCl_3$) δ 150.4, 133.2, 111.7, 108.7, 84.8, 74.8, 40.2.

4.2.10 Synthesis of 4-vinylphenol

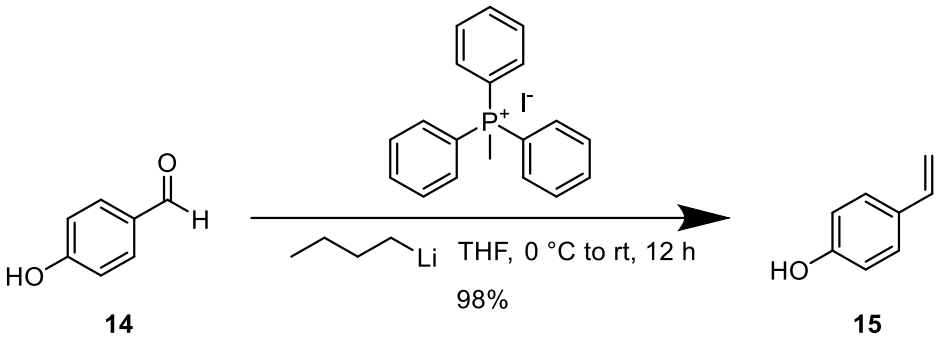

Scheme 34. Synthesis of compound 15

To 100 mL flame dried Schlenk tube vacuum argon cycle applied. Then, methyltriphenylphosphonium iodide (9.93 g, 24.57 mmol) was added to the Schlenk tube and vacuum argon cycle was repeated. 30 mL dry THF was added and cooled down to 0°C. n-BuLi (2.50 M in hexanes, 9.83 mL, 24.57 mmol) was added dropwise and the mixture was stirred for 30 minutes until it became a clear solution. In another flame-dried 20 mL Schlenk tube, compound **14** (1.5 g, 12.28 mmol) was dissolved in 10 mL dry THF. The solution of compound **14** was added dropwise to the above solution of methyl triphenylphosphonium iodide and stirred overnight at room temperature. The reaction was monitored by TLC after 12h, and the resulting solution was quenched with sat. Aq. NH_4Cl. The aqueous layer was extracted with EtOAc (3x50 mL), dried over Na_2SO_4, and concentrated in vacuo. The residue was purified by column chromatography on silica gel Hexane: EtOAc (80:20) solvent system yielding the **15** (98%): ^{1}H NMR (400 MHz, Chloroform-d) δ 7.23 (d, *J* = 8.2 Hz, 2H), 6.72 (d, *J* = 8.2 Hz, 2H), 6.57 (dd, *J* = 17.5, 11.0 Hz, 1H), 5.53 (d, *J* = 17.5 Hz, 1H), 5.29 (s, 1H), 5.05 (d, *J* = 10.8 Hz, 1H). ^{13}C NMR (100 MHz, $CDCl_3$) δ 153.9, 134.6, 129.0, 126.1, 113.8, 110.1.

4.2.11 Synthesis of N, N-dimethyl-4-vinylaniline

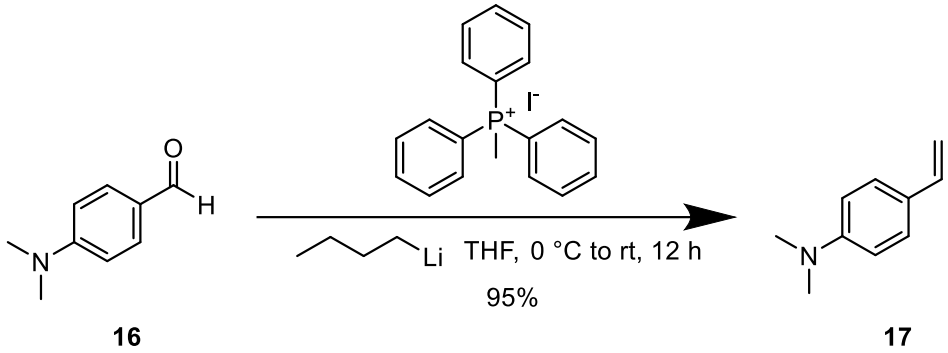

Scheme 35. Synthesis of compound 17

To 100 mL flame dried Schlenk tube vacuum argon cycle applied. Then, methyltriphenylphosphonium iodide (4.88 g, 12.06 mmol) was added to the Schlenk tube and vacuum argon cycle was repeated. 20 mL dry THF was added and cooled to 0°C. n-BuLi (2.50 M in hexanes, 4.83 mL, 12.06 mmol) was added dropwise and the reaction mixture was stirred for 30 min until it became a clear solution. In another flame-dried 20mL Schlenk tube, compound **16** (1.5 g, 10.05 mmol) was dissolved in 10 mL dry THF. Solution of compound **16** was added dropwise to the above solution of methyl triphenylphosphonium iodide and the mixture was stirred overnight at room temperature. The reaction was monitored by TLC after 12h, and the resulting solution was quenched with sat. Aq. NH_4Cl. The aqueous layer was extracted with EtOAc (3x50 mL), dried over Na_2SO_4, and concentrated in vacuo. The residue was purified by column chromatography on neutral alumina Hexane: EtOAc (96:4) solvent system yielding the **17** as yellow liquid (95%): ^{1}H NMR (400 MHz, Chloroform-d) δ 7.35 (d, *J* = 8.8 Hz, 2H), 6.72 (d, *J* = 8.7, 3.3 Hz, 2H), 6.69 – 6.58 (dd, 1H), 5.58 (d, *J* = 17.6 Hz, 1H), 5.06 (d, *J* = 10.9 Hz, 1H), 2.99 (s, *J* = 3.3 Hz, 6H). ^{13}C-NMR (100 MHz, $CDCl_3$): δ 150.3, 136.7, 127.3, 126.3, 112.5, 109.5, 40.7.

4.3 Synthesis of Hybrid Xanthene Core

4.3.1 Synthesis of 10H-phenoselenazine

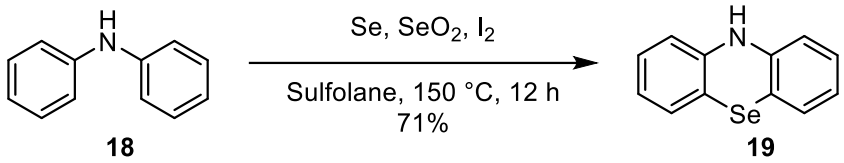

Scheme 36. Synthesis of Compound 19

Diphenylamine was added to a 50 mL Schlenk tube (4.323 g, 25.58 mmol) and dissolved in 5 mL sulfolane. Then selenium powder (1 g, 12.79 mmol), Se_2O (1.704 g, 15.35 mmol), and I_2 (165.2 mg, 1.22 mmol) was added. The reaction mixture was heated to 150 °C and stirred overnight under the argon atmosphere. After 12 h, the solution was filtered through a thin pad of celite and concentrated in vacuo. The crude product purified by column chromatography on silica gel Hexane: EtOAc (10:2) solvent system yielding the **19** as grey solid (71%): ^{1}H NMR (400 MHz, DMSO-d6) δ 8.62 (s, 1H), 7.09 (dd, *J* = 7.5, 1.5 Hz, 2H), 7.03 (td, *J* = 7.7, 1.5 Hz, 2H), 6.82 – 6.73 (m, 4H). ^{13}C-NMR (100 MHz, DMSO-d6): δ 142.2, 128.9, 127.9, 122.2, 115.2, 111.6.

4.3.2 Synthesis of 10-(4-methoxybenzyl)-10H-phenoselenazine

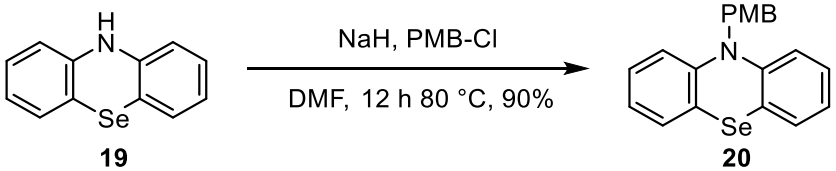

Scheme 37. Synthesis of Compound 20

To a 50 mL Schlenk tube, **19** (650 mg, 2.64 mmol) was added, vacuum argon cycle was applied and solid substance was dissolved in 10 mL dry DMF. NaH (211 mg, 5.28 mmol) was added and solution was stirred for 30 minutes at room temperature.

PMB-Cl (0.713 mL, 5.28 mmol) was added dropwise. The reaction mixture was heated to 80 °C and stirred overnight. Upon completion, the reaction was quenched with water and extracted with Et_2O (3x50 mL), combined organic layers dried over $MgSO_4$. Then, solvent was evaporated under reduced pressure. The crude product was purified by column chromatography on silica gel Hexane: EtOAc (10:1) solvent mixture yielding **20** as white solid (90%): ^{1}H NMR (400 MHz, Chloroform-d) δ 7.22 (dd, *J* = 7.6, 1.6 Hz, 2H), 7.19 (d, *J* = 8.7 Hz, 2H), 6.98 (td, *J* = 8.4, 7.4, 1.6 Hz, 2H), 6.81 (td, *J* = 7.4, 1.2 Hz, 2H), 6.78 – 6.72 (m, 4H), 4.99 (s, 2H), 3.68 (s, 3H). ^{13}C NMR (100 MHz, $CDCl_3$) δ 158.5, 145.0, 129.6, 128.9, 128.2, 127.4, 123.0, 120.6, 117.1, 114.0, 55.2, 53.0.

4.3.3 Synthesis of 3,7-dibromo-10-(4-methoxybenzyl)-10H-phenoselenazine

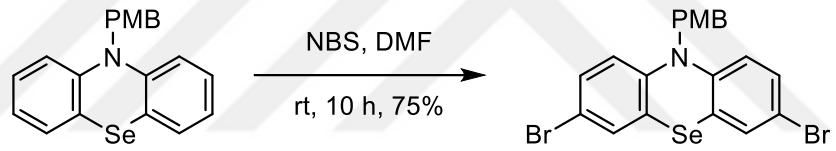

20 **21**

Scheme 38. Synthesis of Compound 21

Compound **20** (200 mg, 0.595 mmol) was dissolved in 5 mL dry DMF, and NBS (264 mg, 1.49 mmol) was gradually added over 4 minutes at 0 °C. After the NBS addition, the reaction mixture was warmed to room temperature and stirred overnight. The resulting mixture was diluted with Et_2O and washed with water (3x20 mL). Organic layer dried over $MgSO_4$ and concentrated in vacuo. The crude product was purified through column chromatography on neutral alumina employing an Hexane: DCM (80:20) as the solvent system, yielding final product as white solid (75%): ^{1}H NMR (400 MHz, Chloroform-d) δ 7.31 (d, *J* = 2.3 Hz, 2H), 7.13 (d, *J* = 8.6 Hz, 2H), 7.08 (dd, *J* = 8.7, 2.3 Hz, 2H), 6.76 (d, 2H), 6.59 (d, *J* = 8.7 Hz, 2H), 4.90 (s, 2H), 3.70 (s, 3H). ^{13}C NMR (100 MHz, $CDCl_3$) δ 158.7, 143.9, 131.7, 130.4, 128.1, 127.8, 122.0, 118.3, 115.6, 114.2, 55.26, 53.2.

4.3.4 Synthesis of 3,7-diiodo-10-(4-methoxybenzyl)-10H-phenoselenazine

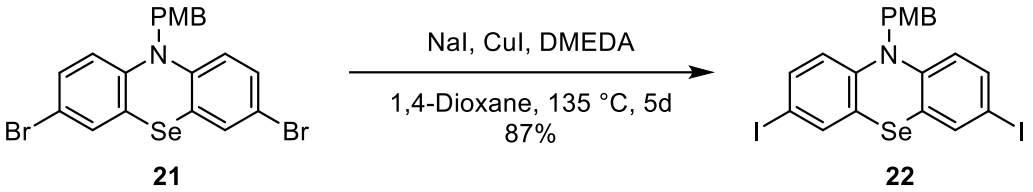

Scheme 39. Synthesis of Compound 22

A hot vacuum argon cycle was applied to the flame-dried sealed tube. Then NaI (223 mg, 1.49 mmol), CuI (71 mg, 372 µmol), and compound 21 (195 mg, 372 µmol) were added to the sealed tube, and the vacuum argon cycle was applied again. Then DMEDA (17 µL, 149 µmol) and 1,4-Dioxane (3 mL) were added while the vessel was flushing with argon, and the vessel cap was secured. The reaction mixture was stirred at 135 °C for five days. Upon completion, the reaction was cooled room temperature, 25% aq. Ammonia solution was added, and the reaction mixture was poured into water. The solution was extracted with DCM (3x30 mL), and the organic layer was dried over Na_2SO_4 and concentrated in vacuo. The crude product was purified by column chromatography on neutral alumina with Hexane: DCM (10:1) yielding the **22** in 87% as white solid : ^{1}H NMR (400 MHz, $CDCl_3$) δ 7.46 (d, *J* = 2.0 Hz, 2H), 7.23 (dd, *J* = 8.6, 2.0 Hz, 2H), 7.11 (d, *J* = 8.6 Hz, 2H), 6.74 (d, *J* = 8.6 Hz, 2H), 6.45 (d, *J* = 8.6 Hz, 2H), 4.87 (s, 2H), 3.69 (s, 3H). ^{13}C NMR (100 MHz, $CDCl_3$) δ 158.8, 144.6, 137.3, 136.3, 128.1, 127.8, 122.4, 118.9, 114.2, 85.8, 55.3, 53.0.

4.3.5 Synthesis of 3,7-dibromo-10H-phenoselenazine

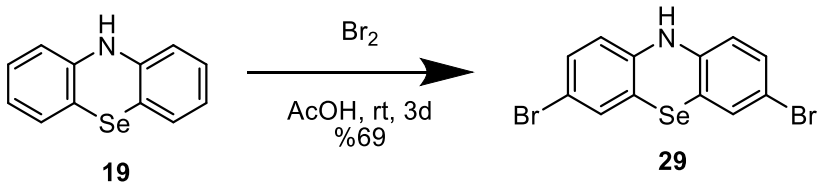

Scheme 40. Synthesis of Compound 29

To flame-dried Schleck tube (100 mL) **19** (460 mg, 1.87 mmol) was added and solid was dissolved in 30 mL glacial acetic acid. The solution was degassed one hour. Then Br_2 (298 µL, 5.61 mmol) was added dropwise and stirred overnight. The reaction was monitored by TLC after 24 h, and another Br_2 (298 µL, 5.61 mmol) was added and stirred for another 24 h. Then, another Br_2 (298 µL, 5.61 mmol) was added and stirred for another 24 h. Spots of mono-brominated, di-brominated, and compound **19** were too close to each other; therefore, the reaction was forced to finish. A solution of 10% Na_2SO_3 was added, and the mixture was stirred at rt for one hour. The resulting suspension was poured into ice/water, and precipitate was filtered through the sintered funnel. The crude product purified by column chromatography on neutral alumina with Hexane: EtOAc (100:15) system yielding the product **29** as black solid (69%): ^{1}H NMR (400 MHz, DMSO-d6) δ 8.85 (s, 1H), 7.34 (d, 2H), 7.18 (dd, *J* = 8.7, 2.4 Hz, 2H), 6.67 (d, *J* = 8.6 Hz, 2H). ^{13}C NMR (100 MHz, DMSO-d6) δ 140.9, 130.6, 130.4, 116.6, 113.5, 113.1.

4.3.6 Synthesis of tert-butyl 3,7-dibromo-10H-phenoselenazine-10-carboxylate

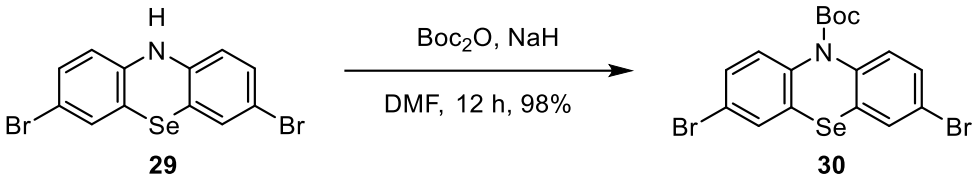

Scheme 41. Synthesis of Compound 30

A solution of **29** (210 mg, 520 µmol) in dry DMF (5 mL) under argon atmosphere at 0 °C NaH (44 mg, 1.09 mmol) was added and stirred for one hour. The reaction mixture was warmed to room temperature, and Boc_2O (240 µL, 1.09 mmol) was added in one portion and stirred overnight at room temperature. The reaction was quenched with water and extracted with Et2O (3x50 mL); the organic layer was dried over MgSO4 and was concentrated under reduced pressure. The crude product purified by column chromatography with Hexane: EtOAc (10:1) system yielding the

compound **30** as white solid (98%): ^{1}H NMR (400 MHz, Chloroform-d) δ 7.55 (d, *J* = 2.1 Hz, 2H), 7.37 – 7.28 (m, 4H), 1.38 (s, 9H). ^{13}C NMR (100 MHz, $CDCl_3$) δ 150.4, 136.3, 130.5, 128.9, 128.6, 127.5, 118.1, 80.9, 26.4.

4.4 Target Molecules

4.4.1 Synthesis of 3,7-bis((4-((tert-butyldimethylsilyl)oxy)phenyl)ethynyl)-10-(4-methoxybenzyl)-10H-phenoselenazine

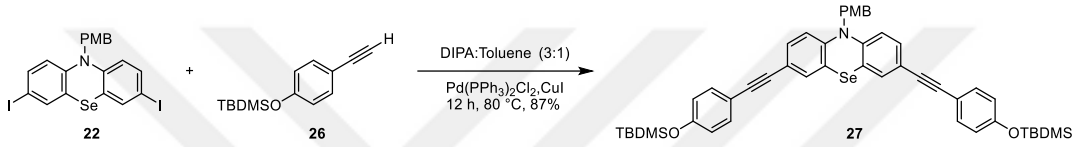

Scheme 42. Synthesis of Compound 27

To a flame-dried Schlenk tube (50 mL) **22** (406 mg, 657 µmol), Pd(PPh3)2Cl2 (92 mg, 131 µmol) and CuI (50 mg, 262 µmol) was added, and vacuum argon cycle was applied. The solid substance was dissolved in the mixture of DIPA: Toluene (3:1, 12 mL), and the solution was degassed for 30 minute. Then, **26** (458 mg, 1.97 mmol) was added to the Schlenk tube. The reaction was heated to 80 °C and stirred for 12 hours under an argon atmosphere. After cooling to room temperature, the yellowish/black mixture was filtered through a thin pad of celite and washed with EtOAc. The filtrate was concentrated in vacuo. Column chromatography (silica gel, Hexane: Ethyl Acetate – 10:1) was performed to isolate the product (473 mg, 87%): ^{1}H NMR (400 MHz, Chloroform-d) δ 7.34 (d, *J* = 2.0 Hz, 2H), 7.28 (dd, *J* = 8.8, 2.2 Hz, 4H), 7.15 (d, *J* = 8.4 Hz, 2H), 7.10 (dd, *J* = 8.5, 2.0 Hz, 2H), 6.77 (d, 2H), 6.74 – 6.69 (m, 4H), 6.65 (d, *J* = 8.5 Hz, 2H), 4.98 (s, 2H), 3.69 (s, 3H), 0.90 (s, 18H), 0.12 (s, 12H). ^{13}C NMR (100 MHz, $CDCl_3$) δ 158.6, 155.7, 144.1, 132.7, 132.1, 130.7, 129.6, 127.9, 120.1, 119.4, 118.3, 116.6, 115.9, 114.0, 89.4, 87.2, 55.1, 53.2, 25.5, 18.1, -4.5.

4.4.2 Synthesis of 4,4'-((10-(4-methoxybenzyl)-10H-phenoselenazine-3,7-diyl)bis(ethyne-2,1-diyl))diphenol

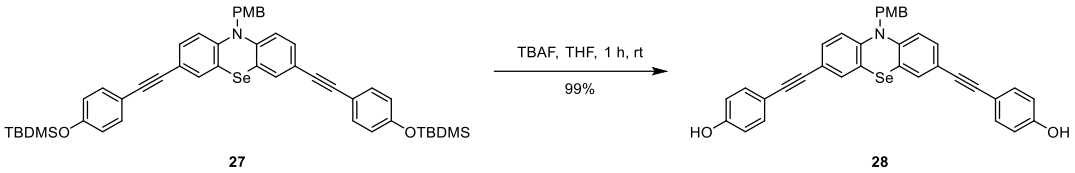

Scheme 43. Synthesis of Compound 28

To a solution of compound **27** (473 mg, 572 µmole) in THF (5 mL), TBAF (1.43 mL, 1.43 mmol) was added in one portion. The reaction was stirred for 3 hours at room temperature and quenched with 10 ml of saturated NH4Cl solution. The reaction was extracted with ethyl acetate (2 x 50 ml). The combined organic layers were dried with Na_2SO_4 and concentrated in vacuo. The residue was purified by column chromatography on silica gel with Hexane: EtOAc (1:1) system yielding the compound **28** (336 mg, 98%): ^{1}H NMR (400 MHz, Chloroform-d) δ 7.46 – 7.43 (m, 2H), 7.39 (d, *J* = 8.4 Hz, 4H), 7.27 – 7.18 (m, 4H), 6.87 (d, *J* = 8.5 Hz, 2H), 6.81 (d, *J* = 8.4 Hz, 4H), 6.76 (d, *J* = 8.5 Hz, 2H), 5.09 (s, 1H), 5.01 (s, 2H), 3.81 (s, 3H).

4.4.3 Synthesis of 4,4'-((10-(4-methoxybenzyl)-10H-phenoselenazine-3,7-diyl)bis(ethyne-2,1-diyl))bis(N,N-dimethylaniline)

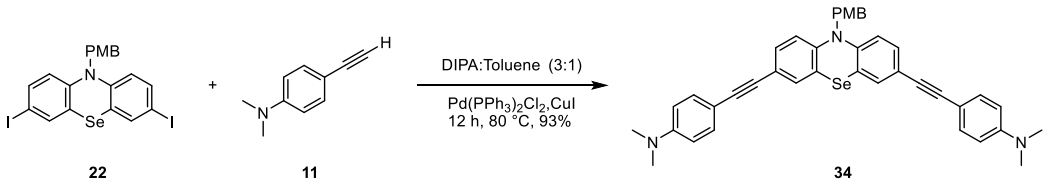

Scheme 44. Synthesis of Compound 34

To a flame-dried Schlenk tube (50 mL) **22** (150 mg, 286 µmol), Pd(PPh3)2Cl2 (40 mg, 57 µmol) and CuI (21 mg 84 µmol) was added, and a vacuum argon cycle was applied. The solid substance was dissolved in the mixture of DIPA: Toluene (3:1, 8 mL), and the resultant mixture was degassed for 30 min. Then, **11** (124 mg, 858

μmol) was added to the Schlenk tube. The reaction was heated to 80 °C and stirred for 12 hours under argon atmosphere. After cooling to room temperature, the black mixture was filtered through a thin pad of celite, and the celite was washed with EtOAc. The filtrate was concentrated in vacuo. Column chromatography (silica gel, Hexane: Ethyl Acetate – 3:1) was performed to isolate the product (172 mg, 93%): ^{1}H NMR (400 MHz, Chloroform-d) δ 7.47 – 7.41 (d, 2H), 7.38 (d, 4H), 7.26 (d, *J* = 8.5 Hz, 2H), 7.20 (dd, *J* = 8.5, 2.0 Hz, 2H), 6.87 (d, *J* = 9.5, 3.1 Hz, 2H), 6.75 (d, 2H), 6.67 (d, 4H), 5.08 (s, 2H), 3.80 (d, *J* = 2.6 Hz, 3H), 3.01 (d, *J* = 3.4 Hz, 12H).

4.4.4 Synthesis of 4,4'-((1E,1'E)-(10-(4-methoxybenzyl)-10H-phenoselenazine-3,7-diyl)bis(ethene-2,1-diyl))bis(N,N-dimethylaniline)

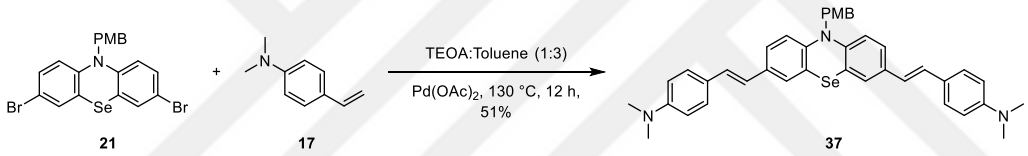

Scheme 45. Synthesis of Compound 37

Under argon atmosphere, **21** (512 mg, 968 μmol) and $Pd(OAc)_2$ (22 mg, 98 μmol) were dissolved in Toluene: TEOA (3:1, 12mL) mixture. Degassed for 30 min afterward, **17** (431 mg, 2.93 mmol) was added, and the reaction was heated to 130 °C for 12 h. After cooling to room temperature, H_2O and EtOAc were added to extract the product. The combined organic layer was washed with brine three times, dried over anhydrous Na_2SO_4, and concentrated in vacuo. The crude mixture purified by column chromatography on silica gel Hexane: EtOAc 10:2 solvent system yielding the product as yellow solid (302 mg, 51%): ^{1}H NMR (400 MHz, Chloroform-d) δ 7.34 (d, *J* = 2.1 Hz, 2H), 7.28 (d, 4H), 7.19 – 7.15 (m, 2H), 7.05 (dd, *J* = 8.2, 2.2 Hz, 2H), 6.84 – 6.73 (m, 4H), 6.71 – 6.64 (m, 4H), 6.64 – 6.57 (m, 4H), 4.97 (s, 2H), 3.68 (s, 3H), 2.88 (s, 12H).

4.4.5 Synthesis of tert-butyl 3,7-bis((E)-4-(dimethylamino)styryl)-10H-phenoselenazine-10-carboxylate

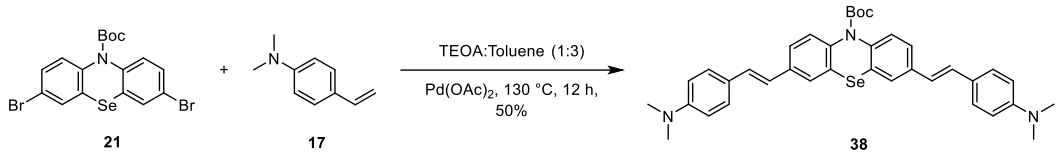

Scheme 46. Synthesis of Compound 38

Under argon atmosphere, **21** (120 mg, 230 µmol) and $Pd(OAc)_2$ (6 mg, 24 µmol) were dissolved in Toluene: TEOA (3:1, 12mL) mixture. Degassed by 30 min afterward, **17** (105 mg, 715 µmol) was added and the reaction was heated to 130 °C for 12 h. After cooling to room temperature, H_2O and EtOAc were added to extract the product. The organic layer was washed with brine three times, dried over anhydrous Na_2SO_4 and concentrated in vacuo. The crude mixture purified by column chromatography on silica gel Hexane: EtOAc (10:2) solvent system yielding the product as yellow solid (76 mg, 50%): ^{1}H NMR (400 MHz, Chloroform-d) δ 7.52 (d, *J* = 2.1 Hz, 2H), 7.40 (d, *J* = 8.5 Hz, 2H), 7.35 – 7.28 (m, 6H), 6.94 (d, *J* = 16.2 Hz, 2H), 6.77 (d, *J* = 16.2 Hz, 2H), 6.63 (d, *J* = 8.5 Hz, 4H), 2.91 (s, 12H), 1.40 (s, 9H).

4.4.6 Synthesis of tert-butyl 3,7-bis((4-((tert-butyldimethylsilyl)oxy)phenyl)ethynyl)-10H-phenoselenazine-10-carboxylate

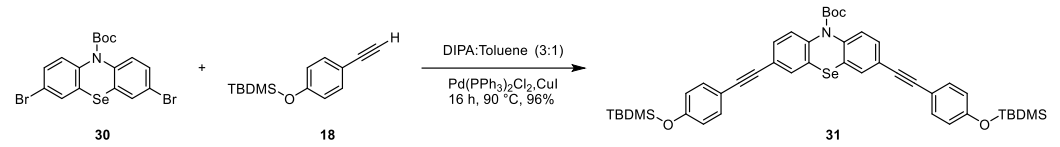

Scheme 47. Synthesis of Compound 31

To a flame-dried Schlenk tube (50 mL) **30** (135 mg, 268 µmol), $Pd(PPh_3)_2Cl_2$ (37 mg, 53 µmol) and CuI (20 mg 106 µmol) was added, and a vacuum argon cycle was

applied. The solid substance was dissolved in the mixture of DIPA: Toluene (3:1, 8 mL), and the resultant solution was degassed for 30 min. Then **18** (217 mg, 937 µmol) was added to the Schlenk tube. The reaction was heated to 90 °C and stirred for 16 hours under the argon atmosphere. After cooling to room temperature, the black mixture filtered through a thin pad of celite, and the celite was washed with EtOAc. The filtrate was concentrated in vacuo. Column chromatography (silica gel, Hexane: Ethyl Acetate – 5:1) was performed to isolate and purify the product as yellow solid (172 mg, 96%): ^{1}H NMR (400 MHz,) δ 7.43 (d, J = 1.5 Hz, 2H), 7.28 (d, J = 8.3 Hz, 2H), 7.22 (d, J = 1.7 Hz, 2H), 7.19 (d, J = 8.6 Hz, 4H), 6.60 (d, J = 8.6 Hz, 4H), 1.27 (s, 9H), 0.77 (s, 18H), 0.00 (s, 12H).

4.4.7 Synthesis of tert-butyl 3,7-bis((4-hydroxyphenyl)ethynyl)-10H-phenoselenazine-10-carboxylate

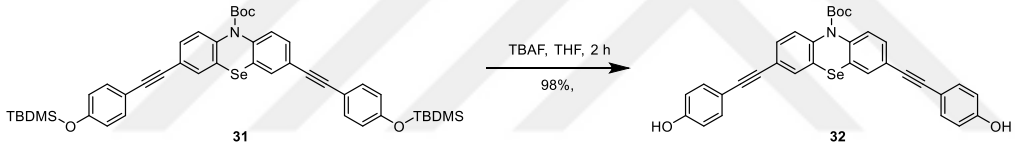

Scheme 48. Synthesis of Compound 32

In 20 mL Schlenk tube **31,** (100 mg, 124µmol) was added and vacuum argon cycle was applied, then solid substance was dissolved in 5 mL dry THF. To the solution, TBAF (1.0 M in THF, 372 µL, 372 µmol) was added and stirred for two hours at room temperature. Then, it was extracted with EtOAc (3x30 mL), and organic layer concentrated under reduced pressure. The crude product was purified by column chromatography on silica gel (1:1 Hexane: EtOAc) yielding the compound **32** as a yellow powder. (98%): ^{1}H NMR (400 MHz, Chloroform-d) δ 7.58 (d, *J* = 1.8 Hz, 2H), 7.40 (d, *J* = 8.3 Hz, 2H), 7.31 (dd, *J* = 8.6, 2.3 Hz, 6H), 6.60 (d, *J* = 8.2 Hz, 4H), 6.19 (s, 1H), 1.42 (s, 9H). ^{13}C NMR (100 MHz, $CDCl_3$) δ 160.47, 152.25, 140.47, 133.38, 130.92, 126.61, 123.26, 117.65, 116.27, 113.87, 90.59, 89.12, 80.71, 28.18.

4.4.8 Synthesis of tert-butyl 3,7-bis((4-(dimethylamino)phenyl)ethynyl)-10H-phenoselenazine-10-carboxylate

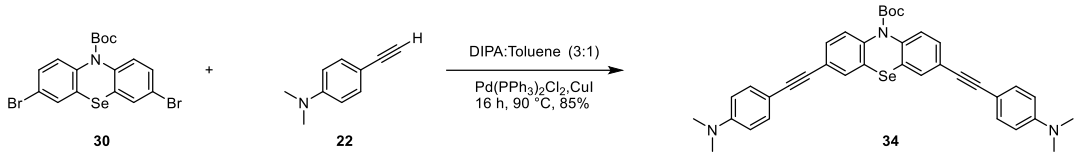

Scheme 49. Synthesis of Compound 34

To a flame-dried Schlenk tube (50 mL) **30** (150 mg, 297 µmol), $Pd(PPh_3)_2Cl_2$ (47 mg, 68 µmol) and CuI (26 mg 126 µmol) was added, and vacuum argon cycle was applied. The solid substance was dissolved in the mixture of DIPA: Toluene (3:1, 8 mL) mixture, and the resultant solution was degassed for 30 min. Then **18** (173 mg, 1.19 mmol) was added to the solution. The reaction was heated to 90 °C and stirred for 16 hours under the argon atmosphere. After cooling to room temperature, the black mixture filtered through a thin pad of celite, and the celite was washed with EtOAc. The filtrate was concentrated in vacuo. Column chromatography (silica gel, Hexane: Ethyl Acetate – 3:1) was performed to isolate the product (235 mg, 85%): ^{1}H NMR (400 MHz,) δ 7.56 (d, *J* = 1.6 Hz, 2H), 7.40 (d, *J* = 8.4 Hz, 2H), 7.34 (d, *J* = 1.7 Hz, 2H), 7.32 (d, *J* = 8.7 Hz, 4H), 6.58 (d, *J* = 8.8 Hz, 4H), 2.92 (s, 12H), 1.40 (s, 8H).

4.4.9 Synthesis of 4,4'-((10H-phenoselenazine-3,7-diyl)bis(ethyne-2,1-diyl))bis(N,N-dimethylaniline)

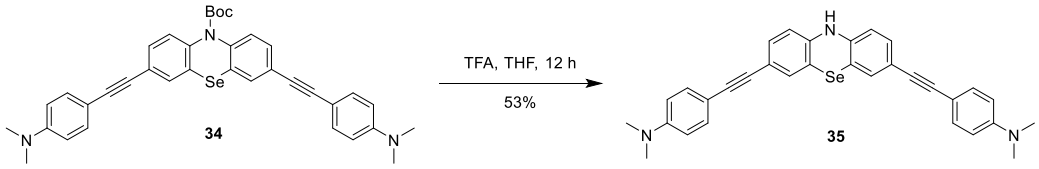

Scheme 50. Synthesis of Compound 35

To a solution of compound **34** (80.0 mg, 0.23 mmol) in 5.0 mL DCM, TFA (2 mL) was added, and solution was stirred 12 hours at room temperature. Upon completion,

the reaction was quenched with saturated $NaHCO_3$ solution. The reaction was extracted with EtOAc (3x20 mL). The organic layer dried over Na_2SO_4 and concentrated in vacuo. The crude product purified via column chromatography on silica gel $CHCl_3$: MeOH (10:1) solvent system yielding the compound **35** as yellow solid (45 mg, 53%): ^{1}H NMR (400 MHz,) δ 7.66 (s, 2H), 7.60 (d, *J* = 9.6 Hz, 2H), 7.03 (d, *J* = 8.5 Hz, 4H), 6.62 (d, *J* = 8.5 Hz, 4H), 6.46 (d, *J* = 8.3 Hz, 2H), 6.33 (s, 1H), 2.84 (s, 12H). ^{13}C NMR (100 MHz, $CDCl_3$) δ 147.13, 141.29, 130.00, 127.68, 127.45, 126.99, 119.76, 112.34, 110.53, 110.04, 108.27, 97.55, 38.22.

REFERENCES

1. Karaman, O.; Alkan, G. A.; Kizilenis, C.; Akgul, C. C.; Gunbas, G. Xanthene dyes for cancer imaging and treatment: A material odyssey. *Coordination Chemistry Reviews* **2023**, *475*, 214841.

2. Daniell, M. D., and J. S. Hill. "A history of photodynamic therapy." *Australian and New Zealand Journal of Surgery* 61.5 **1991,** 340-348.

3. Mitton, D.; Ackroyd, R. A brief overview of photodynamic therapy in Europe. *Photodiagnosis and Photodynamic Therapy* **2008**, *5*(2), 103–111.

4. Raabe, O. Ueber die Wirkung fluoreszierende Stoffe auf infusorien. *Zeitschrift fuer Biologie* **1900**, *39*, 524–526.

5. Roelandts, R. The history of phototherapy: Something new under the sun? *Journal of the American Academy of Dermatology* **2002**, *46*(6), 926–930.

6. Jesionek, A.; Tappeiner, V. H. Therapeutische versuche mit fluoreszierenden stoffen. *Muench Med Wochneshr* **1903**, *47*, 2042–2044.

7. von Tappeiner, H.; Jodlbauer, A. *Die Sensibilisierende Wirkung Fluorescierender Substanzen: Gesammelte Untersuchungen Über Die Photodynamische Erscheinung*; Vogel, 1907.

8. Tappeiner, V. Uber die wirkung der photodynamischen (fluorescierenden) stoffe auf protozoen und enzyme. *Dtsch. Arch. Klin. Med.* **1904**, *80*, 427–487.

9. Hausmann, W. *Über Die Sensibilisierende Wirkung Des Hämatoporphyrins*; 1913.

10. Pushpan, S. K.; Venkatraman, S.; Anand, V. G.; Sankar, J.; Parmeswaran, D.; Ganesan, S.; et al. Porphyrins in photodynamic therapy-a search for ideal

photosensitizers. *Current Medicinal Chemistry-Anti-Cancer Agents* **2002**, *2*(2), 187–207.

11. Thudichum, J. L. Tenth report of the medical officer of the privy council. *London: HM Stationary Office* **1867**.

12. Meyer-Betz, F. Untersuchungen über die biologische (photodynamische) Wirkung des Hämatoporphyrins und anderer Derivate des Blut-und Gallenfarbstoffs. *Dtsch. Arch. Klin. Med* **1913**, *112*(476–450), 366–8576.

13. Schwartz, S.; Absolon, K.; Vermund, H. Some relationships of porphyrins, X-rays and tumors. *Univ Minn Med Bull* **1955**, *27*(7).

14. Dolmans, D. E. J. G. J.; Fukumura, D.; Jain, R. K. Photodynamic therapy for cancer. *Nature Reviews Cancer* **2003**, *3*(5), 380–387.

15. Diamond, I.; Mcdonagh, A.; Wilson, C.; Granelli, S.; Nielsen, S.; Jaenicke, R. Photodynamic therapy of malignant tumours. *The Lancet* **1972**, *300*(7788), 1175–1177.

16. Dougherty, T. J.; Grindey, G. B.; Fiel, R.; Weishaupt, K. R.; Boyle, D. G. Photoradiation therapy. II. Cure of animal tumors with hematoporphyrin and light. *Journal of the national cancer institute* **1975**, *55*(1), 115–121.

17. Kelly, J. F.; Snell, M. E. Hematoporphyrin derivative: a possible aid in the diagnosis and therapy of carcinoma of the bladder. *The Journal of urology* **1976**, *115*(2), 150–151.

18. Dougherty, T. J. ChJ. *Gomer, BW Henderson, G. Jori, D. Kessel, M. Korbelik, J. Moan, and Q. Peng* **1998**, 889–905.

19. Correia, J. H.; Rodrigues, J. A.; Pimenta, S.; Dong, T.; Yang, Z. Photodynamic therapy review: Principles, photosensitizers, applications, and future directions. *Pharmaceutics* **2021**, *13*(9), 1332.

20. Dougherty, T. J.; Gomer, C. J.; Henderson, B. W.; Jori, G.; Kessel, D.; Korbelik, M.; et al. Photodynamic therapy. *Journal of National Cancer Institute* **1998**, *90*(12), 889–905.

21. De Freitas, L. F.; Hamblin, M. R. Antimicrobial photoinactivation with functionalized fullerenes. *Nanobiomaterials in Antimicrobial Therapy: Applications of Nanobiomaterials* **2016**, 1–27.

22. Dabrowski, J. M.; Arnaut, L. G. Photodynamic therapy (PDT) of cancer: from local to systemic treatment. *Photochemical & Photobiological Sciences* **2015**, *14*(10), 1765–1780.

23. Rocha, Luís Gabriel Borges. *Development of a novel photosensitizer for photodynamic therapy of cancer*. **2016**. PhD Thesis.

24. Fitzgerald, F. *Photodynamic Therapy (PDT): Principles, Mechanisms and Applications*; Cancer etiology, diagnosis and treatments; Nova Science Publishers, Incorporated, **2017**.

25. Abrahamse, H.; Hamblin, M. R. New photosensitizers for photodynamic therapy. *Biochemical Journal* **2016**, *473*(4), 347–364.

26. Parab, Shraddha, et al. "Sensitizers in photodynamic therapy." *Nanomaterials for Photodynamic Therapy.* Woodhead Publishing, **2023**. 81-103.

27. Allison, R. R.; Downie, G. H.; Cuenca, R.; Hu, X. H.; Childs, C. J. H.; Sibata, C. H. Photosensitizers in clinical PDT. *Photodiagnosis and Photodynamic Therapy* **2004**, *1*(1), 27–42.

28. Kou, J.; Dou, D.; Yang, L. Porphyrin photosensitizers in photodynamic therapy and its applications. *Oncotarget* **2017**, *8*(46), 81591.

29. Krammer, B.; Plaetzer, K. ALA and its clinical impact, from bench to bedside. *Photochemical & Photobiological Sciences* **2008**, *7*(3), 283–289.

30. Gross, S.; Gilead, A.; Scherz, A.; Neeman, M.; Salomon, Y. Monitoring photodynamic therapy of solid tumors online by BOLD-contrast MRI. *Nature Medicine 2003 9:10* **2003**, *9*(10), 1327–1331.

31. Mroz, P.; Huang, Y.-Y.; Szokalska, A.; Zhiyentayev, T.; Janjua, S.; Nifli, A.-P.; et al. Stable synthetic bacteriochlorins overcome the resistance of melanoma to photodynamic therapy. *The FASEB Journal* **2010**, *24*(9), 3160–3170.

32. Parab, S., Achalla, P. K., Yanamandala, N., Singhvi, G., Kesharwani, P., & Dubey, S. K. Sensitizers in photodynamic therapy. *In Nanomaterials for Photodynamic Therapy* Woodhead Publishing **2023** (pp. 81-103).

33. Chen, X.; Pradhan, T.; Wang, F.; Kim, J. S.; Yoon, J. Fluorescent chemosensors based on spiroring-opening of xanthenes and related derivatives. *Chemical Reviews* **2012**, *112*(3), 1910–1956.

34. Chen, H. J.; Zhou, X. Bin; Wang, A. L.; Zheng, B. Y.; Yeh, C. K.; Huang, J. D. Synthesis and biological characterization of novel rose bengal derivatives with improved amphiphilicity for sono-photodynamic therapy. *European Journal of Medicinal Chemistry* **2018**, *145*, 86–95.

35. Pal, P.; Zeng, H.; Durocher, G.; Girard, D.; Li, T.; Gupta, A. K.; et al. Phototoxicity of Some Bromine-Substituted Rhodamine Dyes: Synthesis, Photophysical Properties and Application as Photosensitizers. *Photochemistry and Photobiology* **1996**, *63*(2), 161–168.

36. Xiao, Y.; Qian, X. Substitution of oxygen with silicon: A big step forward for fluorescent dyes in life science. *Coordination Chemistry Reviews* **2020**, *423*, 213-513.

37. Fu, M.; Xiao, Y.; Qian, X.; Zhao, D.; Xu, Y. A design concept of long-wavelength fluorescent analogs of rhodamine dyes: replacement of oxygen with silicon atom. *Chemical Communications* **2008**, No. 15, 1780–1782.

38. Chai, X.; Cui, X.; Wang, B.; Yang, F.; Cai, Y.; Wu, Q.; et al. Near-Infrared Phosphorus-Substituted Rhodamine with Emission Wavelength above 700 nm for Bioimaging. *Chemistry – A European Journal* **2015**, *21*(47), 16754–16758.

39. Zhou, X.; Lai, R.; Beck, J. R.; Li, H.; Stains, C. I. Nebraska Red: a phosphinate-based near-infrared fluorophore scaffold for chemical biology applications. *Chemical Communications* **2016**, *52*(83), 12290–12293.

40. Liu, J.; Sun, Y. Q.; Zhang, H.; Shi, H.; Shi, Y.; Guo, W. Sulfone-rhodamines: A new class of near-infrared fluorescent dyes for bioimaging. *ACS Applied Materials and Interfaces* **2016**, *8*(35), 22953–22962.

41. Choi, A.; Miller, S. C. Silicon Substitution in Oxazine Dyes Yields Near-Infrared Azasiline Fluorophores That Absorb and Emit beyond 700 nm. *Organic Letters* **2018**, *20*(15), 4482–4485.

42. Brancaleon, L.; Moseley, H. Laser and non-laser light sources for photodynamic therapy. *Lasers in Medical Science* **2002**, *17*(3), 173–186.

43. Gunaydin, G.; Gedik, M. E.; Ayan, S. Photodynamic Therapy for the Treatment and Diagnosis of Cancer–A Review of the Current Clinical Status. *Frontiers in Chemistry* **2021**, *9*, 686303.

44. Agostinis, P.; Berg, K.; Cengel, K. A.; Foster, T. H.; Girotti, A. W.; Gollnick, S. O.; et al. Photodynamic therapy of cancer: an update. *CA: a cancer journal for clinicians* **2011**, *61*(4), 250–281.

45. Juzeniene, A.; Nielsen, K. P.; Moan, J. Biophysical aspects of photodynamic therapy. *Journal of environmental pathology, toxicology and oncology : official organ of the International Society for Environmental Toxicology and Cancer* **2006**, *25*(1–2), 7–28.

46. *Oxygen Dependence of the Photosensitizing Effect of Hematoporphyrin Derivative in NHIK 3025 Cells1 | Cancer Research | American Association for Cancer Research*.

47. Moan, J. On the diffusion length of singlet oxygen in cells and tissues. *Journal of Photochemistry and Photobiology B: Biology* **1990**, *6*(3), 343–344.

48. Moan, J.; Boye, E. Photodynamic effect on DNA and cell survival of human cells sensitized by hematoporphyrin. *Photobiochemistry and Photobiophysics* **1981**, *2*(4–5), 301–307.

49. Sonogashira, K. Development of Pd–Cu catalyzed cross-coupling of terminal acetylenes with sp2-carbon halides. *Journal of Organometallic Chemistry* **2002**, *653*(1–2), 46–49.

50. Frigoli, S.; Fuganti, C.; Malpezzi, L.; Serra, S. A practical and efficient process for the preparation of tazarotene. *Organic Process Research and Development* **2005**, *9*(5), 646–650.

51. Dieck, H. A.; Heck, F. R. Palladium catalyzed synthesis of aryl, heterocyclic and vinylic acetylene derivatives. *Journal of Organometallic Chemistry* **1975**, *93*(2), 259–263

52. Cassar, L. Synthesis of aryl- and vinyl-substituted acetylene derivatives by the use of nickel and palladium complexes. *Journal of Organometallic Chemistry* **1975**, *93*(2), 253–257.

53. Heck, R. F. The Mechanism of Arylation and Carbomethoxylation of Olefins with Organopalladium Compounds. *Journal of the American Chemical Society* **1969**, *91*(24), 6707–6714.

54. Dieck, A.; Heck, R. F. Organophosphinepalladium Complexes as Catalysts for Vinylic Hydrogen Substitution Reactions. *Journal of the American Chemical Society* **1974**, *96*(4), 1133–1136.

55. Rajapaksha, I. N.; Wang, J.; Leszczynski, J.; Scott, C. N. Investigating the Effects of Donors and Alkyne Spacer on the Properties of Donor-Acceptor-Donor Xanthene-Based Dyes. *Molecules* **2023**, *28*(13), 4929.

56. Liu, D.; He, Z.; Zhao, Y.; Yang, Y.; Shi, W.; Li, X.; et al. Xanthene-Based NIR-II Dyes for in Vivo Dynamic Imaging of Blood Circulation. *Journal of the American Chemical Society* **2021**, *143*(41), 17136–17143.

APPENDICES

A. NMR Spectra

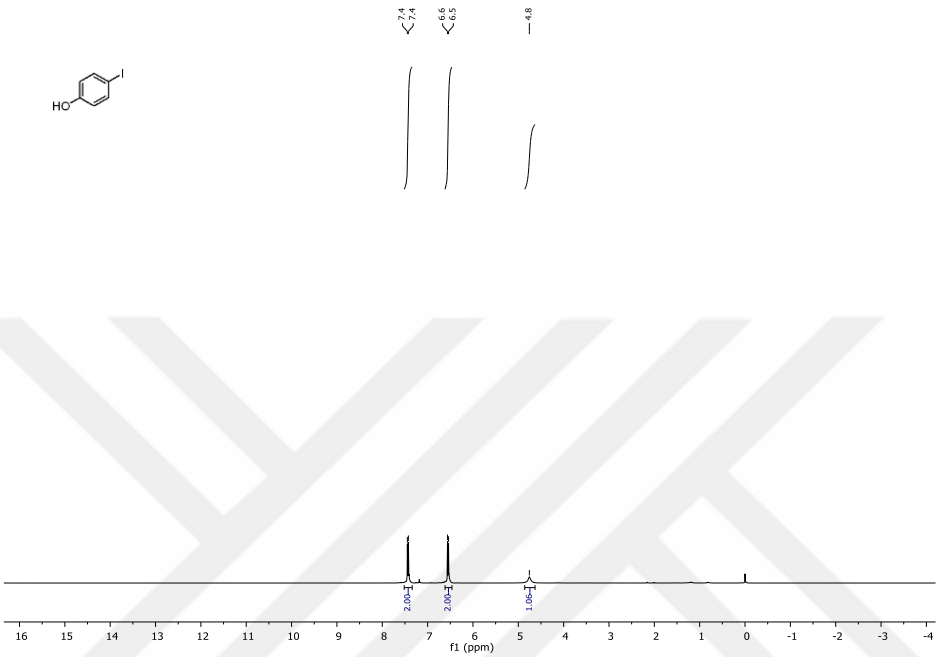

Figure A. ^{1}H NMR of Compound 2 in $CDCl_3$

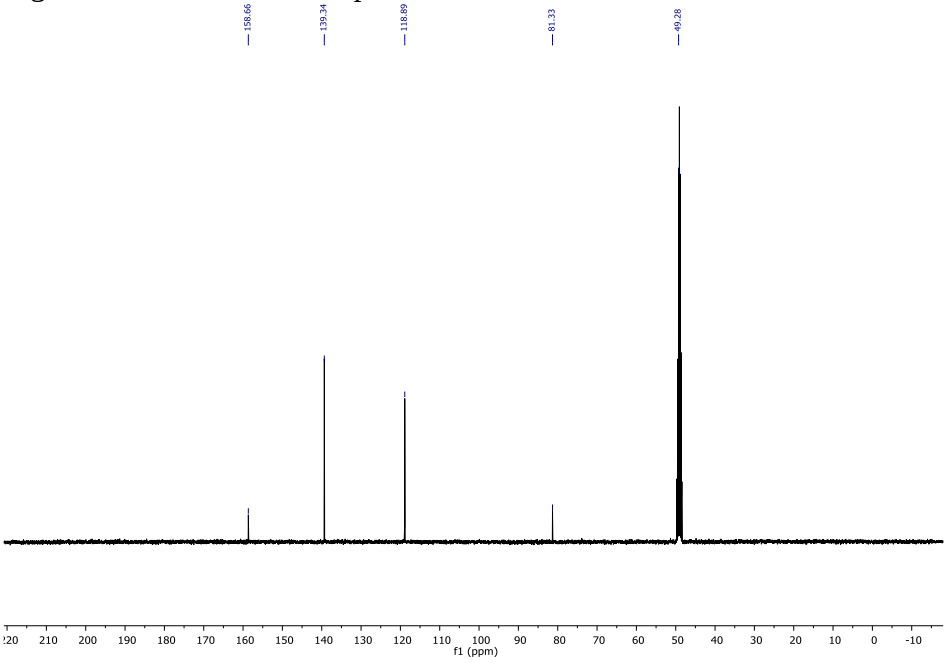

Figure A. 2. ^{13}C NMR of Compound 2 in $CDCl_3$

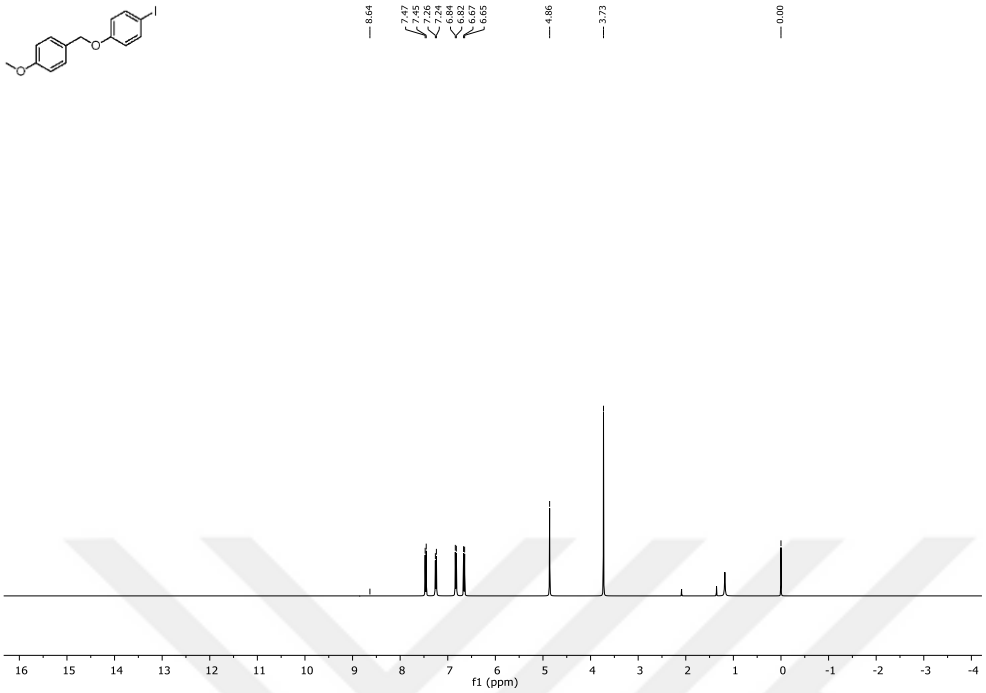

Figure A. 3. ^{1}H NMR of Compound 6 in $CDCl_3$

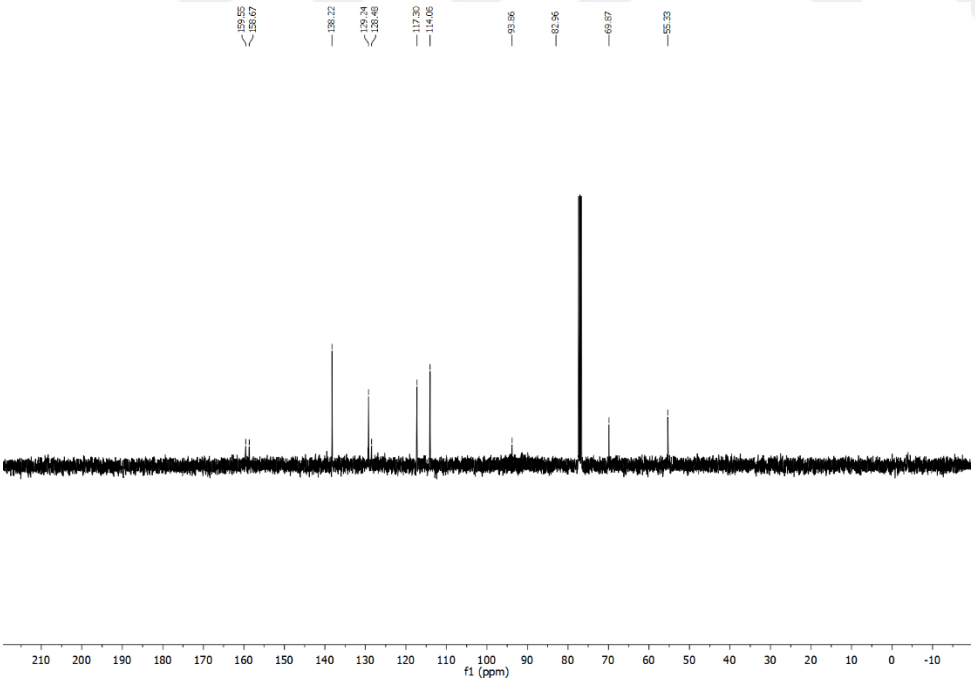

Figure A. 4. ^{13}C NMR of Compound 6 in $CDCl_3$

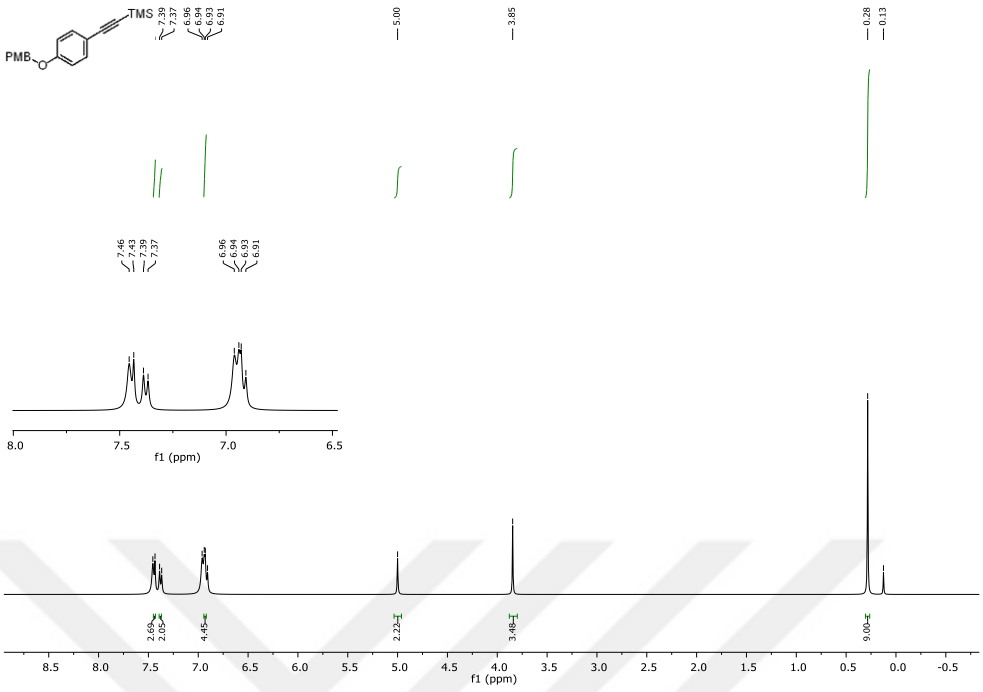

Figure A. 5. ^{1}H NMR of Compound 7 in $CDCl_3$

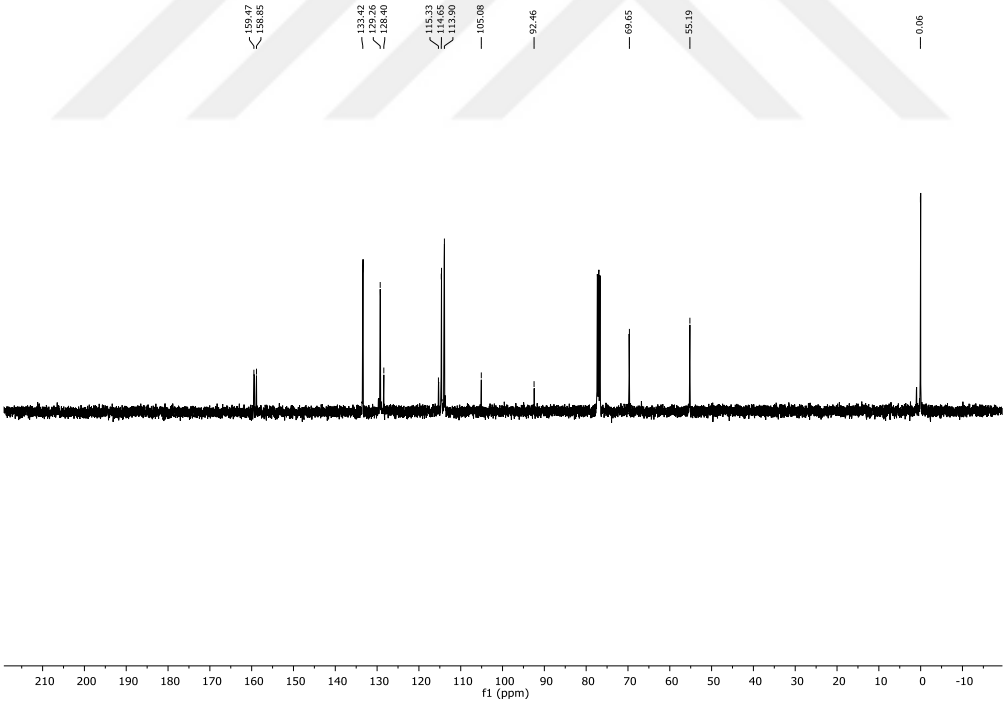

Figure A. 6. ^{13}C NMR of Compound 7 in $CDCl_3$

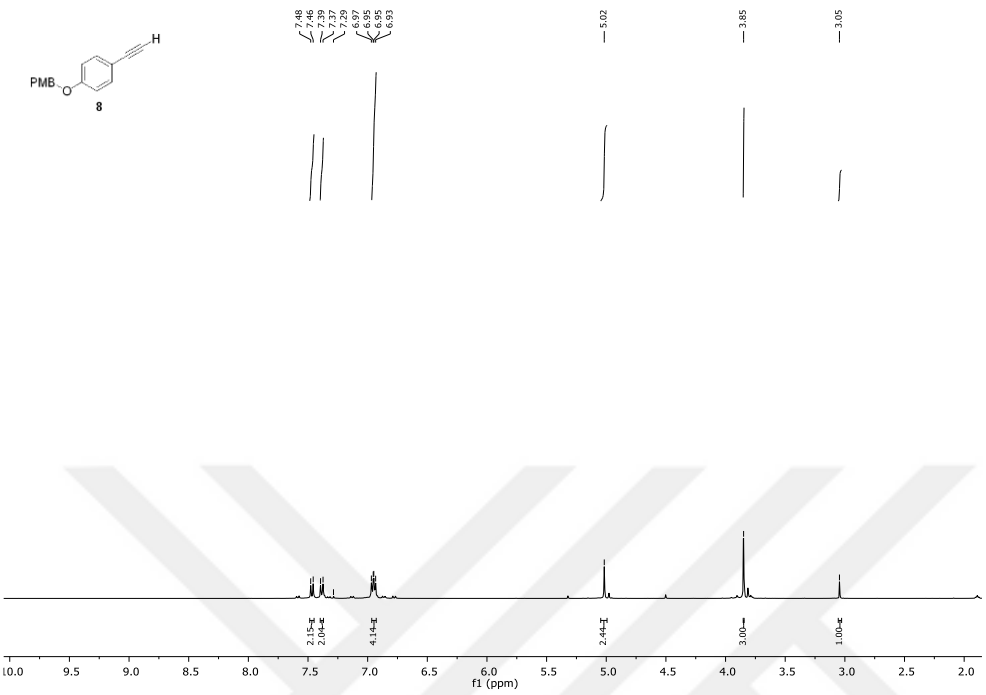

Figure A. 7. ^{1}H NMR of Compound 8 in $CDCl_3$

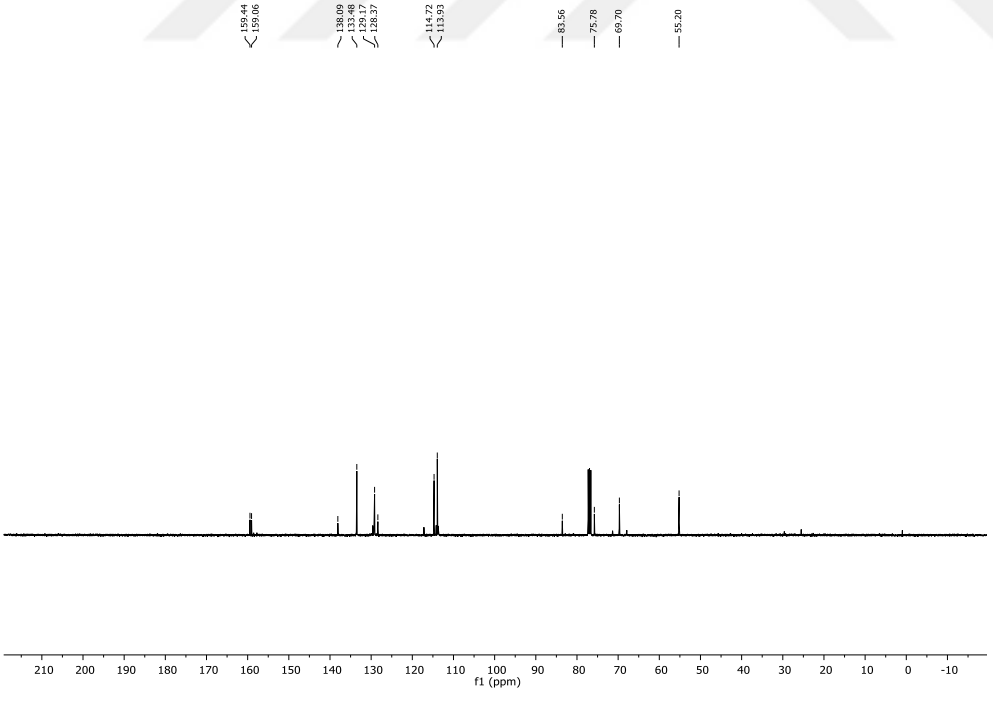

Figure A. 8. ^{13}C NMR of Compound 8 in $CDCl_3$

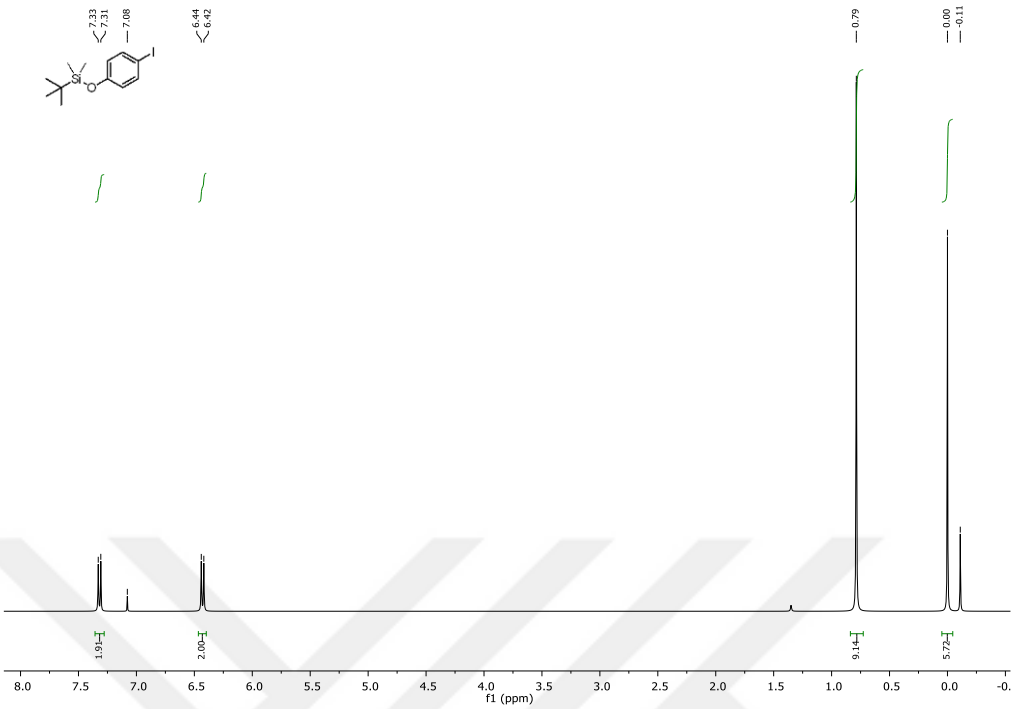

Figure A. 9. ^{1}H NMR of Compound 24 in $CDCl_3$

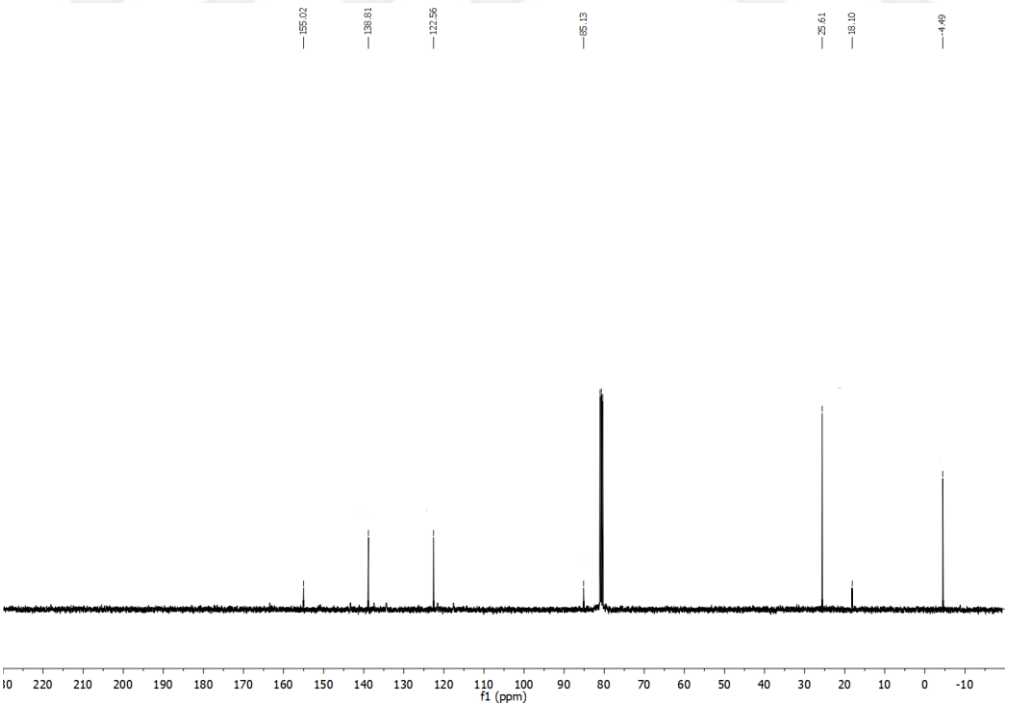

Figure A. 10. ^{13}C NMR of Compound 24 in $CDCl_3$

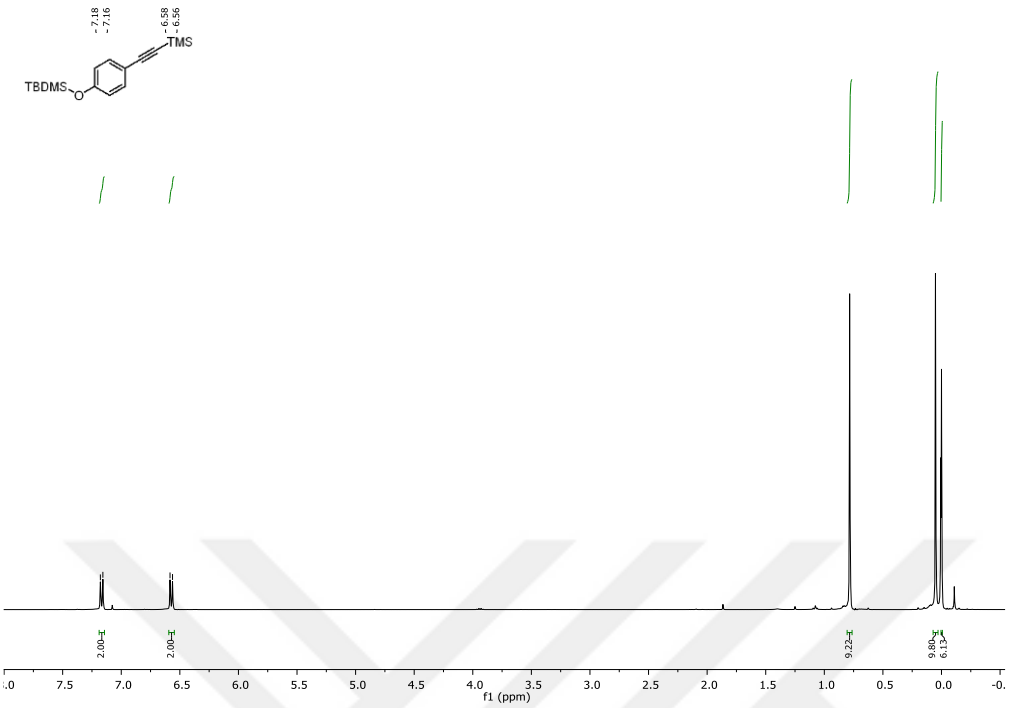

Figure A. 11. ^{1}H NMR of Compound 25 in $CDCl_3$

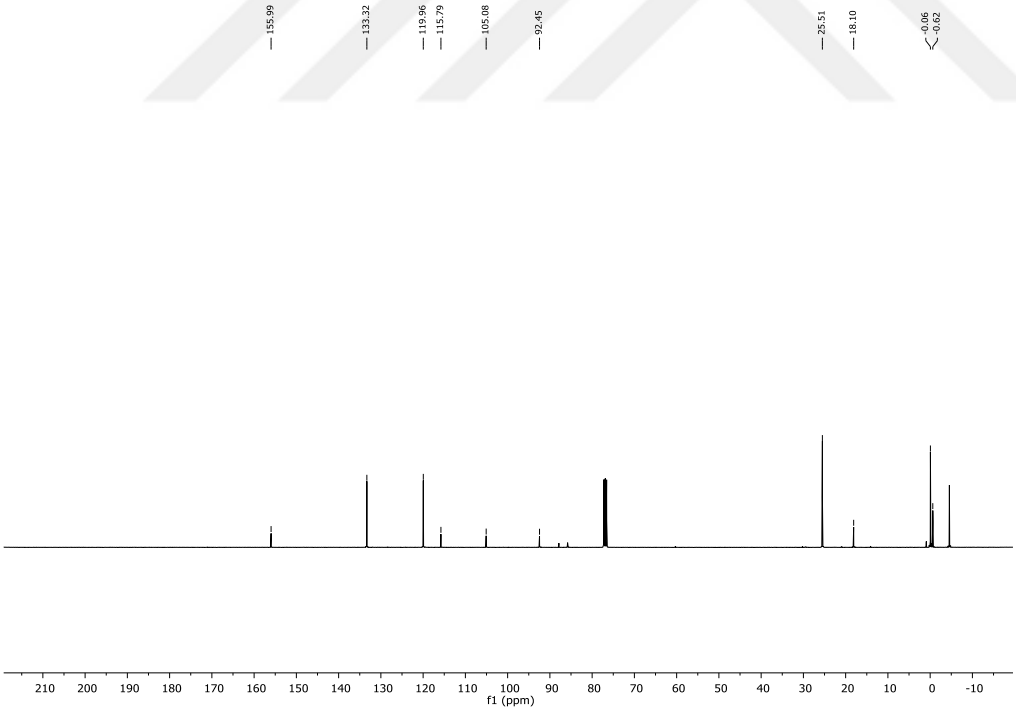

Figure A. 12. ^{1}H NMR of Compound 25 in $CDCl_3$

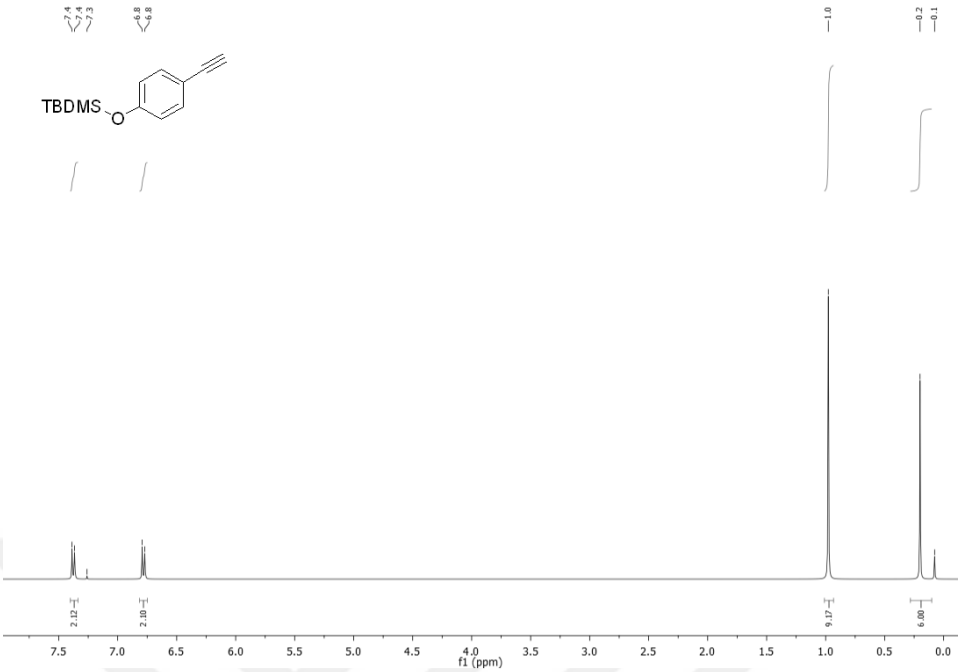

Figure A. 13. ^{1}H NMR of Compound 26 in $CDCl_3$

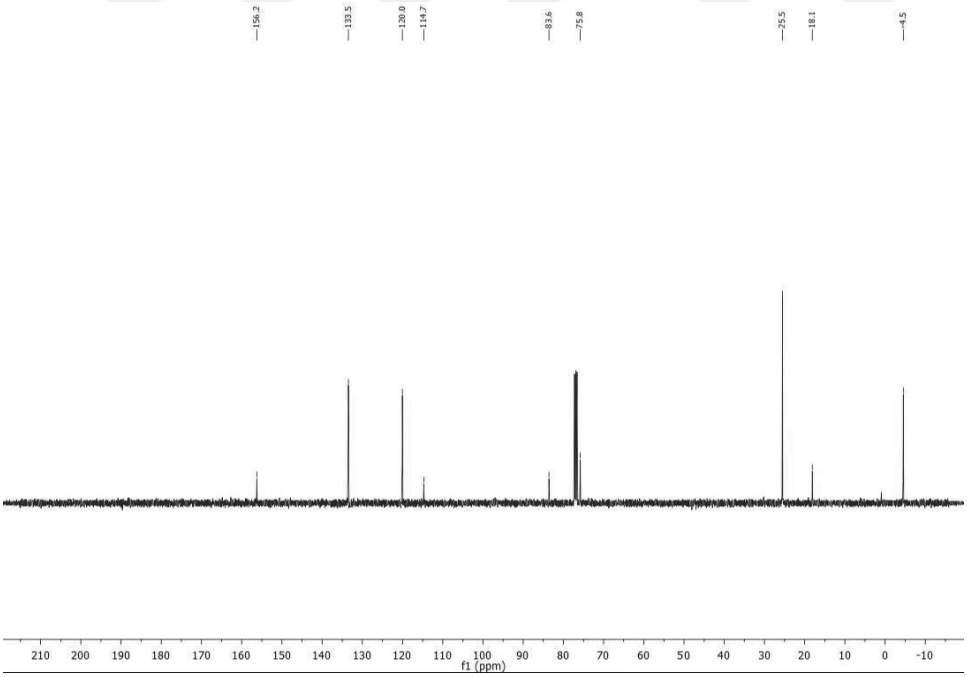

Figure A. 14. ^{13}C NMR of Compound 26 in $CDCl_3$

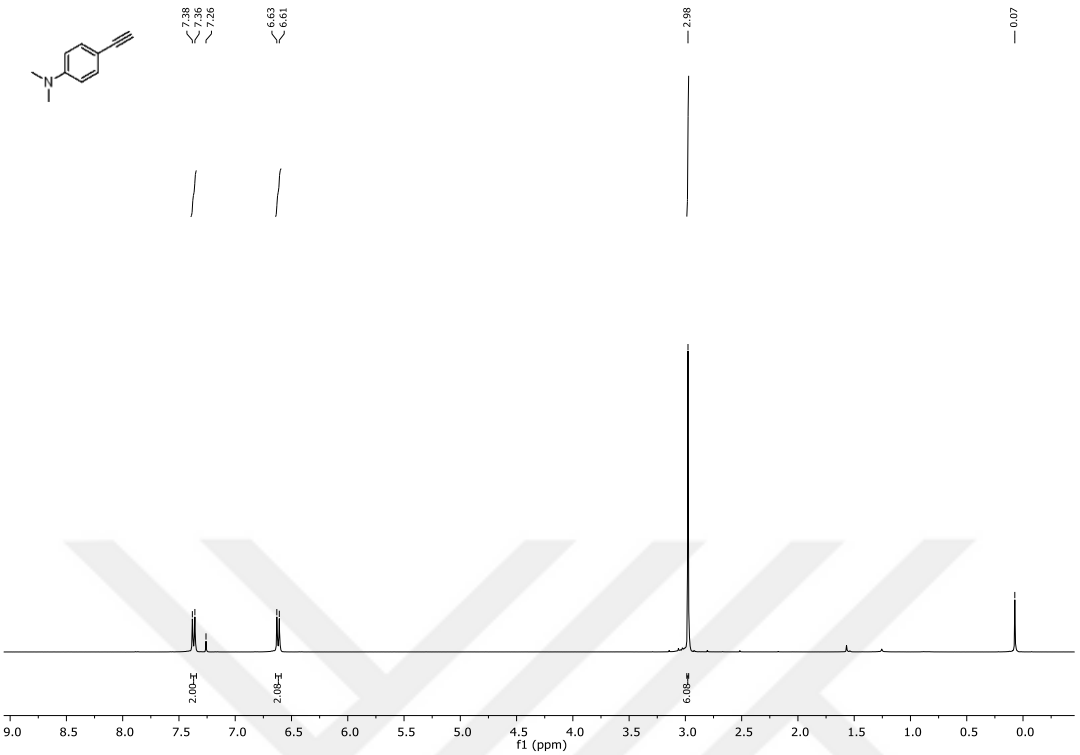

Figure A. 15. ^{1}H NMR of Compound 11 in $CDCl_3$

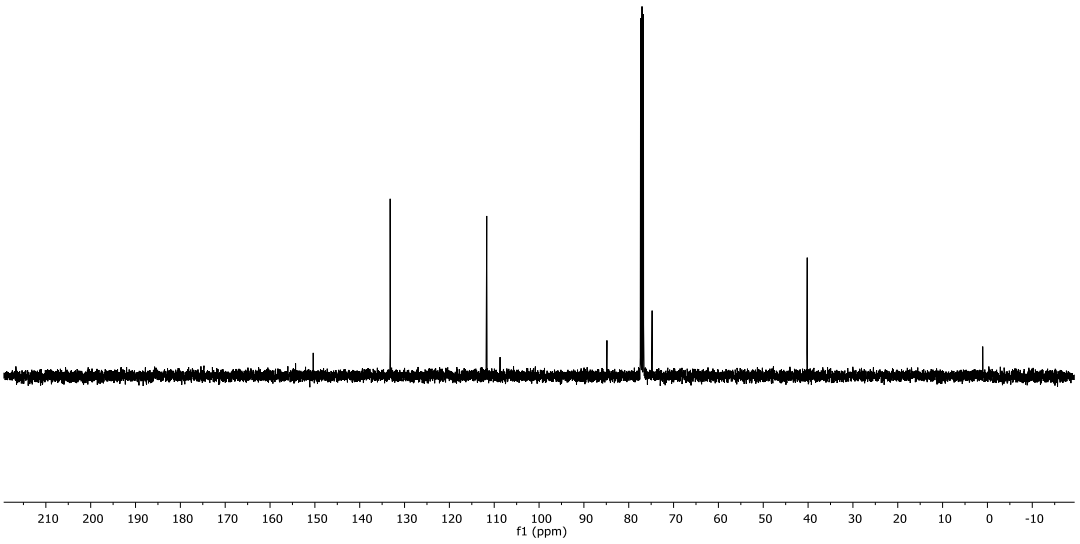

Figure A. 16. ^{13}C NMR of Compound 11 in $CDCl_3$

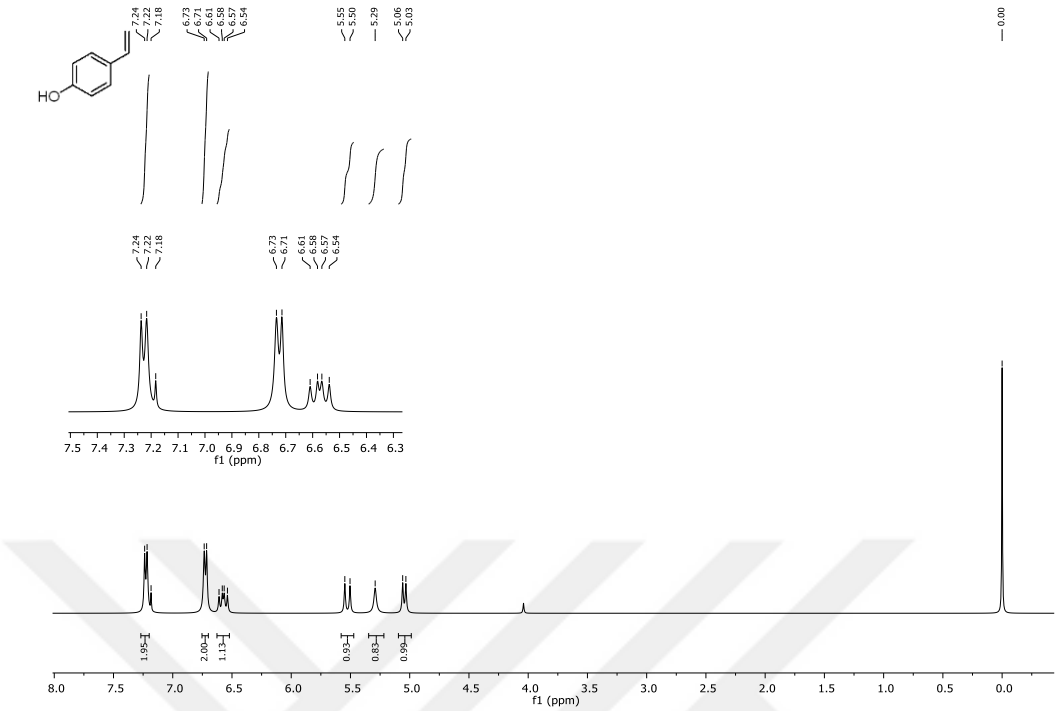

Figure A. 17. ^{1}H NMR of Compound 15 in $CDCl_3$

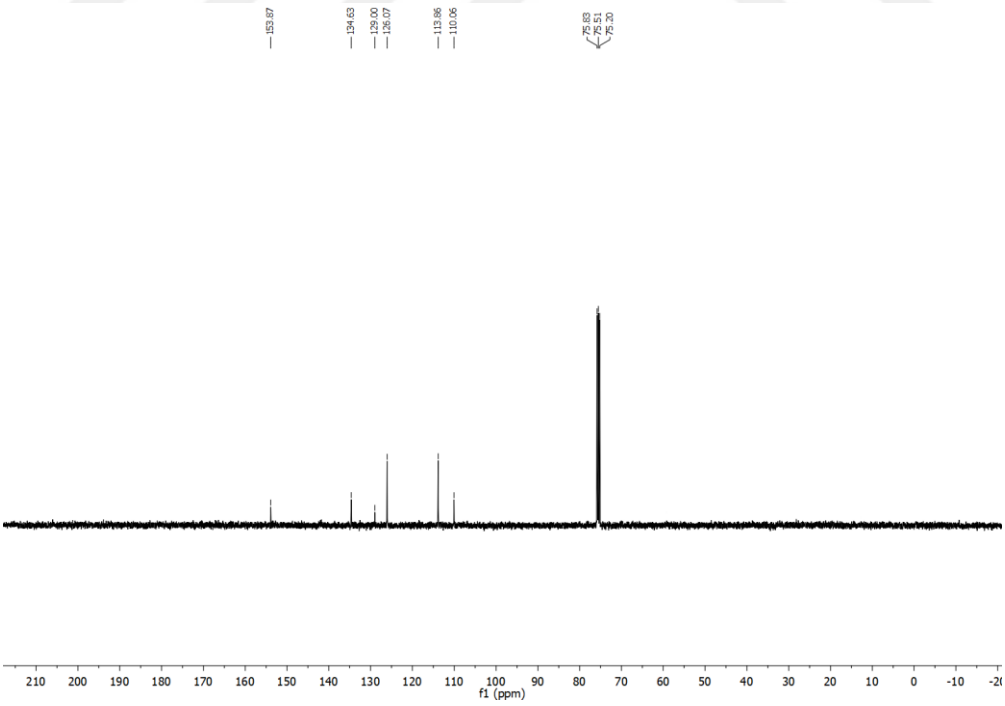

Figure A. 18. ^{13}C NMR of Compound 15 in $CDCl_3$

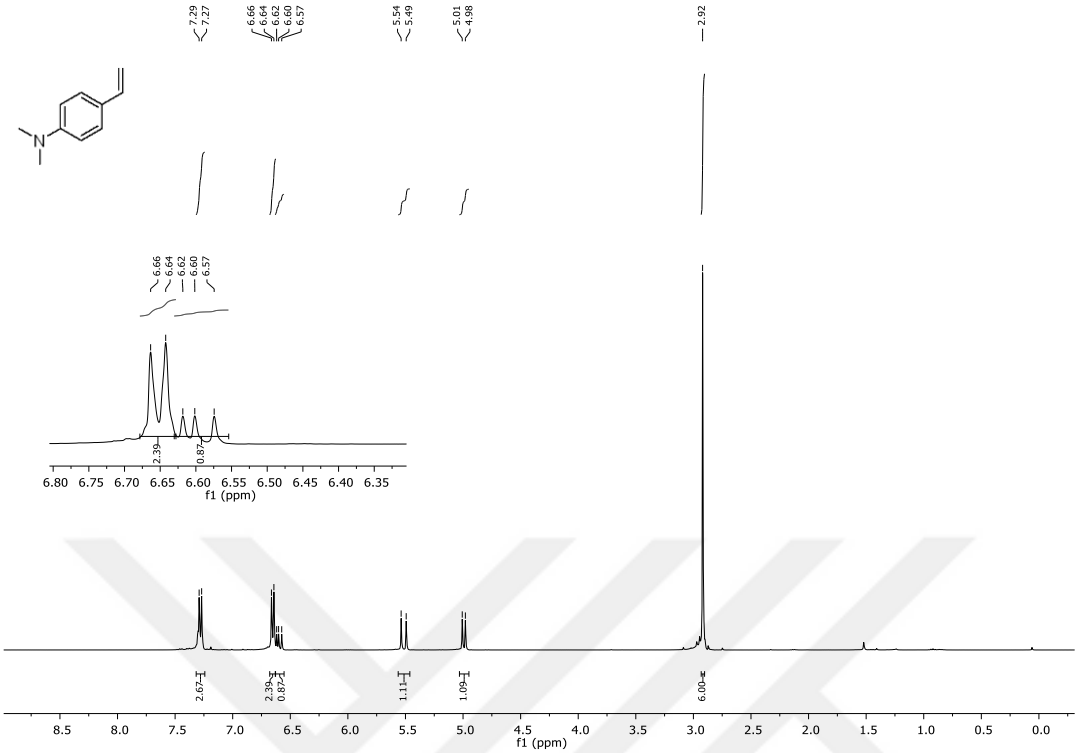

Figure A. 19. ^{1}H NMR of Compound 17 in $CDCl_3$

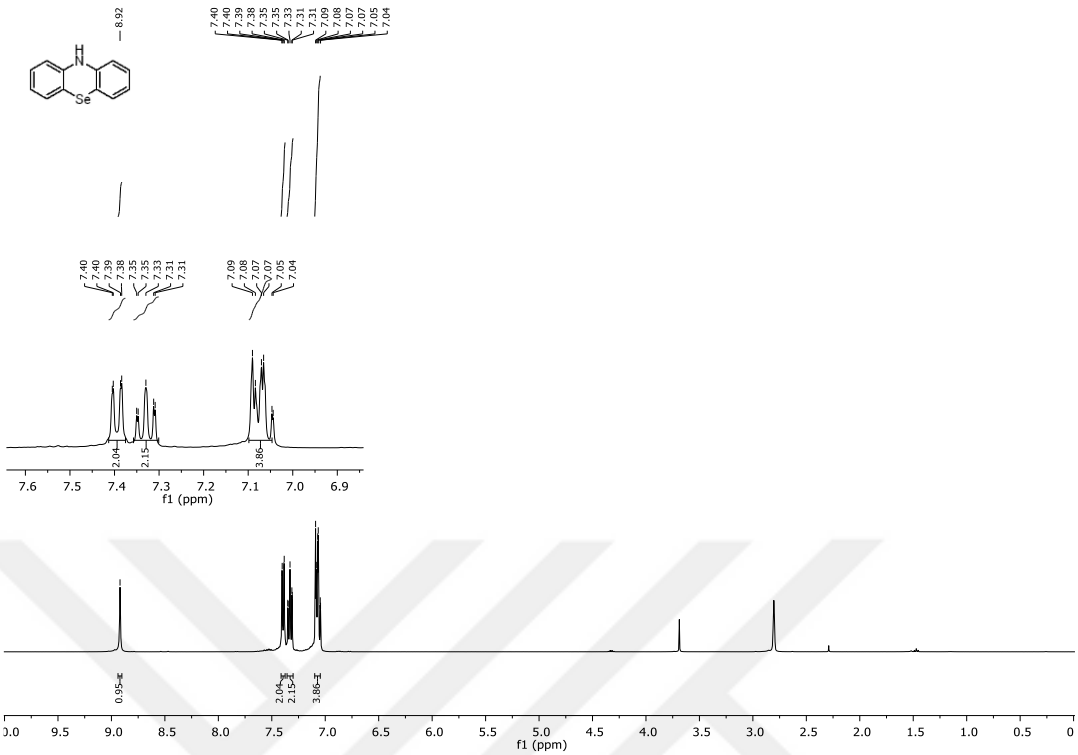

Figure A. 20. ^{1}H NMR of Compound 19 in DMSO-d6

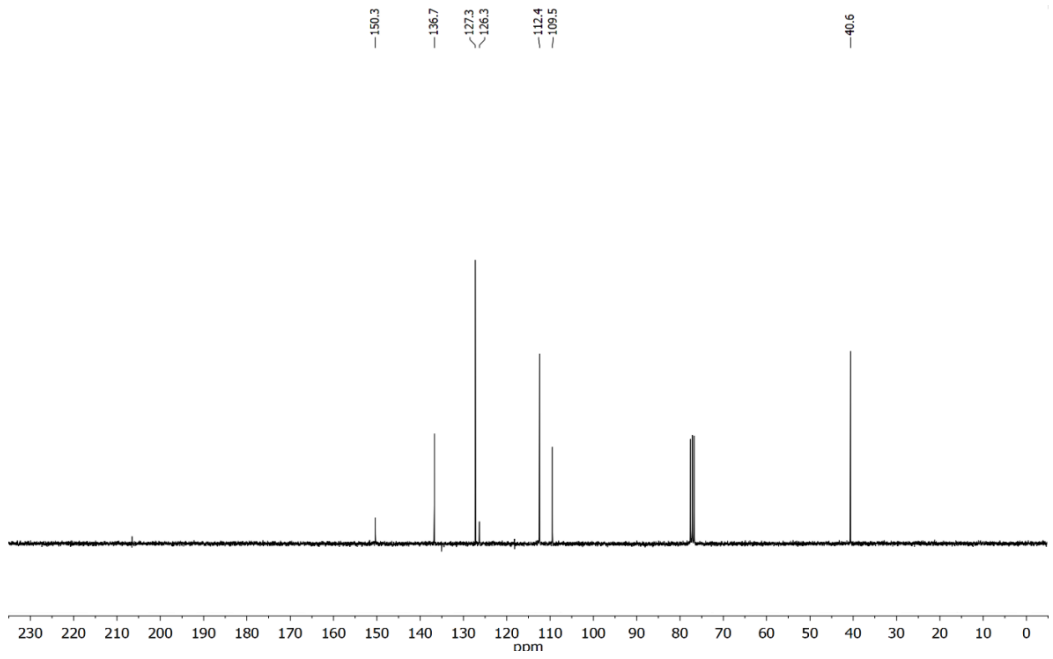

Figure A. 21. ^{13}C NMR of Compound 19 in DMSO-d6

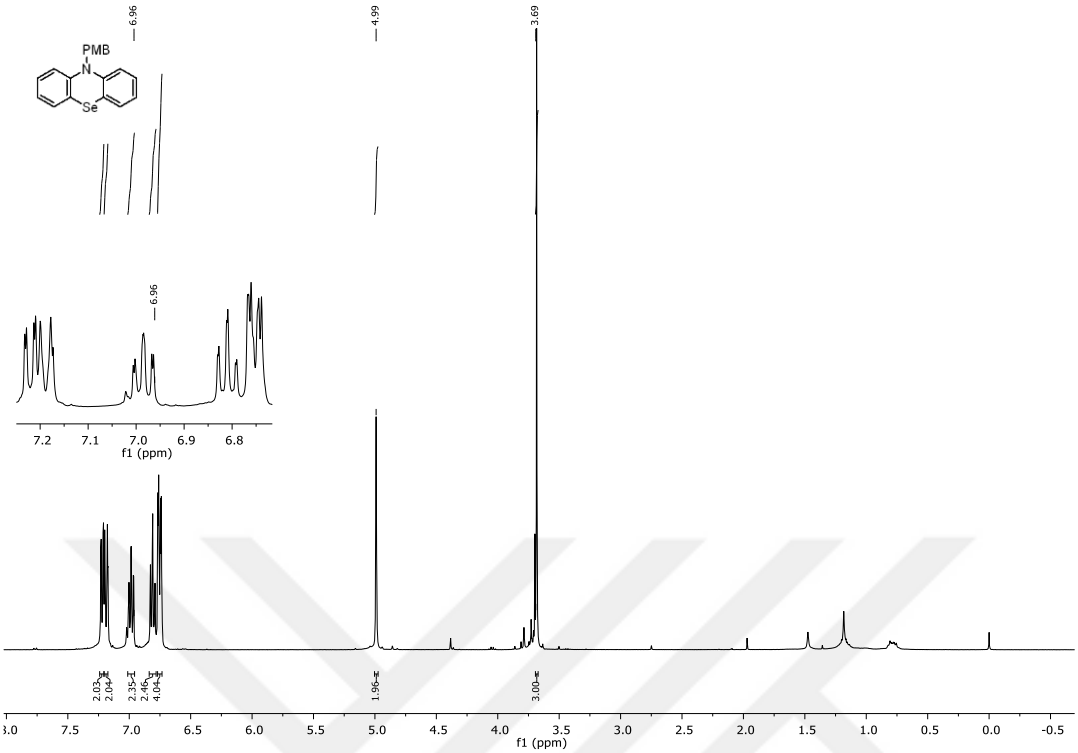

Figure A. 22. ^{1}H NMR of Compound 20 in $CDCl_3$

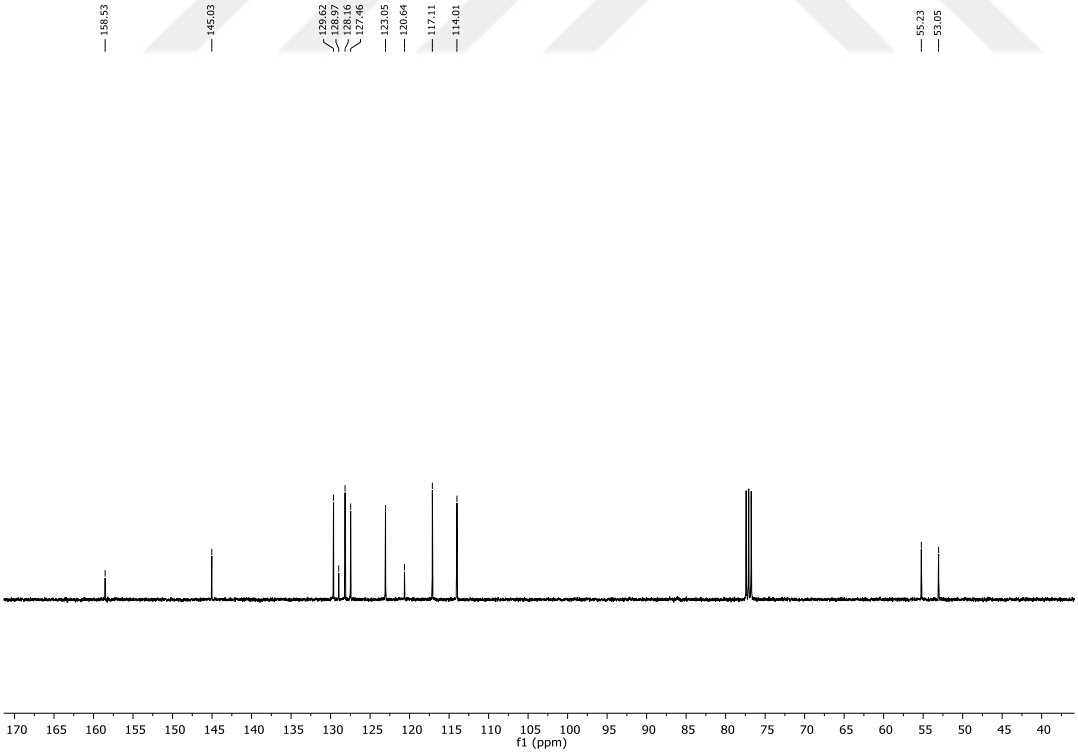

Figure A. 23. ^{13}C NMR of Compound 20 in $CDCl_3$

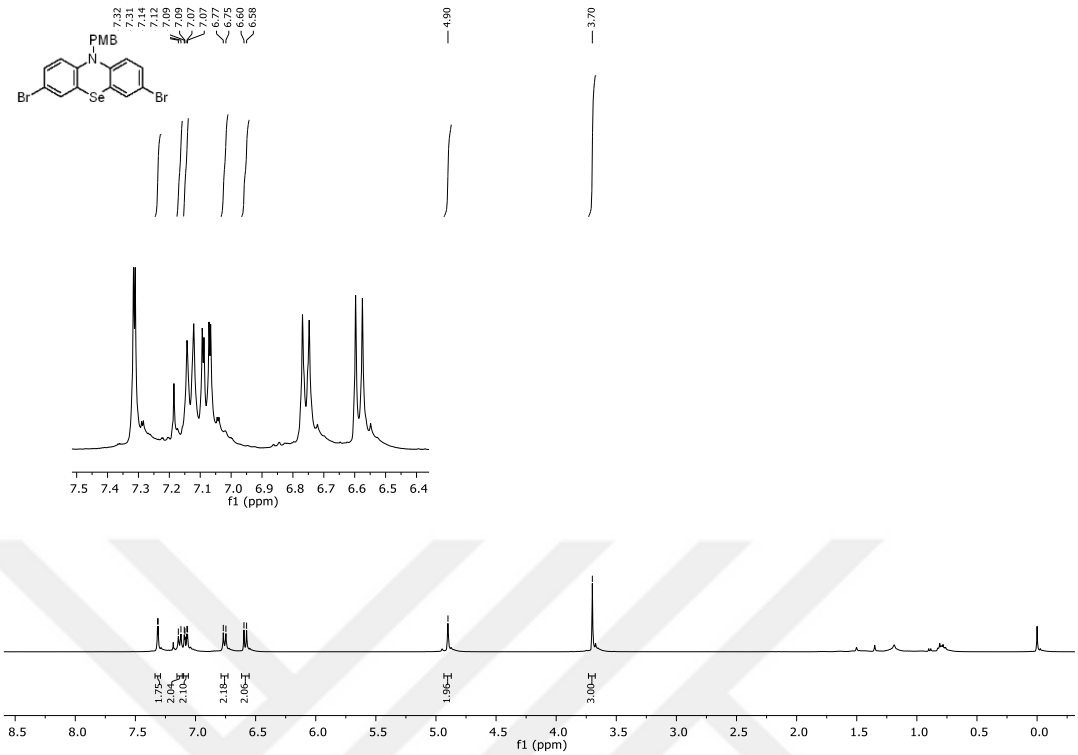

Figure A. 24. ^{1}H NMR of Compound 21 in $CDCl_3$

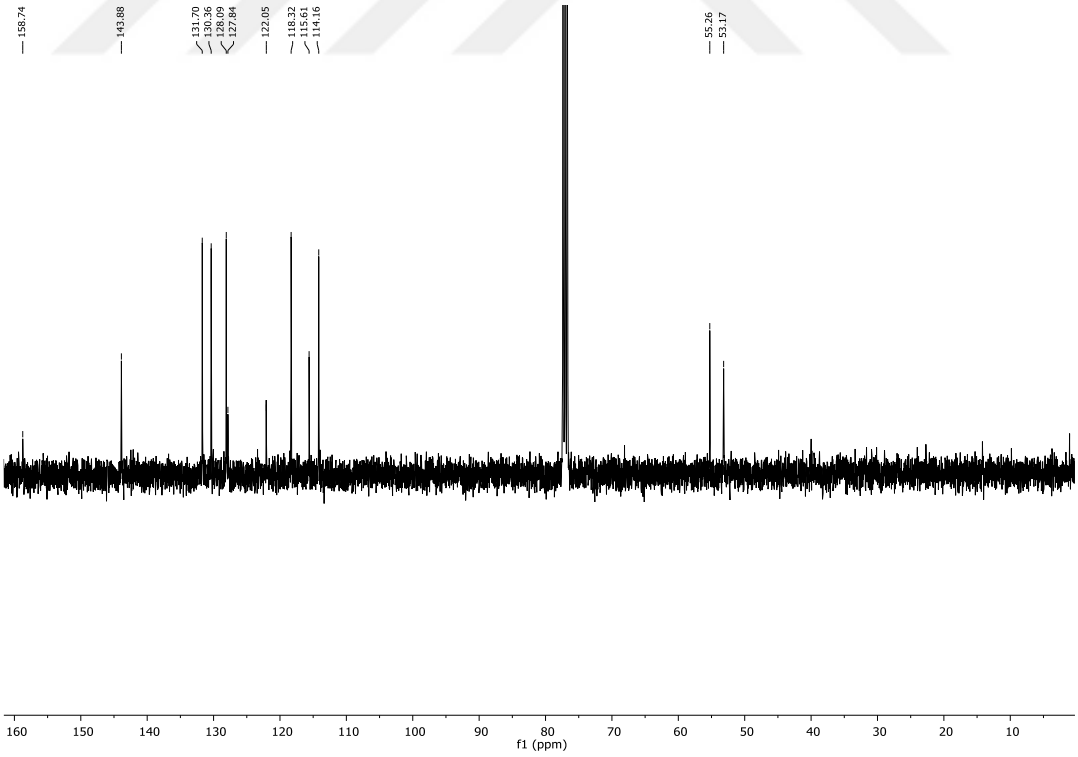

Figure A. 25. ^{13}C NMR of Compound 21 in $CDCl_3$

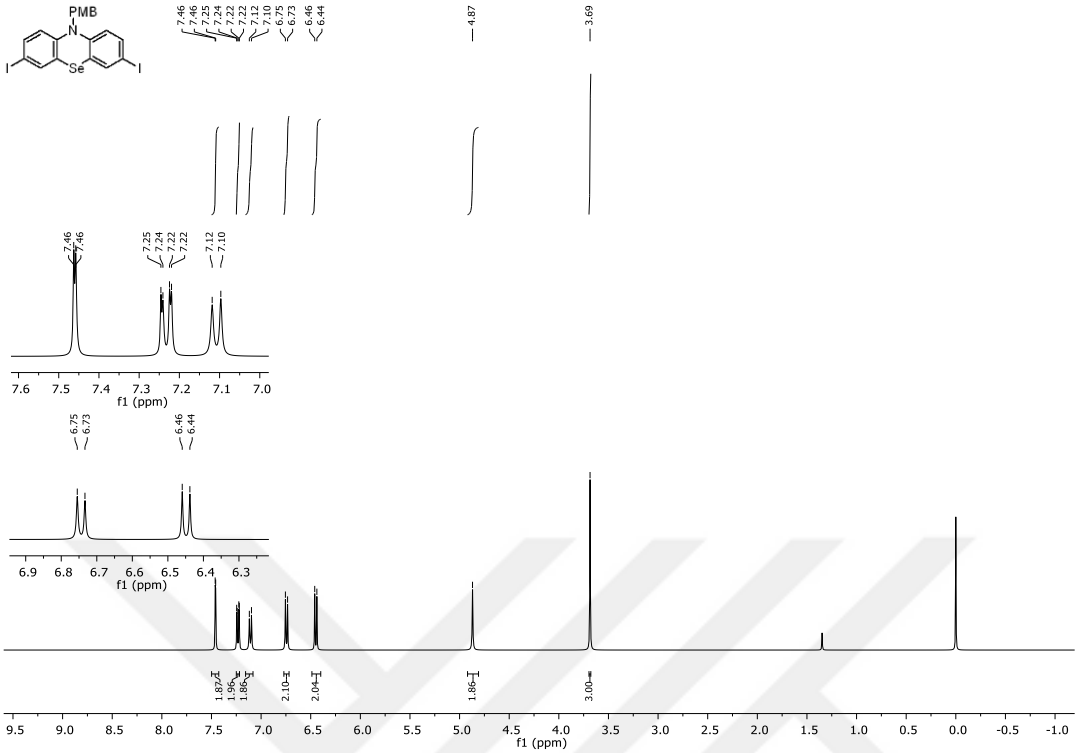

Figure A. 26. ^{1}H NMR of Compound 22 in $CDCl_3$

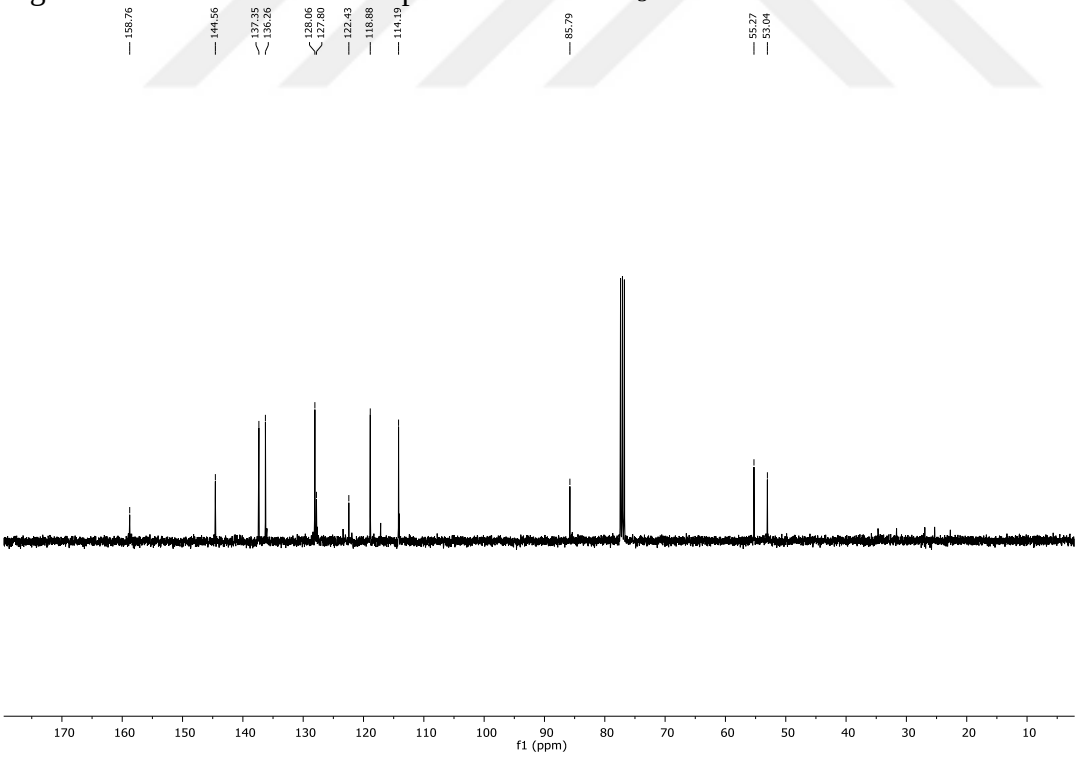

Figure A. 27. ^{13}C NMR of Compound 22 in $CDCl_3$

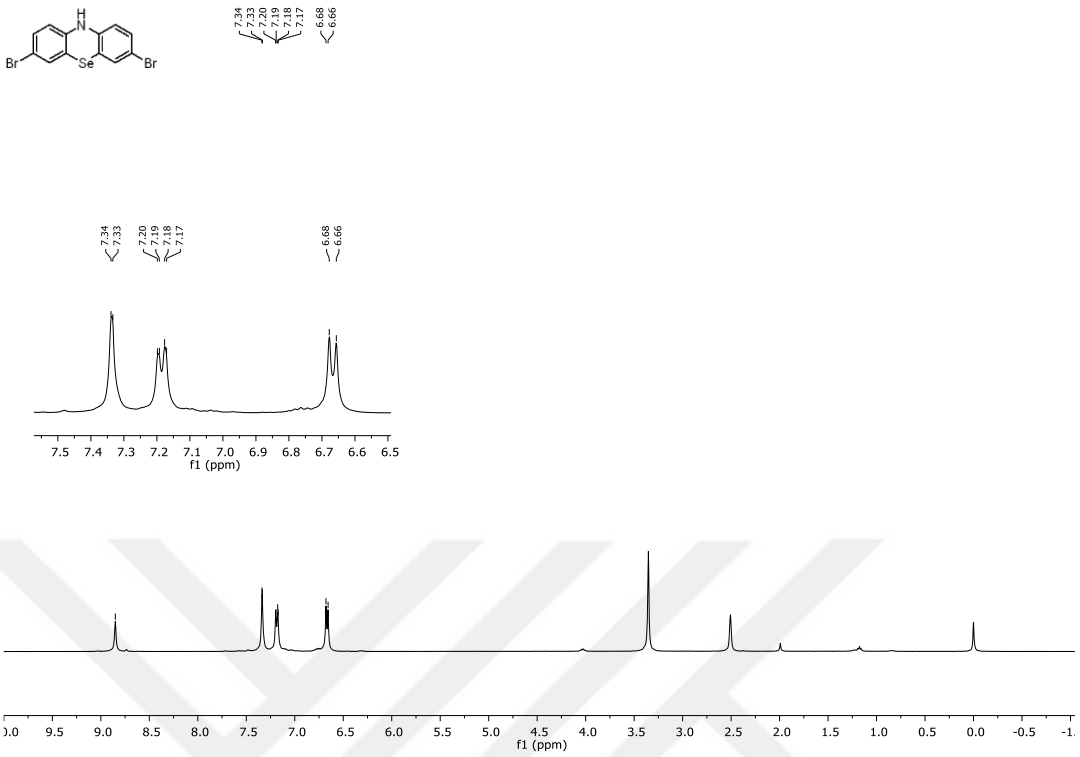

Figure A. 28. ^{1}H NMR of Compound 29 in DMSO-d6

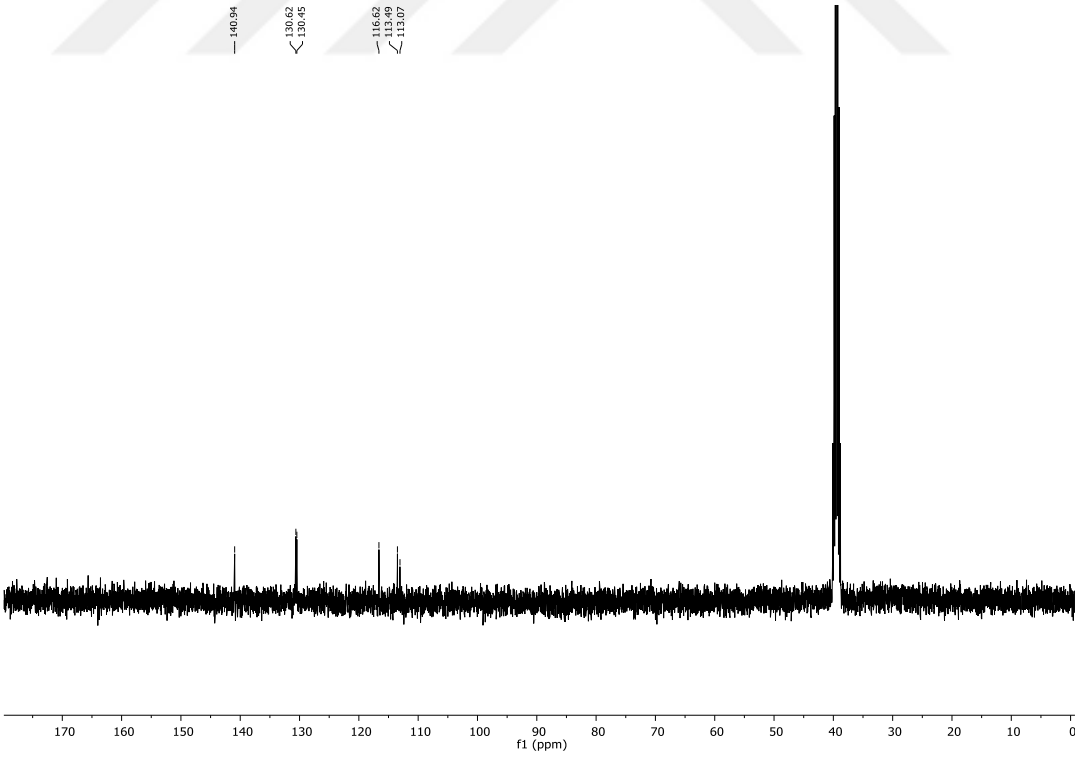

Figure A. 29. ^{13}C NMR of Compound 20 in DMSO-d6

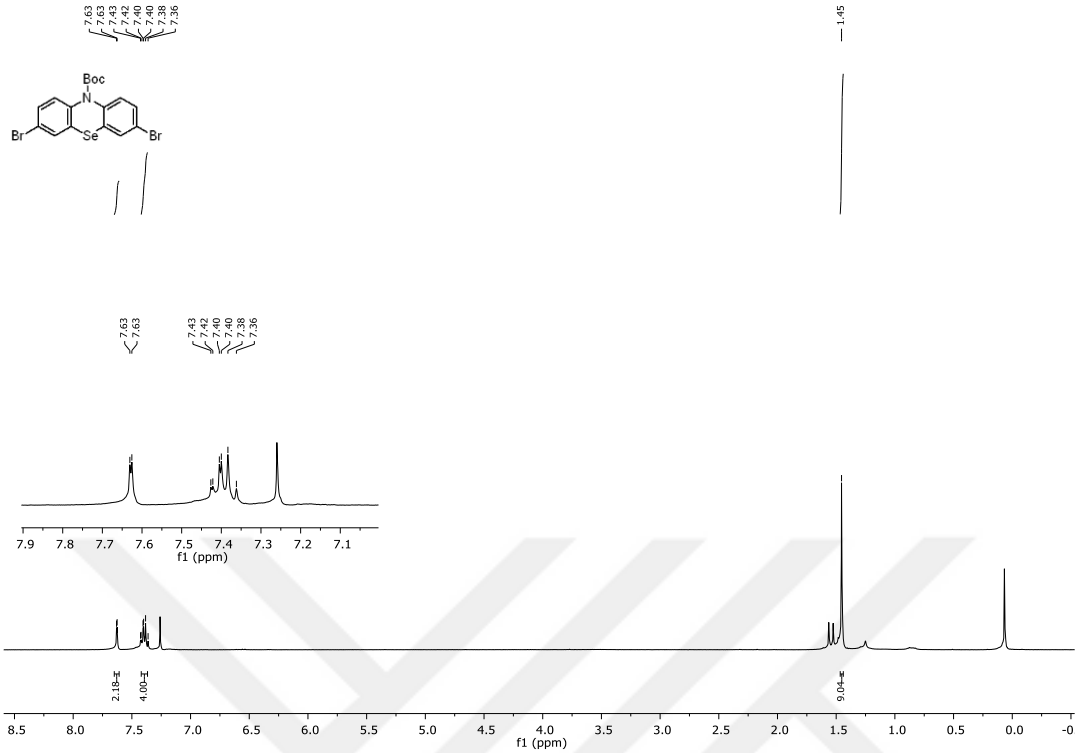

Figure A. 30. ^{1}H NMR of Compound 30 in $CDCl_3$

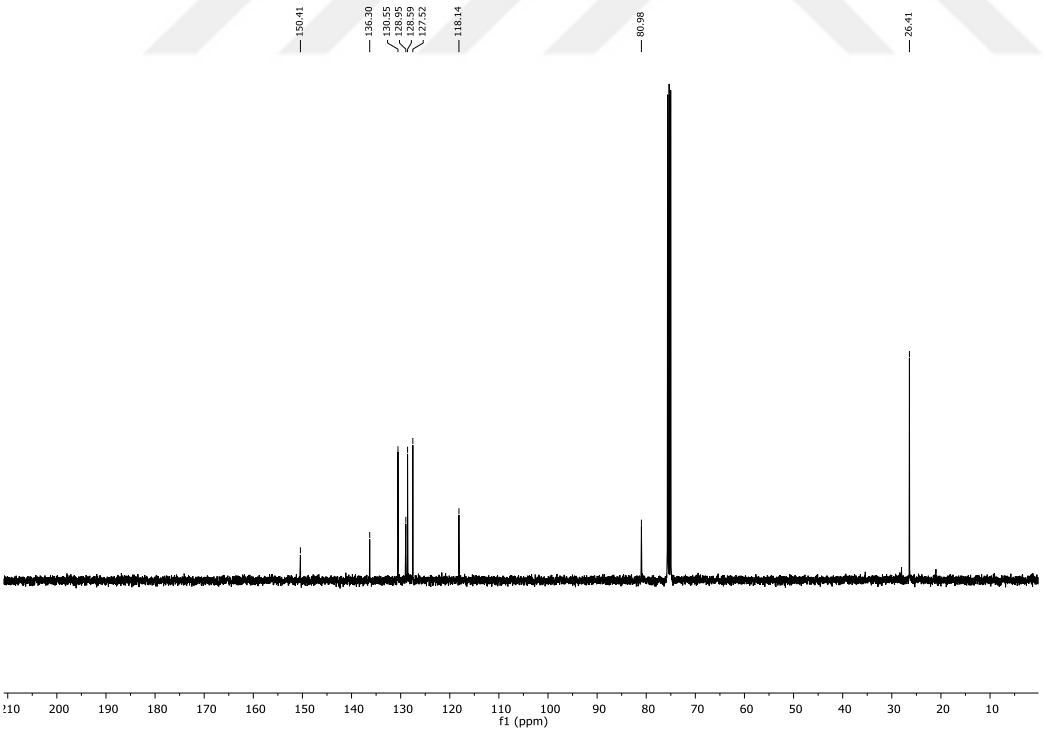

Figure A. 31. ^{13}C NMR of Compound 30 in $CDCl_3$

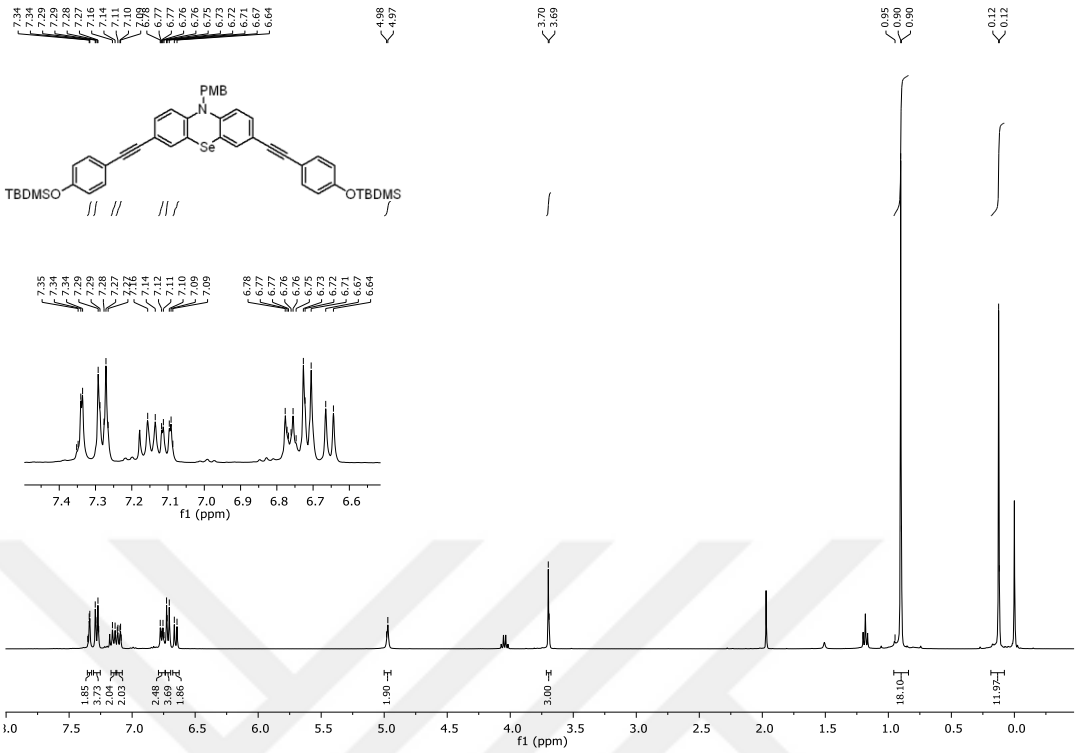

Figure A. 32. ^{1}H NMR of Compound 27 in $CDCl_3$

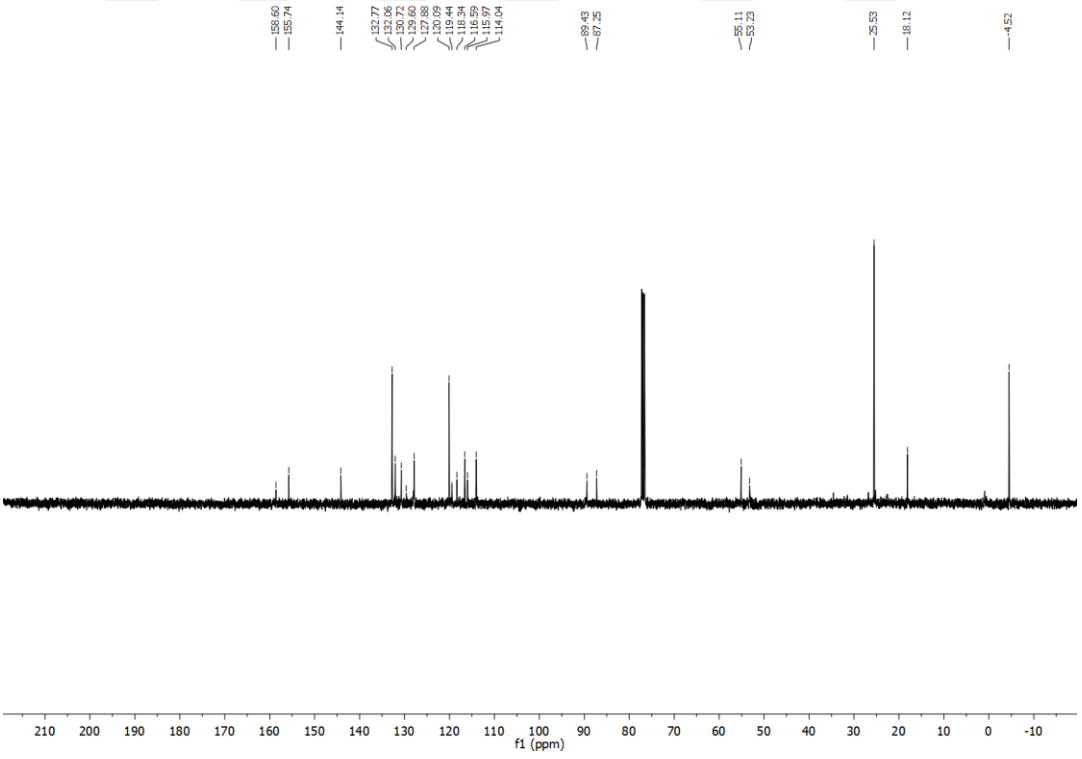

Figure A. 33. ^{13}C NMR of Compound 27 in $CDCl_3$

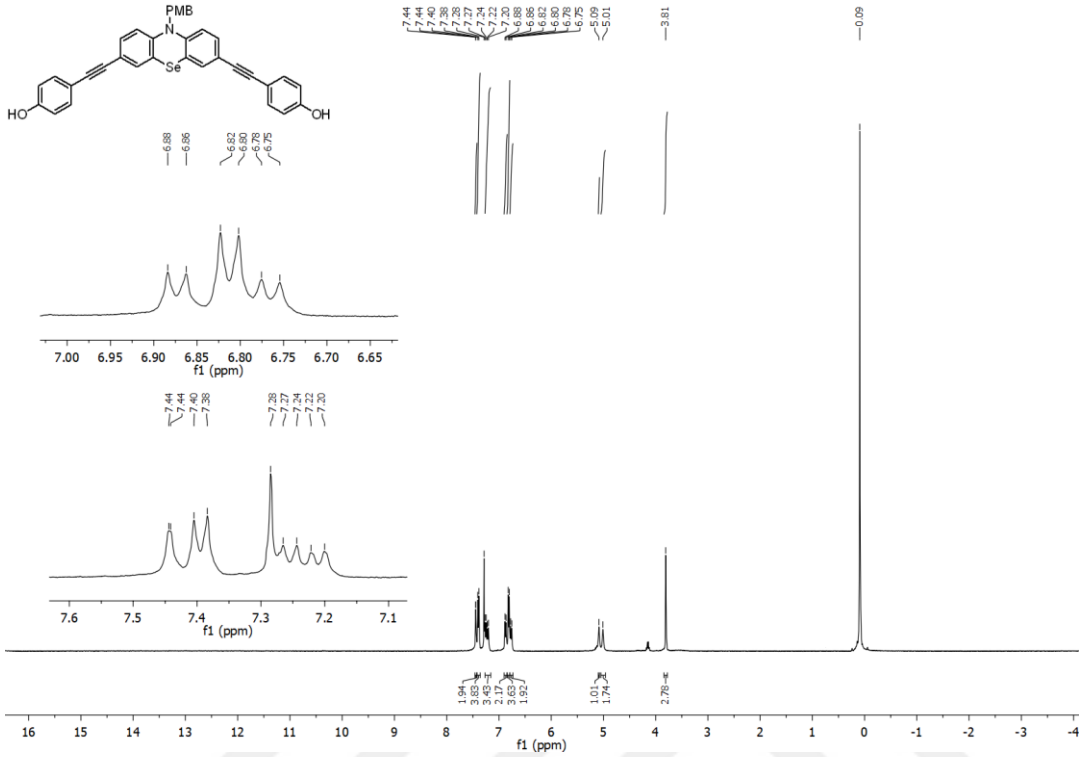

Figure A. 34. ^{1}H NMR of Compound 28 in $CDCl_3$

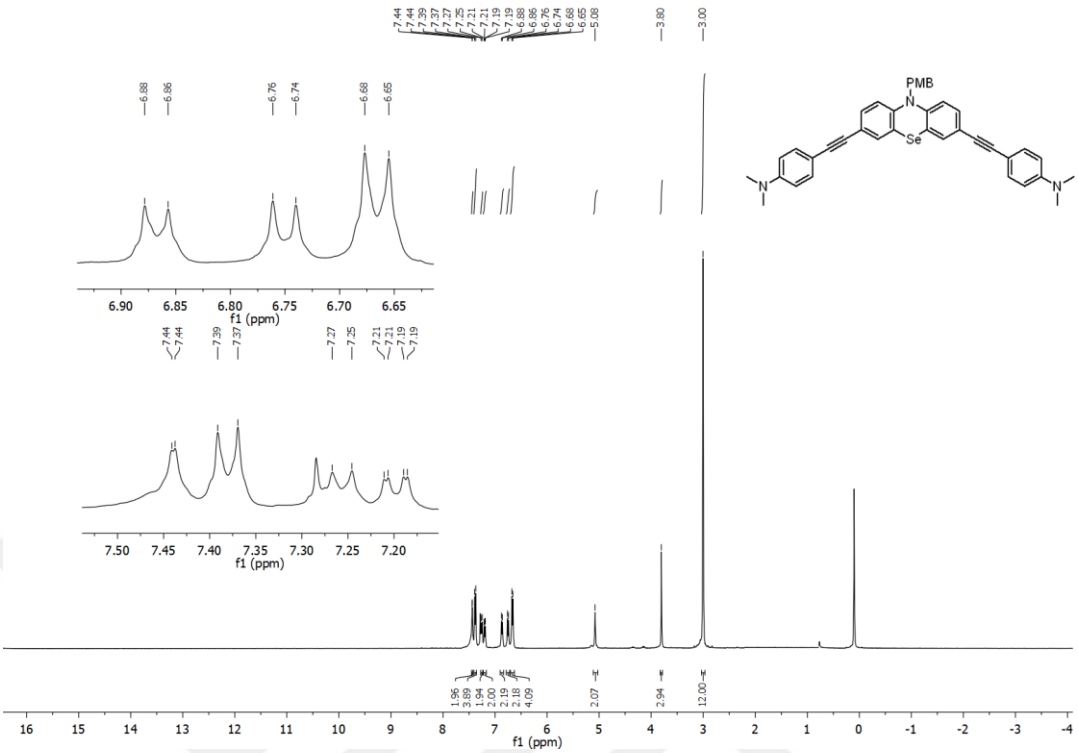

Figure A. 35. ^{1}H NMR of Compound 34 in $CDCl_3$

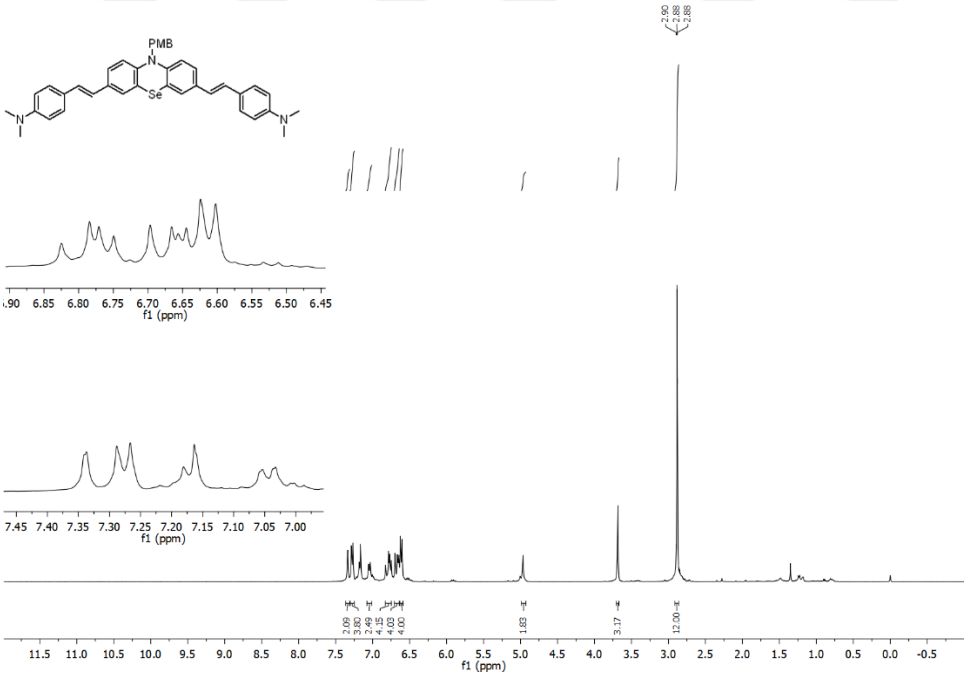

Figure A. 36. ^{1}H NMR of Compound 37 in $CDCl_3$

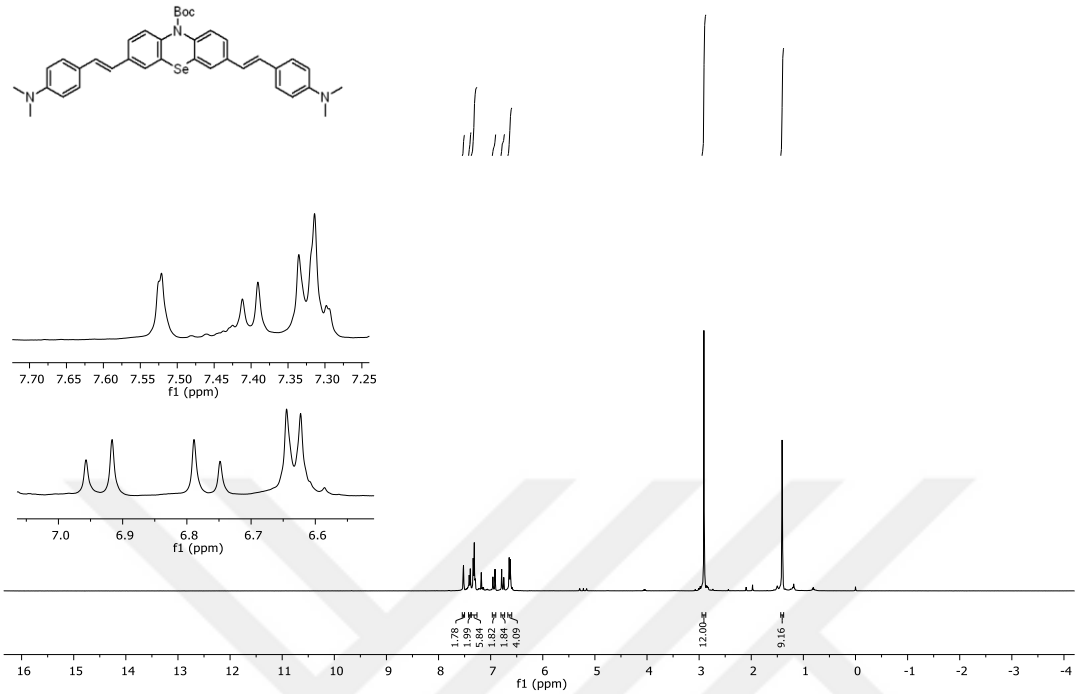

Figure A. 37. ^{1}H NMR of Compound 38 in $CDCl_3$

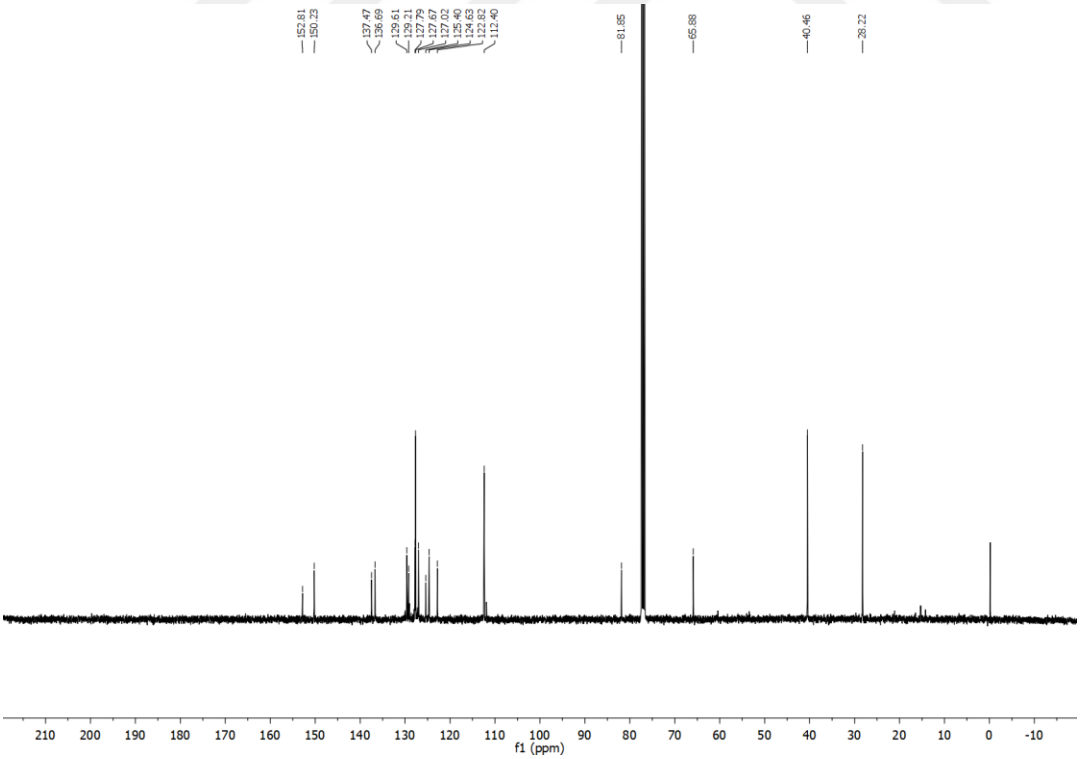

Figure A. 38. ^{13}C NMR of Compound 38 in $CDCl_3$

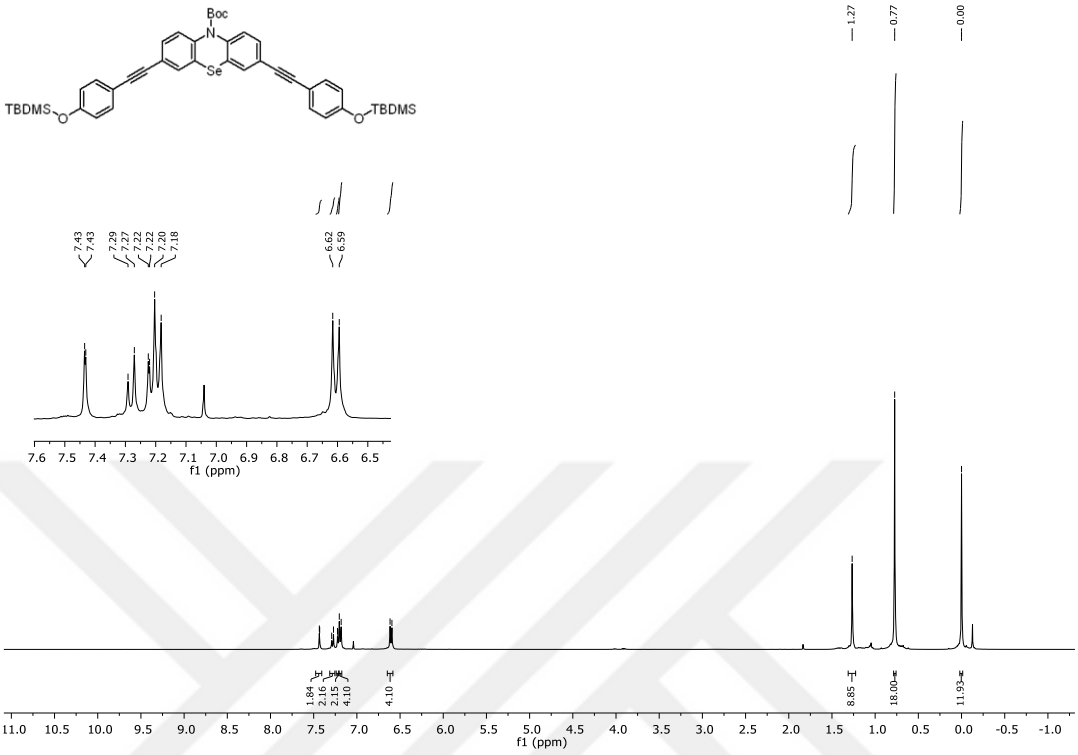

Figure A. 39. ^{1}H NMR of Compound 31 in $CDCl_3$

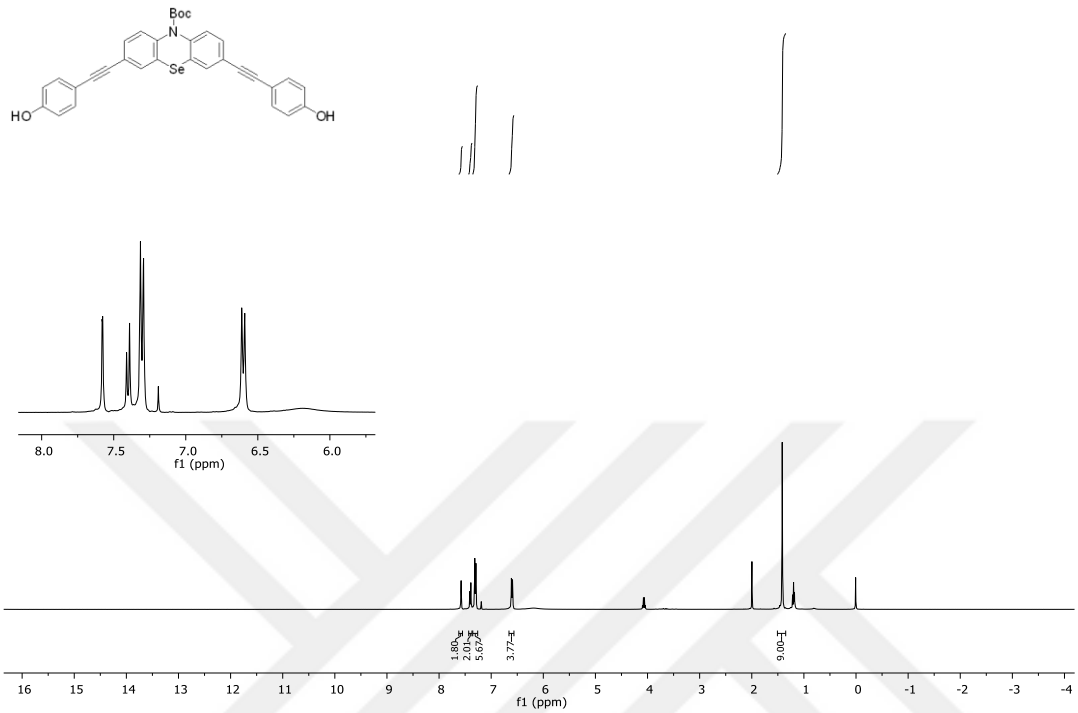

Figure A. 40. ^{1}H NMR of Compound 32 in $CDCl_3$

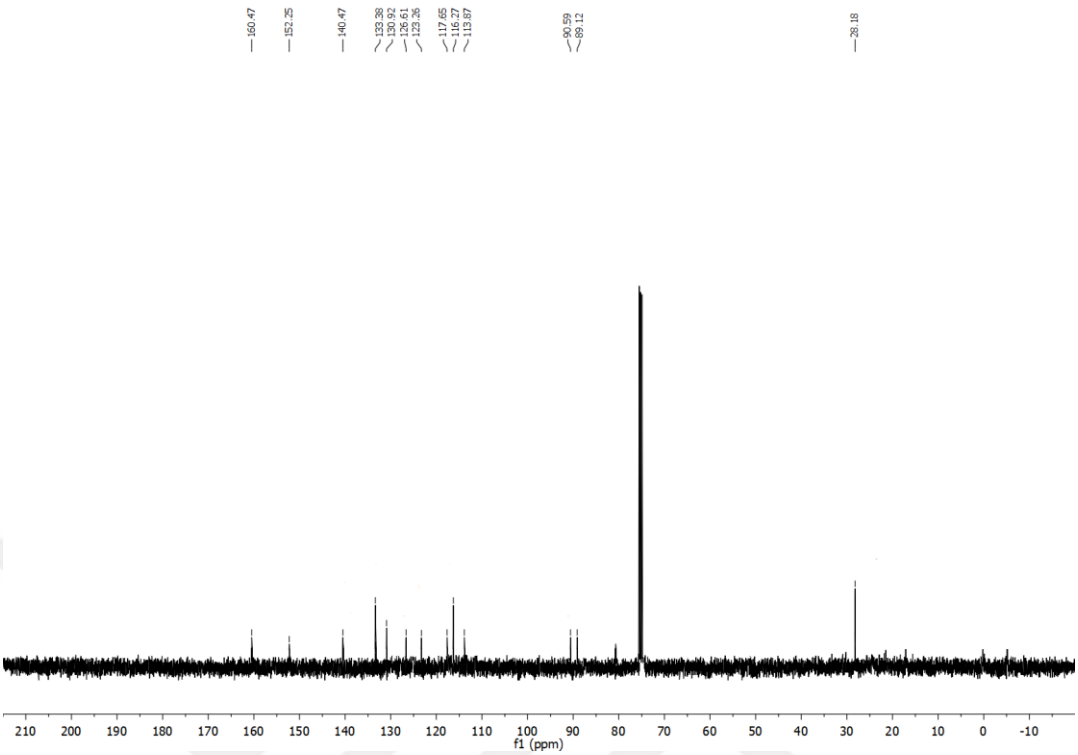

Figure A. 41. ^{13}C NMR of Compound 32 in $CDCl_3$

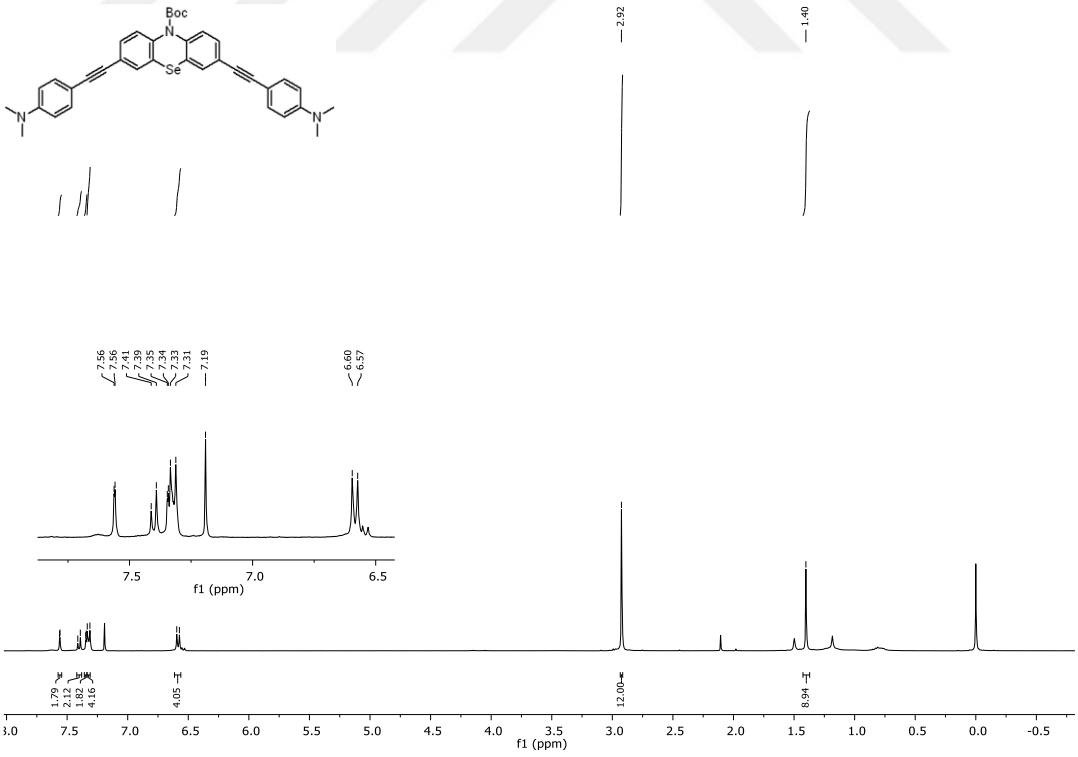

Figure A. 42. ^{1}H NMR of Compound 34 in $CDCl_3$

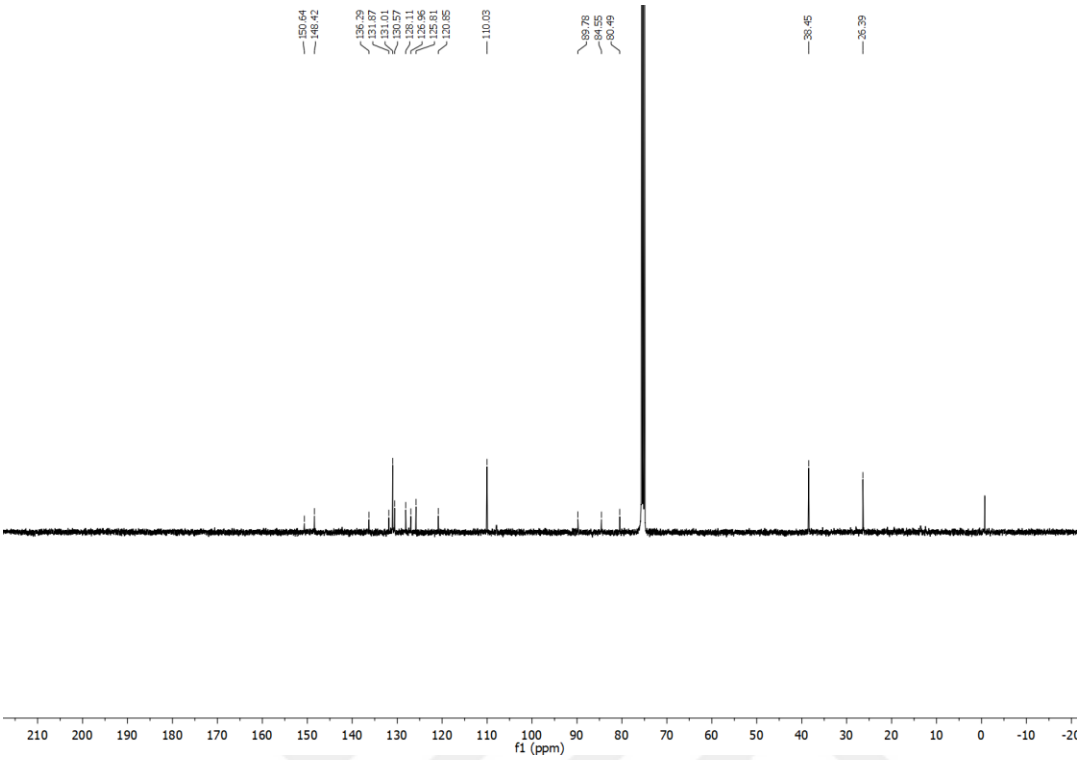

Figure A. 43. 13C NMR of Compound 34 in CDCl3

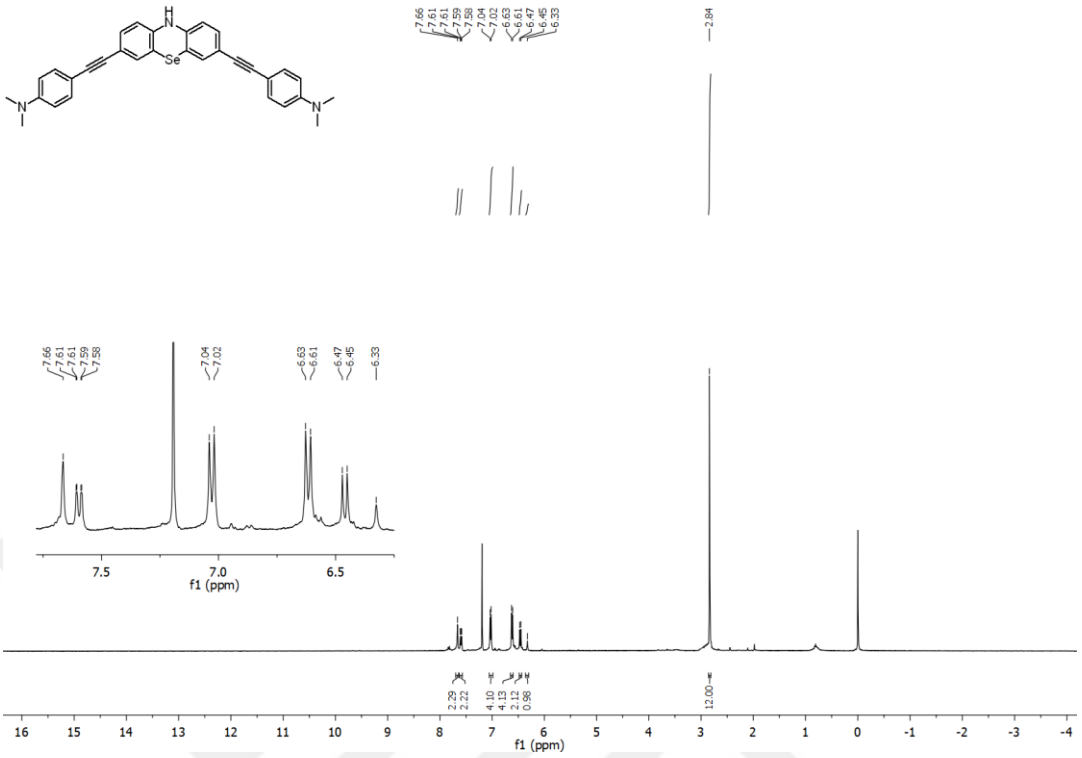

Figure A. 44. ^{1}H NMR of Compound 35 in $CDCl_3$

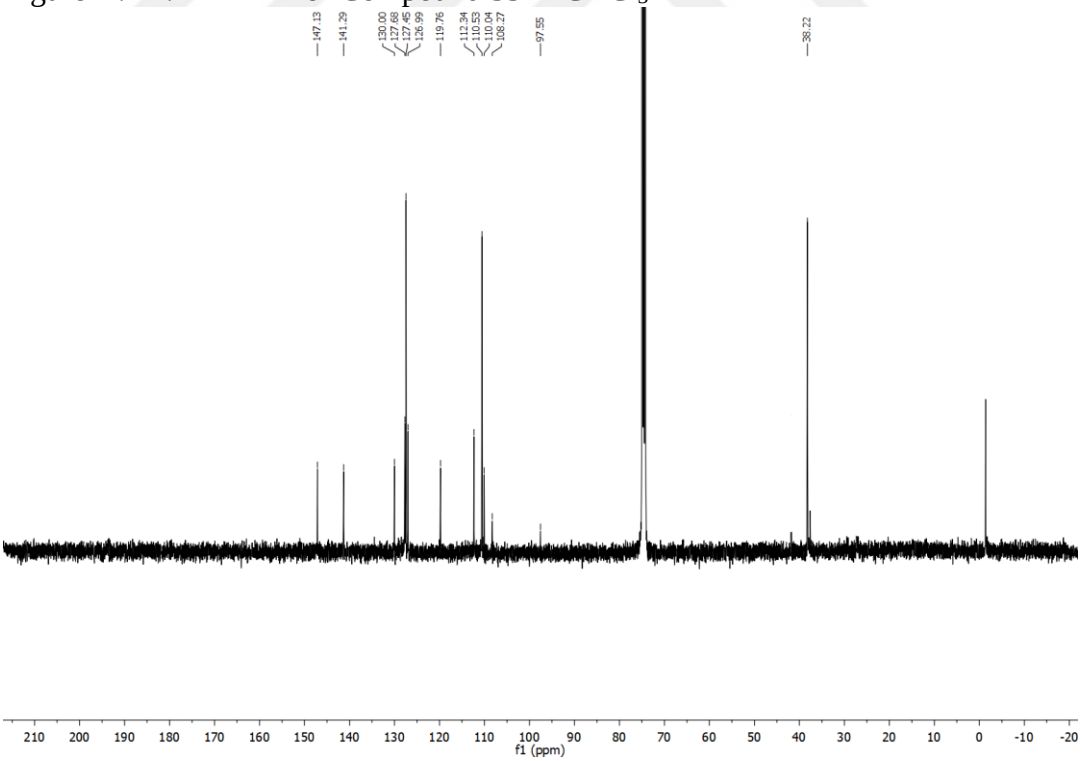

Figure A. 45. ^{13}C NMR of Compound 35 in $CDCl_3$